AER/AGS Special Report 128

Alberta Energy Regulator

Geological Interpretation of Merged 2021–2024 Airborne Geophysics Datasets, Alberta

AGS
ALBERTA GEOLOGICAL SURVEY

AER/AGS Special Report 128

Geological Interpretation of Merged 2021–2024 Airborne Geophysics Datasets, Alberta

G.P. Lopez, D. McGill, A. Brem and J. McKenzie

Ronacher McKenzie Geoscience Inc.

January 2026

ISBN 978-1-4601-5741-1

Lopez, G.P., McGill, D., Brem, A. and McKenzie, J. (2026): Geological interpretation of merged 2021–2024 airborne geophysics datasets, Alberta; Alberta Energy Regulator / Alberta Geological Survey, AER/AGS Special Report 128, 137 p.

Publications in this series have undergone only limited review and are released essentially as submitted by the author.

Authors address:
G.P. Lopez, D. McGill, A. Brem and J. McKenzie
Ronacher McKenzie Geoscience Inc.
6 – 2140 Regent Street
Sudbury, ON P3E 5S8
Canada

Tel: 705.419.1508
Email: info@rmgeoscience.com

Published January 2026 by:
Alberta Energy Regulator
Alberta Geological Survey
Suite 205
4999 – 98 Avenue NW
Edmonton, AB T6B 2X3
Canada

Tel: 780.638.4491
Email: AGS-Info@aer.ca
Website: ags.aer.ca

Contents

Appendices

Digital Appendix A – Interpretation – GIS files

The appendix is in the accompanying folder entitled 'Digital Appendix A – Interpretation – GIS files,' located in the download zip file.

Digital Appendix B – Airborne magnetic map products

The appendix is in the accompanying folder entitled 'Digital Appendix B – Airborne magnetic map products,' located in the download zip file.

Digital Appendix C – Automatic detection – Fathom Geophysics vector and raster products

The appendix is in the accompanying folder entitled 'Digital Appendix C – Automatic Detection – Fathom Geophysics vector and raster products,' located in the download zip file.

Foreword

The Alberta Geological Survey (AGS) outsourced the geological interpretation of several high-resolution airborne magnetic geophysical surveys conducted by the Alberta Energy Regulator (AER) / AGS over the entire province of Alberta between 2021 and 2024. This report provides merged raster and vector datasets and an interpretation of these newly merged datasets. This release does not replace the previous interpretive reports and data releases provided by Ronacher McKenzie Geoscience Inc. (RMG), as they delve into greater detail for each survey area of Alberta. The interpretation focused on modifying the boundaries of known basement domains, dividing domains into subdomains, identifying brittle and ductile structures, and identifying potential igneous intrusions.

All production of the geophysical products and interpretation of data were completed by RMG, as well as the subcontractor Fathom Geophysics LLC (Fathom), with oversight and approval from the AER and the AGS. The aeromagnetic data from the 2021–2024 surveys were used to create various gridded and raster filter products to aid RMG's interpretation. Fathom generated automatic structure detection, radial symmetry detection, depth to basement filters, and other geophysical products, which also aided RMG in their interpretation. These newly merged datasets were used to conduct a province-wide geophysical interpretation, made in conjunction with the previous interpretations. This release includes all of the geophysical vector and raster products and GIS files.

This work was completed under the Mineral Grant provided by the Government of Alberta dated June 22, 2021.

Geological Interpretation of the 2021-2024 Aeromagnetic Data

Merging of Airborne Magnetic Interpretation Products

Alberta

Prepared For:

Alberta Geological Survey

Alberta Energy Regulator | AGS ALBERTA GEOLOGICAL SURVEY

Prepared By:

Gloria Lopez, PhD, P.Geo.
Darcy McGill, P.L. (Geo.)
Arjan Brem, PhD, P.Geo.
Jenna McKenzie, P.Geo.
Ronacher McKenzie Geoscience Inc.

RONACHER MCKENZIE GEOSCIENCE

March 28, 2025

TABLE OF CONTENTS

FIGURES

TABLES

APPENDICES

DIGITAL APPENDICES

1.0 SUMMARY

The Alberta Geological Survey ("AGS") contracted Ronacher McKenzie Geoscience ("RMG") to provide a province-wide geological interpretation of the high-resolution aeromagnetic surveys acquired over Alberta between 2021 and 2024. This report presents the results of the seamless integration of the geological interpretations that were conducted by RMG for the Shield, southern Alberta, central Alberta, and northern Alberta into a single project area that covers most of Alberta and provides updates to previous interpretations. This report supplements the GIS files produced for this project.

Between 2021 and 2024, the Alberta Energy Regulator ("AER") contracted EON Geosciences, Sander Geophysics Limited, and Xcalibur Multiphysics to fly aeromagnetic surveys covering different parts of the province in four main survey areas: Shield (northeastern Alberta), northern Alberta, central Alberta and southern Alberta. Additional aeromagnetic data from legacy surveys were also acquired for complete coverage of these four project areas. EON Geosciences integrated all datasets and created a merged gridded magnetic data set for the entire province.

RMG created derivative and filter products from the merged measured data to enhance and highlight different features to aid in geological interpretations. Grid-based derivative and filter products were calculated from the total magnetic intensity ("TMI") and International Geomagnetic Reference Field ("IGRF")-removed residual magnetic intensity ("RMI") grids. The various digital products are included in the digital appendix delivered with this report.

Fathom Geophysics performed automatic detection on the merged gridded magnetic data to generate structure, radial symmetry, and fabric orientation products. These products supported the geological interpretation. Fathom Geophysics' final report is attached as an appendix to this report and the various digital products are included in the digital appendix delivered with this report.

The new high-quality airborne magnetic data and filter products enable improved understanding of the architecture of the basement in Alberta. The observations were integrated with and calibrated against existing results of legacy geophysical and geological studies, and previous regional interpretations. Care was taken to avoid mistaking potential cultural magnetic response for geology-related anomalies.

The following conclusions are made:

- The higher resolution of the new magnetic data allows for further subdivision of domains into subdomains in the crystalline basement based on variations of internal magnetic fabrics. Significant modifications to existing basement domains were made by editing the tectonic domain boundaries defined by previous studies and by dividing known domains into subdomains.
- Basement anomalies were delineated. These range from small single lobe circular anomalies to larger multi-lobe rounded asymmetrical anomalies that may represent potential intrusions.

- Known ductile structures were recognized, including the Charles Lake, Leland Lake, and Great Slave Lake shear zones, the Snowbird tectonic zone, the Red Deer trend, and the Eyehill High. New ductile structures were defined and characterized, including the High Level and Steen River shear zones, and the previously recognized but forgotten Beatty River Fault.
- New brittle faults were delineated. Few regional faults of the Western Canada Sedimentary Basin reported in literature show a spatial correlation with the magnetic lineaments.
- The new magnetic data provide further insight into the geology of Alberta and demonstrate relationships between basement features not previously identified.

The interpretation of the new high-quality aeromagnetic data for Alberta may help to refine current tectonic models. In particular, the magnetic data suggest that north-central Alberta has more basement complexity adjacent to the Snowbird tectonic zone, and between the Buffalo Head domain and the Charles Lake shear zone than previously recognized, and further investigation is required to understand its tectonic history, controls on the deposition of Paleozoic strata, and potential sources, pathways and traps for mineralization.

2.0 PROJECT OVERVIEW

The Alberta Geological Survey ("AGS") commissioned Ronacher McKenzie Geoscience ("RMG") to merge the products of the geological interpretations of the four recent high-resolution aeromagnetic surveys over Alberta and complete a province-wide interpretation of the magnetic data. The geophysical surveys were conducted by EON Geosciences Inc., Sander Geophysics Ltd., and Xcalibur Multiphysics between 2021 and 2024. The geological interpretations were conducted by RMG for the Canadian Shield, northern Alberta, and southern Alberta regions in 2024 (Lopez et al., 2024a; Lopez et al., 2024b; Brem et al., 2024), and the central Alberta region in 2025 (Lopez et al., 2025). The goal of this project is to merge these separate interpretation products into seamless files and interpret the merged data. The merged magnetic dataset was provided by the AGS.

The objectives of the merging project are to:

- Review the merged magnetic dataset.
- Create filter and derivative products for the merged dataset.
- Combine and review previous domain interpretations of the crystalline basement conducted by RMG.
- Combine and review previous anomalies interpreted as granitoids by RMG.
- Combine and review previous lineaments interpreted by RMG including major ductile structures, brittle faults, and dikes.
- Review the boundaries of the major lithotectonic units.

- Produce a merged lithotectonic map for the province of Alberta.
- Summarize the work, including province-wide interpretations, in a report with recommendations.

Universal Transverse Mercator ("UTM") coordinates were provided in the datum of WGS 84 zone 11N for all aeromagnetic digital files (vector and map files). Figures herein are projected to NAD 83 zone 11N unless otherwise labeled.

2.1 Previous Regional Studies

Previous regional studies that involve geophysical acquisition and/or geological interpretations include:

- The pioneering work by Hoffman (1988, 1989), Ross et al. (1989, 1991, 1994), and Villeneuve et al. (1993), in which aeromagnetic and gravity data were used to subdivide the basement in Alberta into tectonic domains.
- Misra et al. (1991) interpreted numerous lineaments based on satellite imagery. Their work assumed that fractures that outline fault blocks in the basement control the orientation of faults in the sedimentary cover and hence, the orientation of lineaments that appear on satellite images.
- Burwash et al. (1994) provided a geological interpretation of the basement rocks based on petrography, whole-rock geochemistry, and isotopic age determinations carried out on core samples collected from petroleum wells that have penetrated the crystalline basement. The authors also provided a metamorphic evolution of the basement of Alberta based on historical and new U–Pb, Rb–Sr, K–Ar, $^{40}Ar/^{39}Ar$ and Sm–Nd geochronology (Burwash et al., 2000a).
- Edwards et al. (1998) completed a regional interpretation of magnetic and gravity data in central Alberta using the horizontal gradient to infer the locations of steep basement faults. Results identified distinctive orthogonal sets of NE, NW and N-S/E-W lineament systems, which may have controlled the deposition and deformation of Phanerozoic sedimentary units. Later, Edwards and Brown (1999) integrated potential-field data with paleobathymetry and available seismic data to resolve whether basement structures controlled Devonian reef deposition, but results were equivocal.
- The Lithoprobe seismic reflection program was a national research project that studied the 3D structure and evolution of the subsurface in Canada. Lithoprobe data interpretation for Alberta can be found in Eaton et al. (1995; 1999), Hope et al. (1999), Lemieux et al. (2000), Ross and Eaton (2002) and Ross (2002), among others.
- Pilkington et al. (2000) used potential field data and anomaly enhancement methods to emphasize the internal character of domains and refined the basement subdivisions by Ross et al. (1994).
- Hope and Eaton (2002) modelled the crustal structure beneath the Western Canada Sedimentary Basin ("WCSB") using numerical simulation of five regional gravity and magnetic anomalies in Alberta

that had previously been constrained by Lithoprobe seismic and electromagnetic studies (Kimiwan High, Thorsby Low, Red Deer High, Eyehill High, and Vulcan structure). Their results provided confirmation or alternative interpretations for these anomalies enhancing the understanding of the tectonic history.

- Lyatsky et al. (2005; and references therein) used potential field data and anomaly enhancement methods to identify lineaments in central and southern Alberta. This work supported the conclusions by Eaton et al. (1995) that basement faults have a control on hydrocarbon traps in the Central Alberta basin.

2.2 Recent Advances

The new state-of-the-art aeromagnetic and gravity surveys are of higher resolution than many previous surveys and allow better and more accurate analysis and interpretation of the data, particularly since much legacy aeromagnetic and gravity data were acquired using very large line spacings and without the spatial accuracy made possible by satellite positioning and navigation systems.

Secondly, over the past two decades, advances in computing power have enabled new geophysical data processing methods and visualization techniques, particularly for large scale datasets. In addition, 3D integration and modelling of subsurface data is now commonplace, enabled by these same computing advances.

2.3 RMG Qualifications

Ronacher McKenzie Geoscience is a Canadian consulting company operating globally. RMG's mission is to use intelligent geoscientific data integration to help mineral explorers focus on what matters to them. We help a growing number of clients understand the factors that control the location of mineral deposits.

With a variety of professional experience, our team's services include:

- Data integration, analysis, and interpretation
- Geophysical services
- Project generation and property assessment
- Exploration project management
- Independent technical reporting
- Project promotion
- Lands management

The primary author of this report is Gloria Lopez, PhD, P.Geo., Senior Geologist at RMG and a geologist in good standing with the Association of Professional Engineers and Geoscientists of Alberta (#181673) and

Professional Engineers and Geoscientists Newfoundland and Labrador (#11213). Dr. Lopez has over two decades of experience working as an economic geologist.

A second co-author of this report is Mr. Darcy McGill, BSc, P.Geo. (Limited), P.L. (Geo). Mr. McGill is a Senior Geophysicist at RMG and a geophysicist in good standing with the Association of Professional Geoscientists of Ontario (APGO #2010) and Professional Licensee with the Association of Professional Engineers and Geoscientists of Alberta (#316505). Mr. McGill has worked in geophysical data acquisition, processing, and interpretation for mineral exploration since 1995.

A third co-author of this report is Arjan Brem, PhD, P.Geo., Associate Geologist at RMG and a geoscientist in good standing with the Association of Professional Geoscientists of Ontario (#3798) and with the Association of Professional Engineers and Geoscientists of Alberta (#289121). Dr. Brem has worked globally as a structural geologist in the petroleum and mining industry since 2007.

A fourth co-author of this report is Ms. Jenna McKenzie, Hons BSc, P.Geo. Ms. McKenzie is the co-founder and Principal Geophysicist to RMG and a geoscientist in good standing with the Association of Professional Geoscientists of Ontario (APGO #1653) and the Association of Professional Engineers and Geoscientists of Alberta (#315719). Ms. McKenzie has worked as a geophysicist since 2001 in the exploration and mining industry on a variety of exploration properties with specific focus on geophysics surveying and interpretation.

Additionally, Fathom Geophysics completed automatic structure detection, depth to basement analysis and radial symmetry analysis for intrusion detection on behalf of RMG.

3.0 PROJECT LOCATION

The project area encompasses the Canadian Shield and the Athabasca Basin in the northeast, the northern to southern Plains, and the Foothills in the west (Figure 3-1). The geophysical survey areas lie between latitudes 49° and 60°N, and longitudes 110° and 120°W.

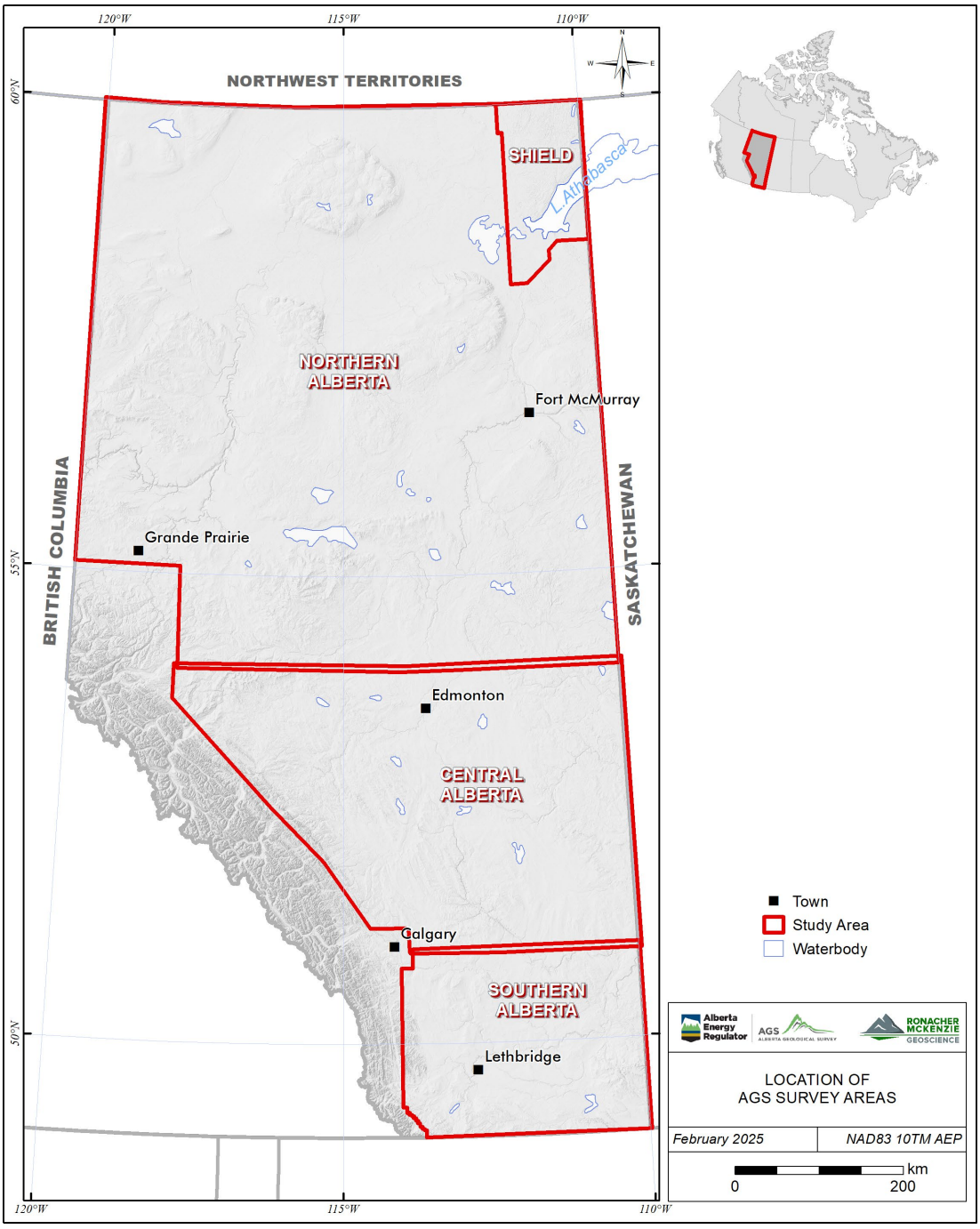

Figure 3-1. Location map showing extent of magnetic survey areas.

4.0 GEOLOGICAL SETTING

The project area covers the Alberta Plains, the Canadian Shield in the northeast, and the Cordilleran foothills in the west (Prior et al., 2013). The area encompasses the Archean to Proterozoic crystalline basement, overlain by the Proterozoic Athabasca Basin in the northeast and the Middle Cambrian to Cenozoic Western Canada Sedimentary Basin ("WCSB") in the remainder of the area. Crystalline basement of the Canadian Shield is only exposed in the northeastern corner of the project area.

4.1 Crystalline Basement

The crystalline basement in Alberta is comprised of Archean and Paleoproterozoic domains (Ross et al., 1994; Figure 4-1) that were assembled into Laurentia during the Paleoproterozoic. These basement domains were defined based on a combination of potential field data, integration with geochronology, isotope geochemistry of basement core samples, and Lithoprobe seismic studies. This integration led to the existing interpretation of basement domains as tectonic domains (Hoffman, 1988; Ross et al., 1991; Villeneuve et al., 1993; Ross et al., 1994; Pilkington et al., 2000). The authors corroborated their interpretation by analogy with geophysical signatures of exposed geological subdivisions of the Canadian Shield and the earlier subdivisions of Hoffman (1988, 1989). Building upon these interpretations, Pilkington et al. (2000) created an internally consistent compilation of magnetic and gravity data for Alberta (and northeastern British Columbia) and used automated interpretation methods to refine basement domain boundaries and to further characterize their internal structure.

Alberta's basement domains and related tectonic interpretations were compiled by Pană et al. (2021). Thus, lithotectonic basement domains in Alberta encompass the Proterozoic Buffalo Head, Chinchaga, Hottah, and Wabamun terranes; the Thorsby remnant of oceanic lithosphere; the Great Bear, Ksituan, Rimbey and Taltson magmatic arcs; the Lacombe metavolcanic and metasedimentary back-arc basin; the Archean Nova slice of the Slave craton; and the Archean Loverna, Vulcan, Eyehill, and Medicine Hat domains of the Hearne Province (Figure 4-2). Pană et al. (2021) excluded the Buffalo Head High and Utikuma basement domains of Pilkington et al. (2000), the Kiskatinaw and Matzhiwin domains of Villeneuve et al. (1993) and Pilkington (2000), and the Rae basement domain of Pilkington et al. (2000).

Further characterization of the crustal architecture in 3D has benefitted from integration with Lithoprobe deep seismic reflection studies (e.g., Eaton et al., 1999; Lemieux et al., 2000; Ross and Eaton, 2002). Additionally, lithological and geochronological controls on basement rocks were obtained from the analysis of sparse core samples from oil wells by Ross et al. (1991), Villeneuve et al. (1993), and Burwash et al. (unpublished data 1994) (Figure 4-2).

The recent compilation of Pană et al. (2021) provides an excellent and condensed description of the tectonic assembly of Alberta's crystalline basement and the studies that led to its current interpretation.

Major structural elements of the basement are the Snowbird tectonic zone in central Alberta, the Vulcan Low in southern Alberta, the Charles Lake and Leland Lake shear zones in the northeast, and the Great Slave Lake Shear Zone in the northwest of the province.

The topography of the crystalline basement is constrained by basement top picks encountered in oil and gas wells and interpreted basement surface available from the AGS (Alberta Geological Survey 2021). Elevation of the basement surface ranges from 454 m above sea level in the northeastern corner of Alberta down to 5,146 m below sea level near the Cordilleran deformation front in the west of the project area (Figure 4-3) (Alberta Geological Survey 2021a).

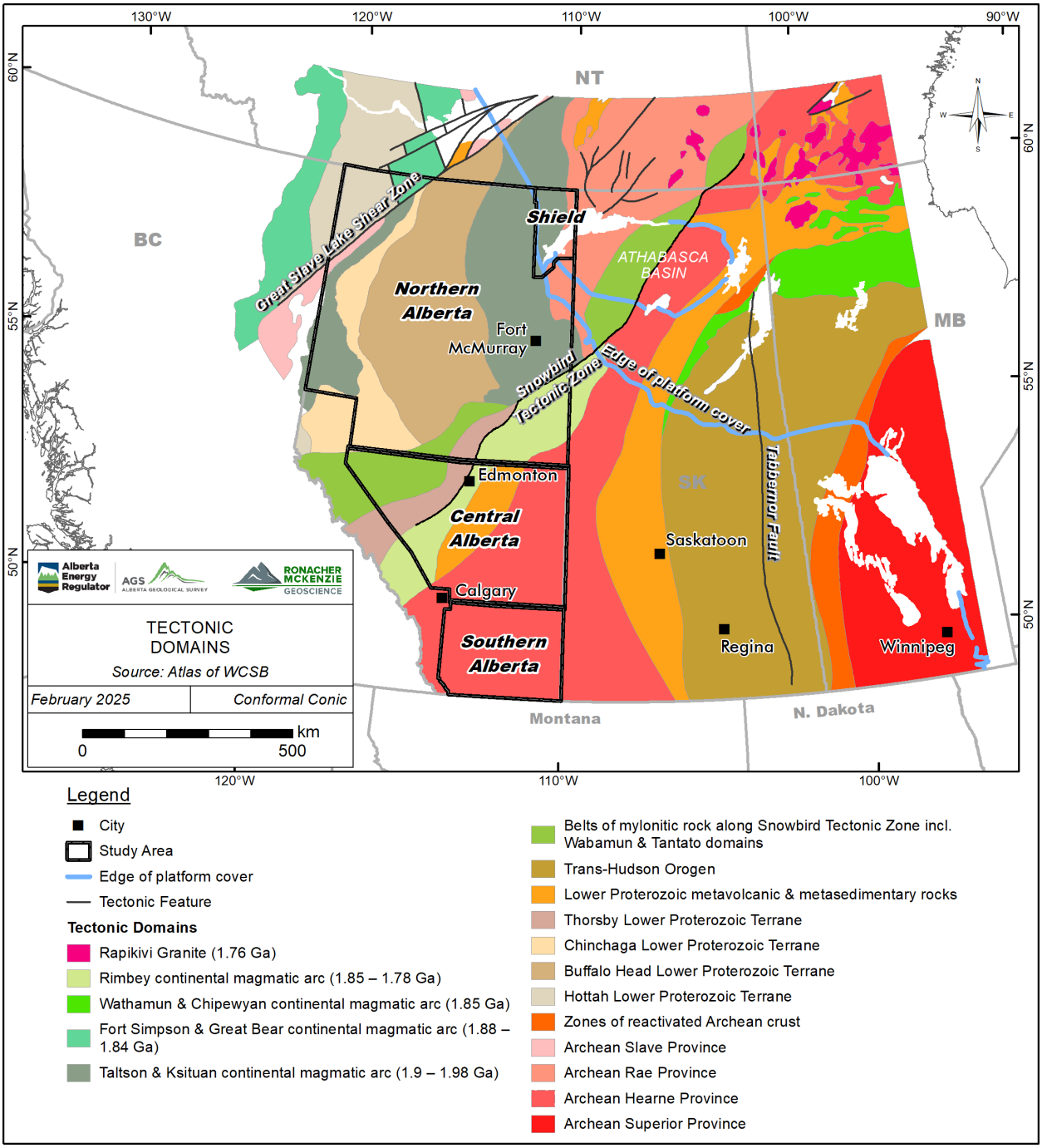

Figure 4-1. Tectonic basement domains in Western Canada (modified from Ross et al., 1994).

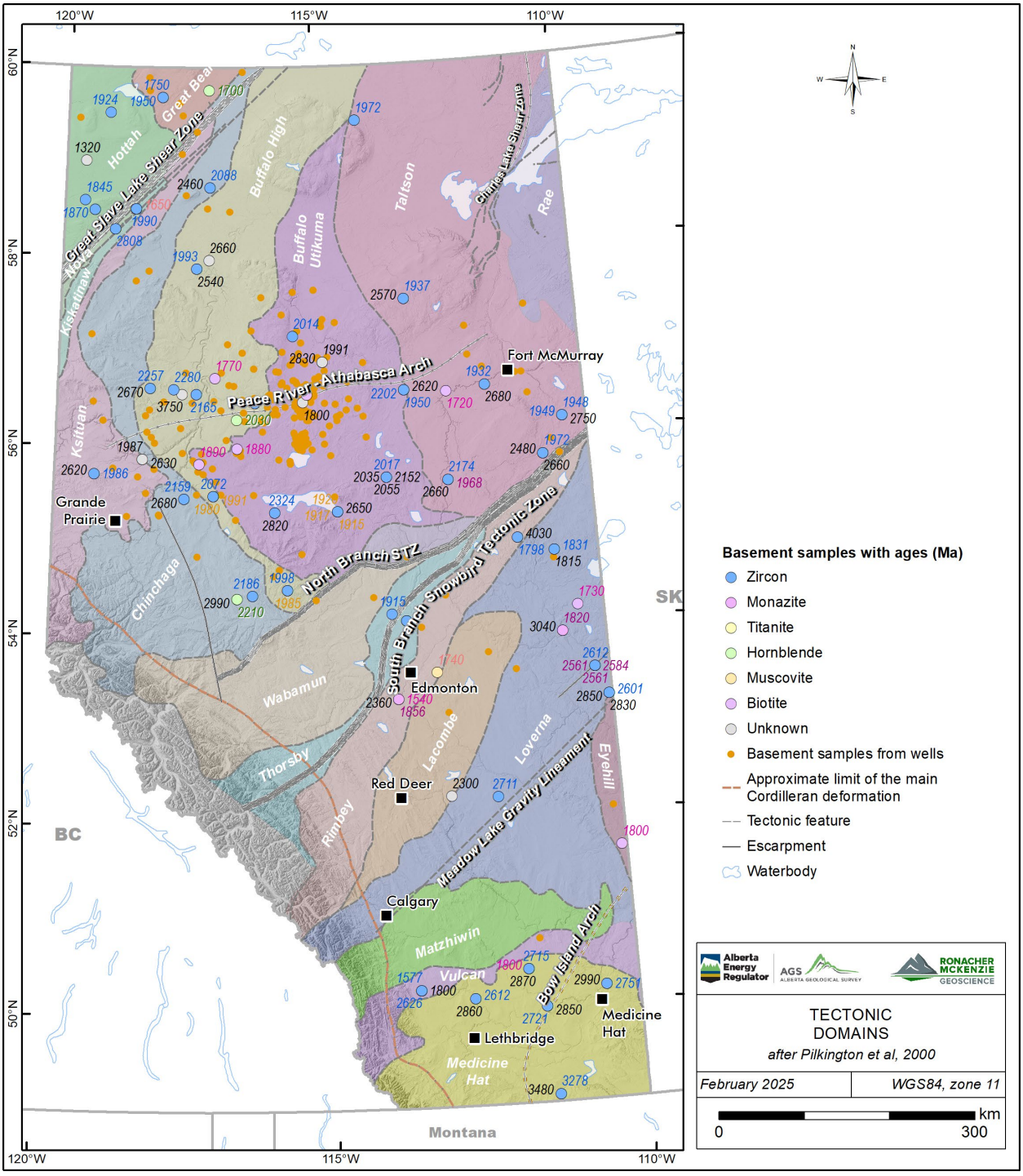

Figure 4-2. Tectonic domains of Alberta after Pilkington et al. (2000). Selected structural lineaments (grey) from Pană et al. (2021). Radiometric ages from Ross et al. (1991), Villeneuve et al. (1993), and Burwash et al. (unpublished data 1994).

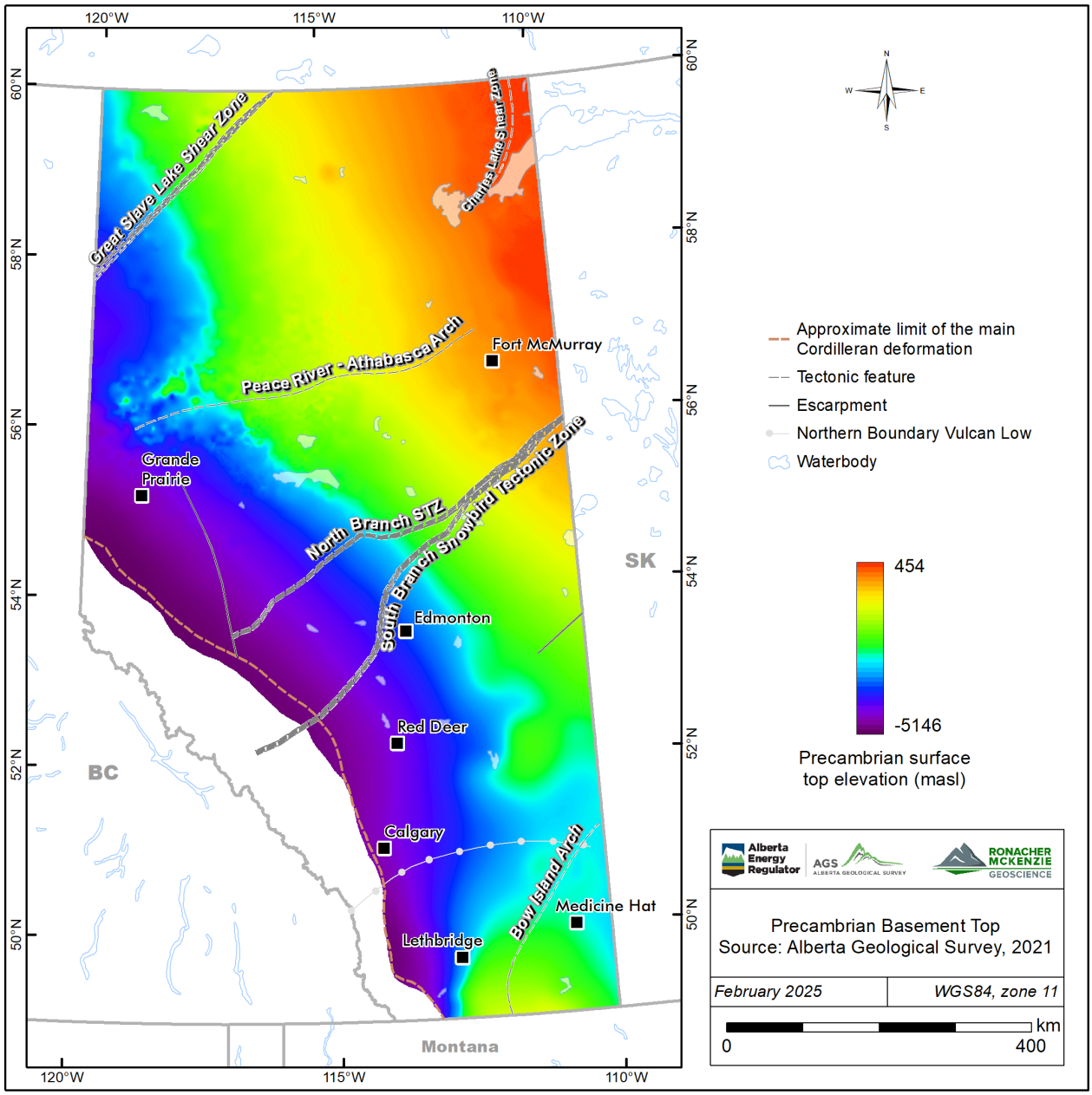

Figure 4-3. Modelled Precambrian basement top surface in Alberta. Data from the Alberta Geological Survey (2021a). Selected structural lineaments (grey) from Pană et al. (2021).

4.2 Athabasca Basin

The Athabasca Basin comprises Late Paleoproterozoic to Early Mesoproterozoic (ca. 1760 Ma and 1500 Ma) quartzose fluvial sequences of the Athabasca Group. These sequences, which are bound by unconformities, are deposited in distinct stacked NE-trending sub-basins with a total preserved aggregate thickness estimated at 1150 m (e.g., Ramaekers et al., 2007). About ten percent of the Athabasca Basin is present in northeastern

Alberta. Further descriptions of the Athabasca Group units in Alberta that may be relevant to the interpretation of geophysical surveys can be found in Lopez et al. (2024a).

4.3 Western Canada Sedimentary Basin

Across most of Alberta, the crystalline basement is covered by the Phanerozoic wedge-shaped Western Canada Sedimentary Basin ("WCSB"). The thickness of the sedimentary strata increases towards the Rocky Mountains, from its erosional edge at the Canadian Shield in the northeast to approximately 5.1 km in the west.

The WCSB stratigraphy reflects the deposition of strata during two different, subsequent tectonic settings (Mossop and Shetsen, 1994).

- Cambrian to Middle Jurassic passive continental margin, dominated by carbonates, mudstones and minor evaporites; and
- Middle Jurassic to Oligocene foreland basin dominated by clastic sequences.

Major structural features of the sedimentary basin are the Peace River Arch (O'Connell, 1994), Tathlina Arch, Bow Island Arch, McDonald Fault, and the Fox Creek and Meadow Lake escarpments. Brief descriptions of these structural elements and additional relevant features are provided in previous RMG reports for northern, central and southern Alberta (Lopez et al., 2024b; Brem et al., 2024; Lopez et al., 2025). A comprehensive review of the many structural elements identified in the Alberta Plains is provided in the AGS compilation by Pană et al. (2021) and related "Structural Elements in the Alberta Plains Interactive App and Map" (Alberta Geological Survey, 2021b).

Other localized structures in the WCSB include astroblemes, which are eroded remnants of meteorite impact craters. In Alberta, the most relevant due to its larger size is the Steen River astrobleme (Mazur, 1999; Molak et al., 2001; Walton et al., 2017; McGregor et al., 2020). A complete list of confirmed and inferred astroblemes in Alberta can be found in the AGS interactive application (Alberta Geological Survey 2021b).

4.4 Kimberlite Fields and Minettes

Three Cretaceous age kimberlite fields occur in northern Alberta. These kimberlite fields are the Mountain Lake, Buffalo Head Hills, and Birch Mountains fields (Eccles, 2011). These fields are aligned on an ENE-trend that has not been adequately explained. Brief descriptions of Alberta's kimberlite fields are provided in the previous RMG report for northern Alberta (Lopez et al., 2024b). Abundant literature exists about Alberta's kimberlite fields and comprehensive reviews and summaries are provided by Dufresne et al. (1996), Eccles (2011) and Banas et al. (2016).

In southern Alberta, near the US border, potassic dykes, small plugs and an intrusive complex of Eocene age are exposed. Most of these potassic igneous rocks that intrude the Cretaceous sequences of the WCSB are classified as alkaline and peralkaline minettes. Temporally and spatially, they relate to the more extensive Sweet Grass Hills intrusive complex ca. 20 km to the south in Montana. Brief descriptions of these minettes

are provided in the RMG report for southern Alberta (Brem et al., 2024). AGS publications about Alberta's minettes include a comprehensive report by Rukhlov and Pawlowicz (2012).

4.5 Surficial Geology

Alberta is blanketed by Neogene fluvial deposits, glaciogenic materials and postglacial sediments of variable thickness and distribution overlying the bedrock surface. Modelled surficial sediment thickness values range from less than 1 m to as much as 360 m (Atkinson et al., 2020). Maximum thicknesses occur along a northwesterly trend from Peace River to Cold Lake in north-central Alberta, and in the northwest corner of the province.

5.0 AEROMAGNETIC SURVEY DATA

5.1 Data Review

The Alberta Energy Regulator ("AER") contracted EON Geosciences, Sander Geophysics Limited, and Xcalibur Multiphysics to fly aeromagnetic surveys covering different portions of the province (Figure 5-1). The Shield dataset was collected by EON Geosciences in 2021. The northern Alberta dataset was collected by EON Geosciences, Sander Geophysics Limited, and Xcalibur Multiphysics between February 2021 and May 2022. The southern Alberta and central Alberta datasets were collected by EON Geosciences between October 2022 and March 2023, and September 2023 and March 2024, respectively (Alberta Geological Survey, 2024).

Additional aeromagnetic data from legacy surveys were included to complete coverage of the project areas. Integrated datasets are available to the public through AGS's website (Alberta Geological Survey, 2024). The legacy data sets include the following surveys:

- Marguerite River (northern Alberta and Saskatchewan, data acquired 2017) – only portions in Alberta were used
- Hotchkiss (northern Alberta, data acquired 1996)
- Dunvegan (northern Alberta, data acquired 1995-1996)
- Leduc (A,B,C) (central Alberta, data acquired 1997)

EON Geosciences merged the data from the four survey areas (Shield, North, Central, South) to produce a single contiguous magnetic dataset. The merged data for Alberta was provided to RMG by the AGS. RMG (Section 5.2) and Fathom Geophysics (Section 5.3) created derivative and filter products from the merged data grids to enhance and highlight different features in the measured data to aid in geological interpretation.

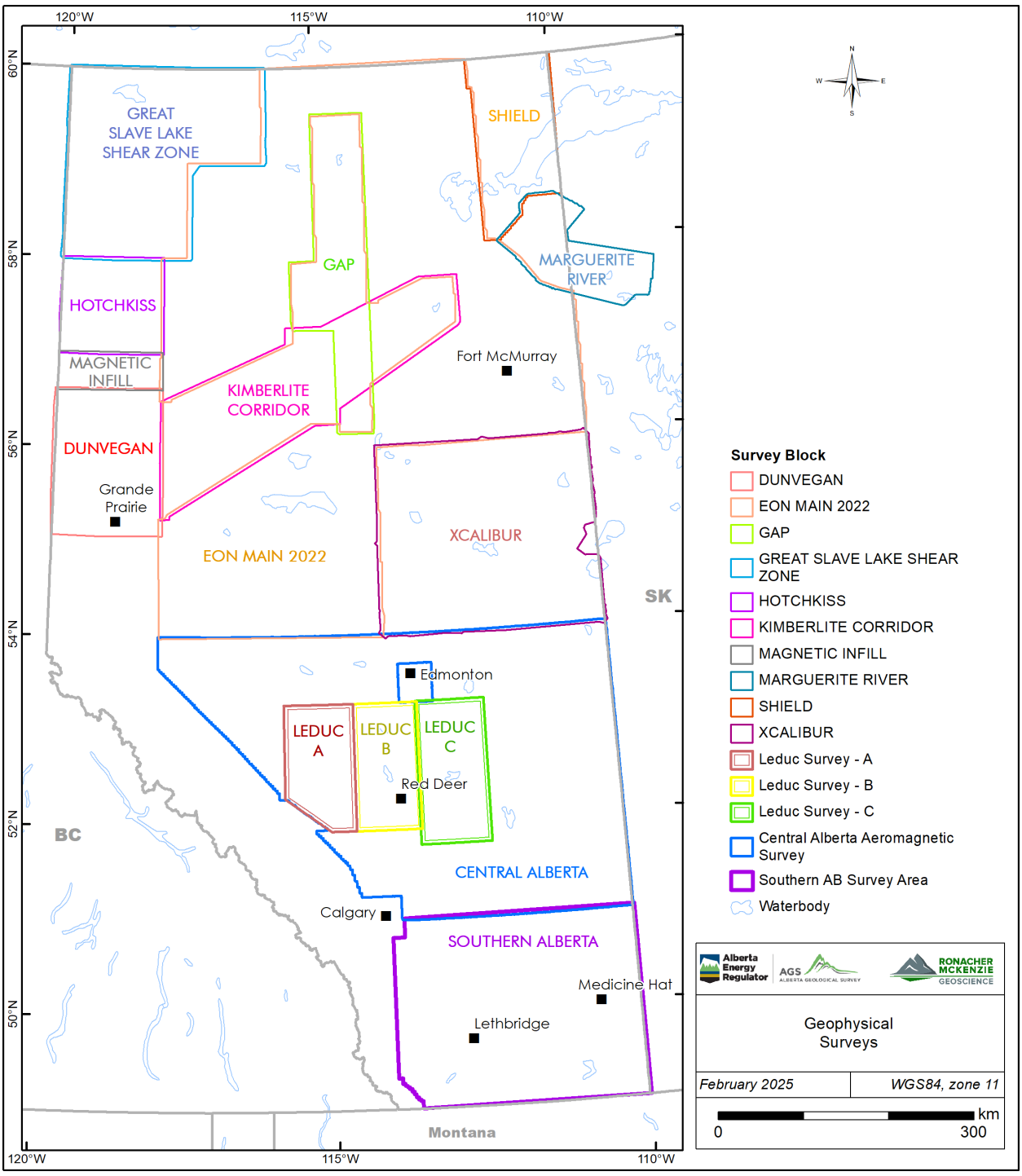

Figure 5-1. Alberta airborne survey blocks, including legacy data.

5.2 Derivative and Filter Products

Grid-based filter products were calculated from the total magnetic intensity ("TMI") and International Geomagnetic Reference Field ("IGRF")-removed residual magnetic intensity ("RMI") grids (Table 5-1). The various filter products were used to enhance and highlight different features in the measured data to aid in geological interpretation. RGB ternary images were also created from selected filter products to produce pseudo-structure and pseudo-geology maps.

Given the large spatial extents of the merged data set, and corresponding variations in the orientation of the magnetic field, pole reduction of the TMI and RMI data was completed by Fathom Geophysics using a differential pole reduction algorithm that uses the actual IGRF inclination and declination values at each data point, as opposed to standard pole reduction algorithms that use averaged values for inclination and declination.

Table 5-1. Magnetic Filter Products.

Product	Abbreviation	Description
Total Magnetic Intensity	TMI	Measured data.
Residual Magnetic Intensity	RMI	Measured data, IGRF removed.
TMI/RMI, Pole Reduced	RTP	Transform to vertical magnetic field, simplifies anomaly shapes.
X Horizontal Derivative	DX	Highlights near surface features in N-S direction.
Y Horizontal Derivative	DY	Highlights near surface features in E-W direction.
1st Vertical Derivative	VD1	Highlights near surface features.
2nd Vertical Derivative	VD2	Enhances subtle near surface features.
Analytic Signal (Total Gradient)	AS	Highlights discrete magnetic bodies and zones of high gradients.
Total Horizontal Derivative	THD	Highlights horizontal changes in the total field.
1st Vertical Derivative of Total Horizontal Derivative	THD_VD1	Enhances THD.
Tilt Angle (Derivative)	TD	Tilt angle between vertical and horizontal derivatives, highlights magnetic contacts, amplitude independent.
Total Horizontal Derivative of Tilt Angle	TD_THD	Used with TD to estimate depth of discrete magnetic sources.
Area	AREA	Highlights discrete areas.
Edge	EDGE	Highlights edges of discrete areas.
Geology	GEOLOGY	Pseudo-geology map. Ternary image (RMI/RTP, VD1, VD2) only, no grid data.
Structure	STRUCTURE	Pseudo-structure map. Ternary image (DX, DY, VD1) only, no grid data.
Differential Upward Continuation	DIF_XXX_YYY	Highlights features at selected approximate depths.

Selected filter products are presented in Figure 5-2 through Figure 5-10. All filter products are included in Digital Appendix B.

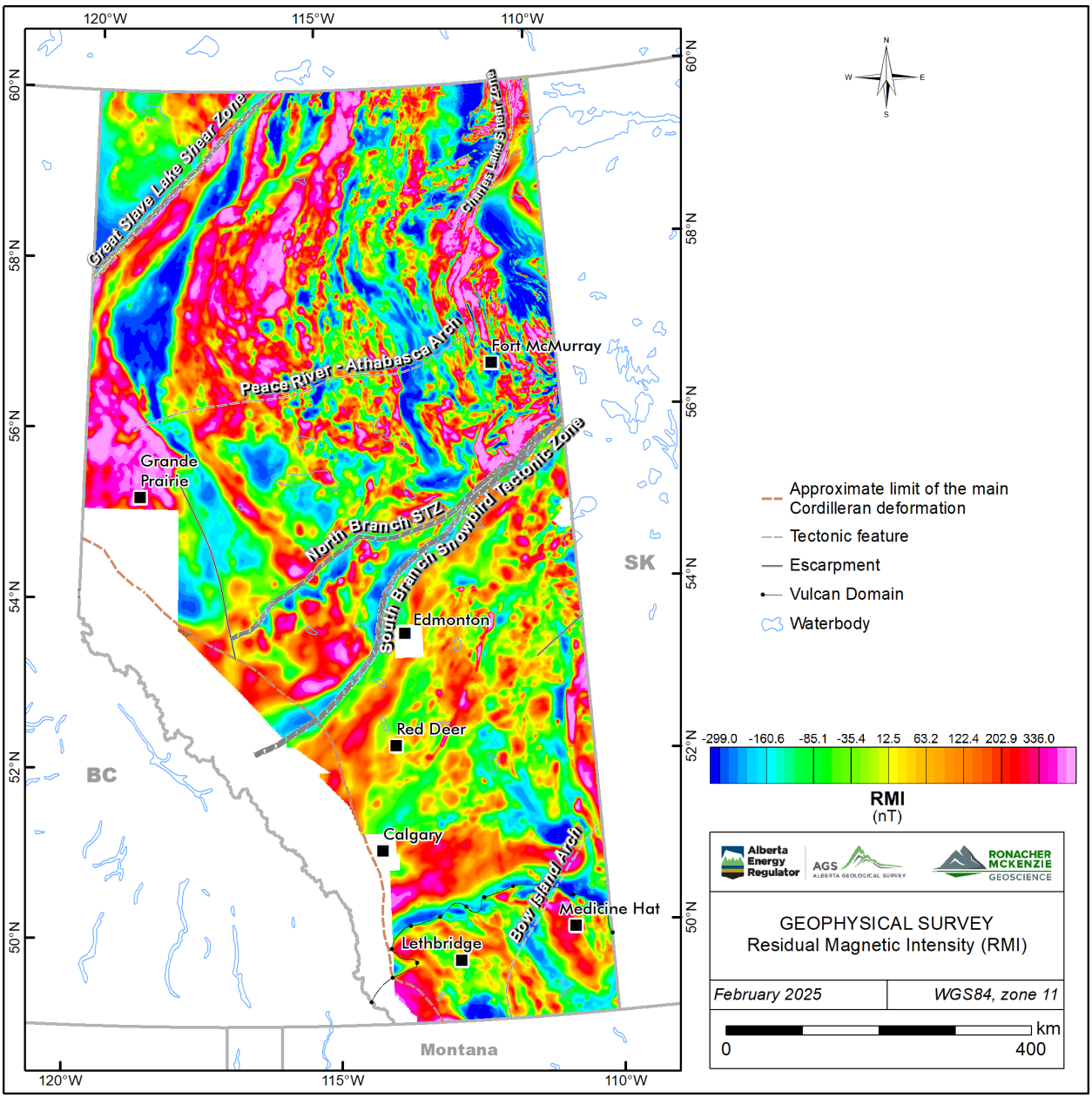

Figure 5-2. Residual Magnetic Intensity ("RMI"). Selected structural lineaments from Pană et al. (2021).

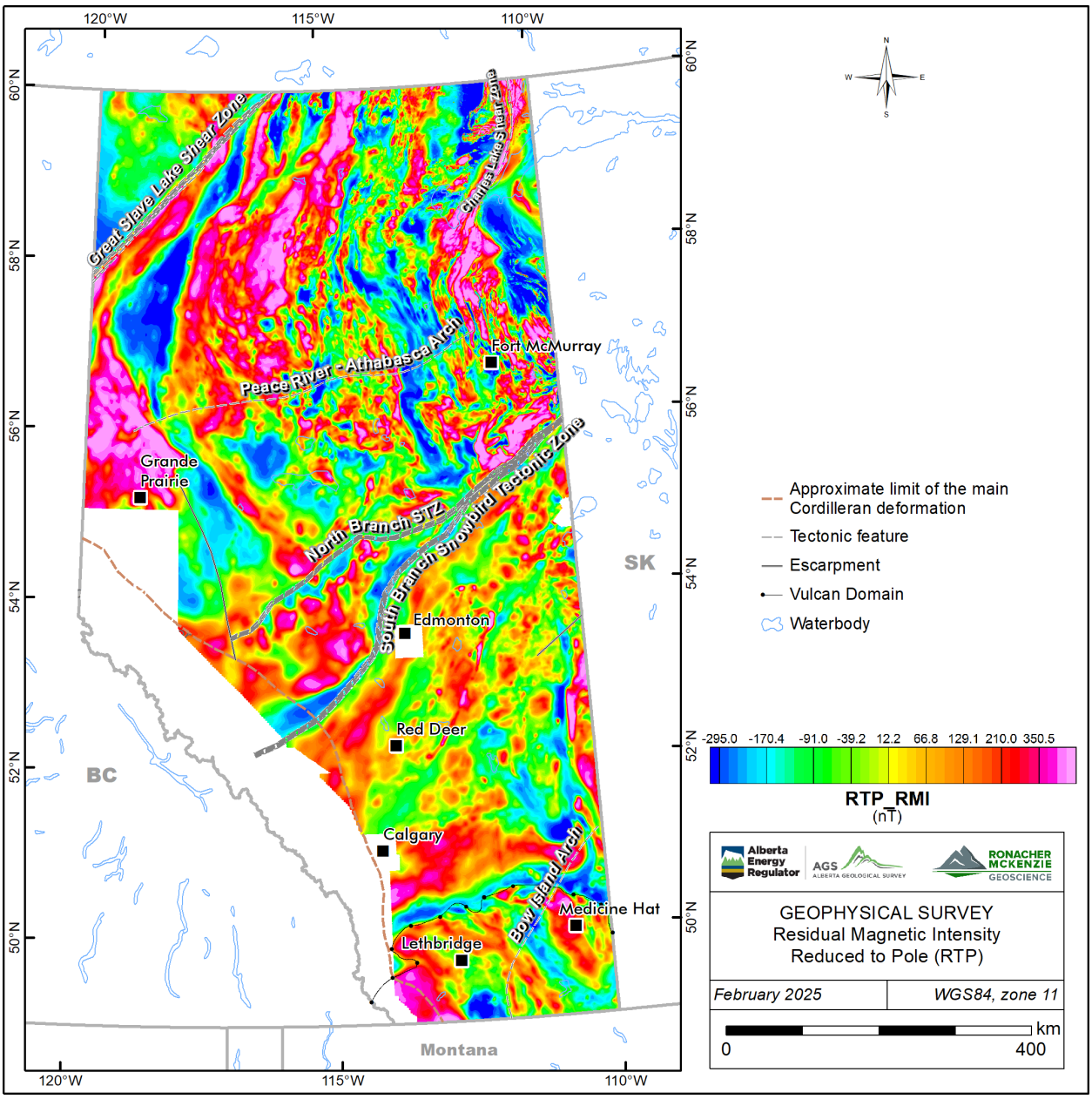

Figure 5-3. RMI, reduced to pole. Selected structural lineaments from Pană et al. (2021).

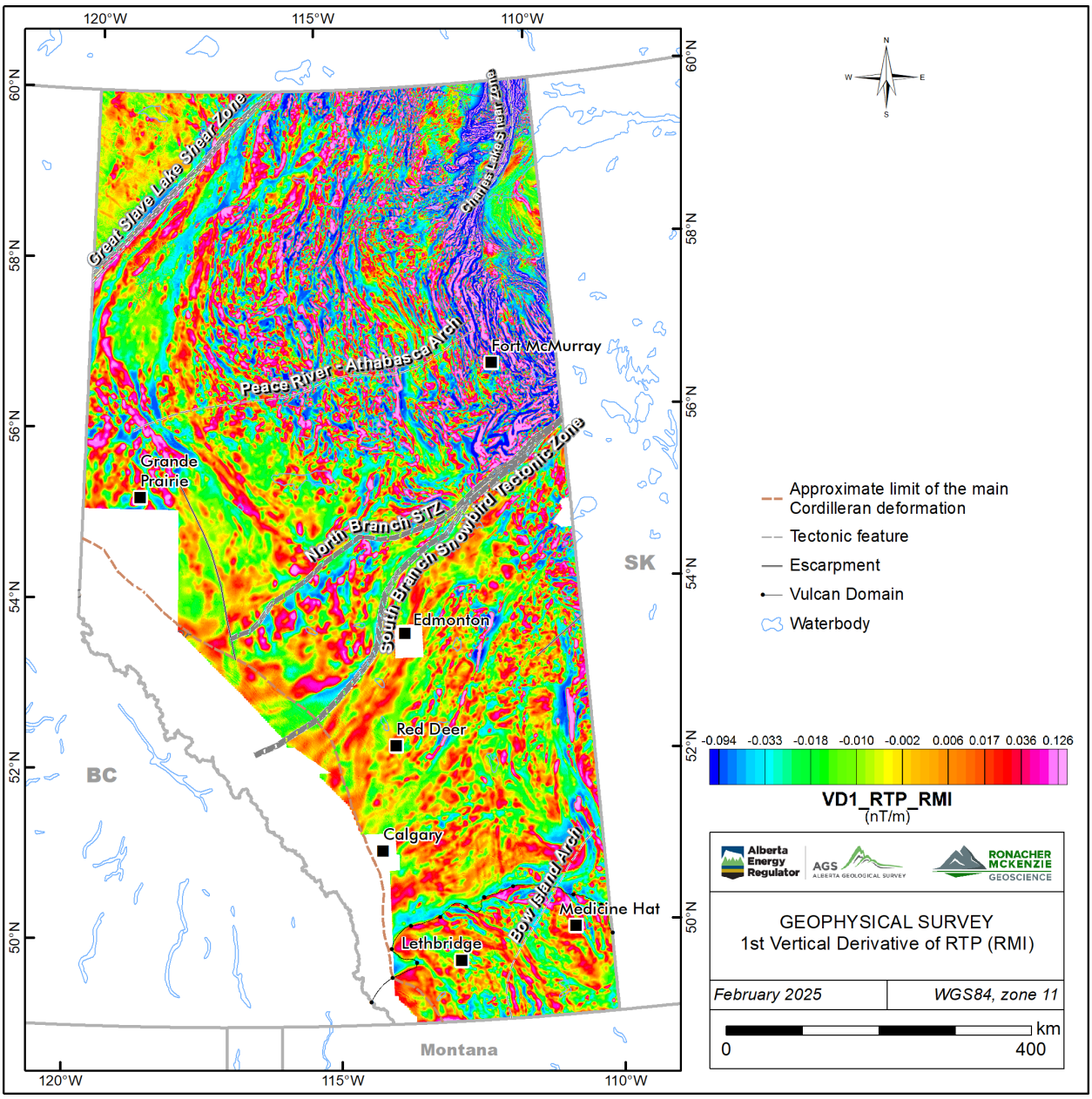

Figure 5-4. RMI, reduced to pole, 1st vertical derivative. Selected structural lineaments from Pană et al. (2021).

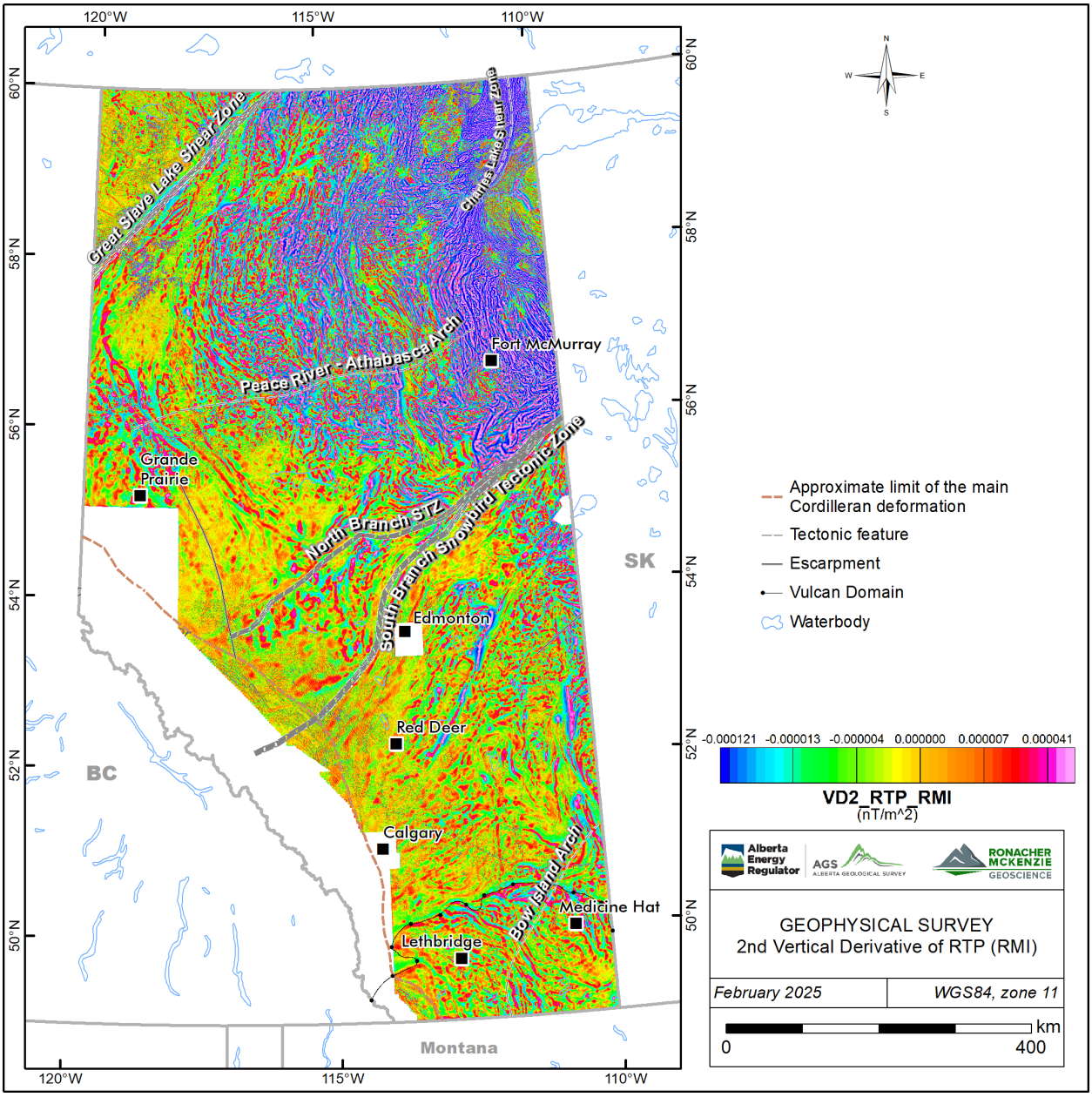

Figure 5-5. RMI, reduced to pole, 2nd vertical derivative. Selected structural lineaments from Pană et al. (2021).

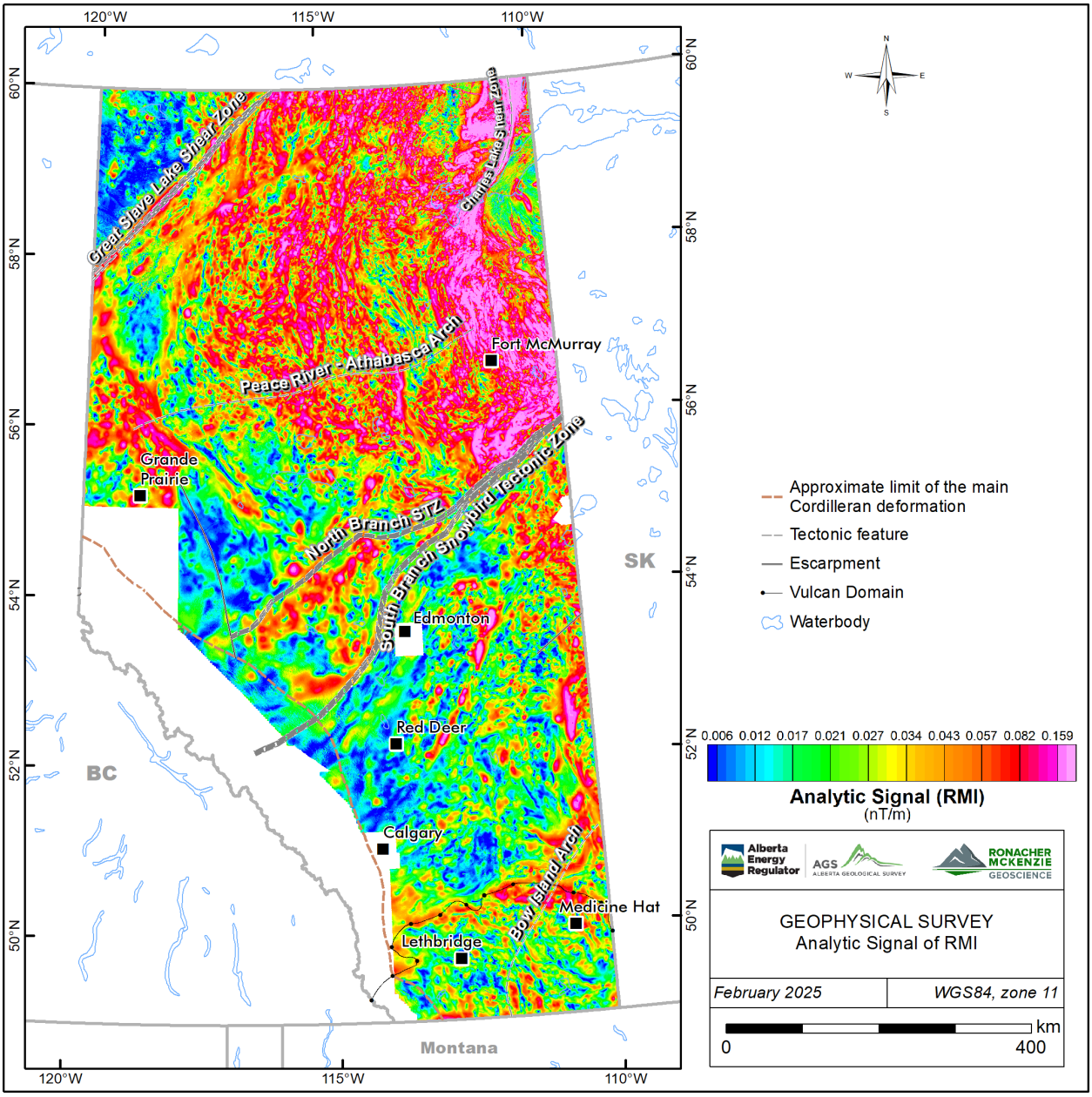

Figure 5-6. RMI, Analytic Signal. Selected structural lineaments from Pană et al. (2021).

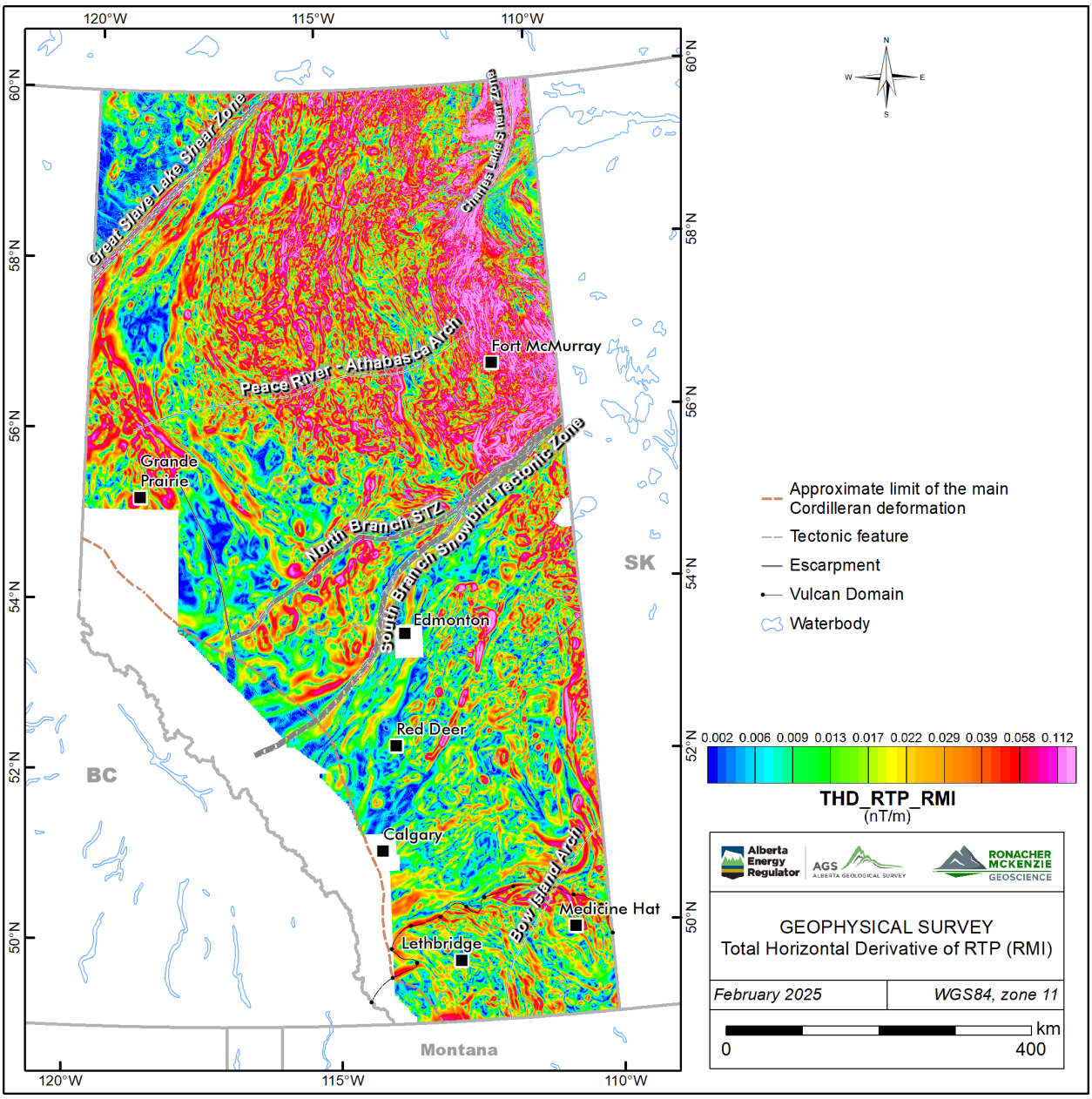

Figure 5-7. RMI, reduced to pole, total horizontal derivative. Selected structural lineaments from Pană et al. (2021).

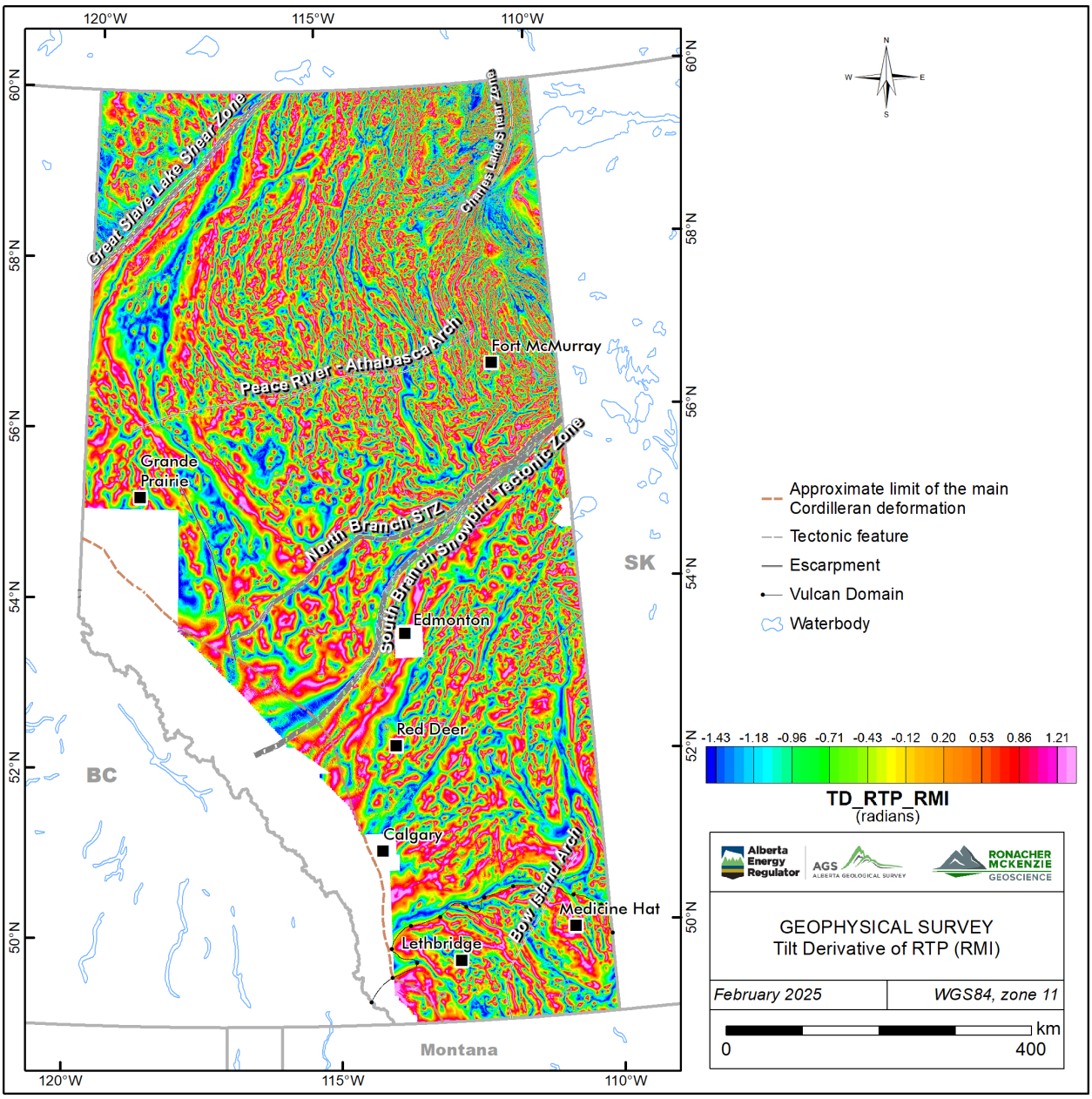

Figure 5-8. RMI, reduced to pole, tilt angle. Selected structural lineaments from Pană et al. (2021).

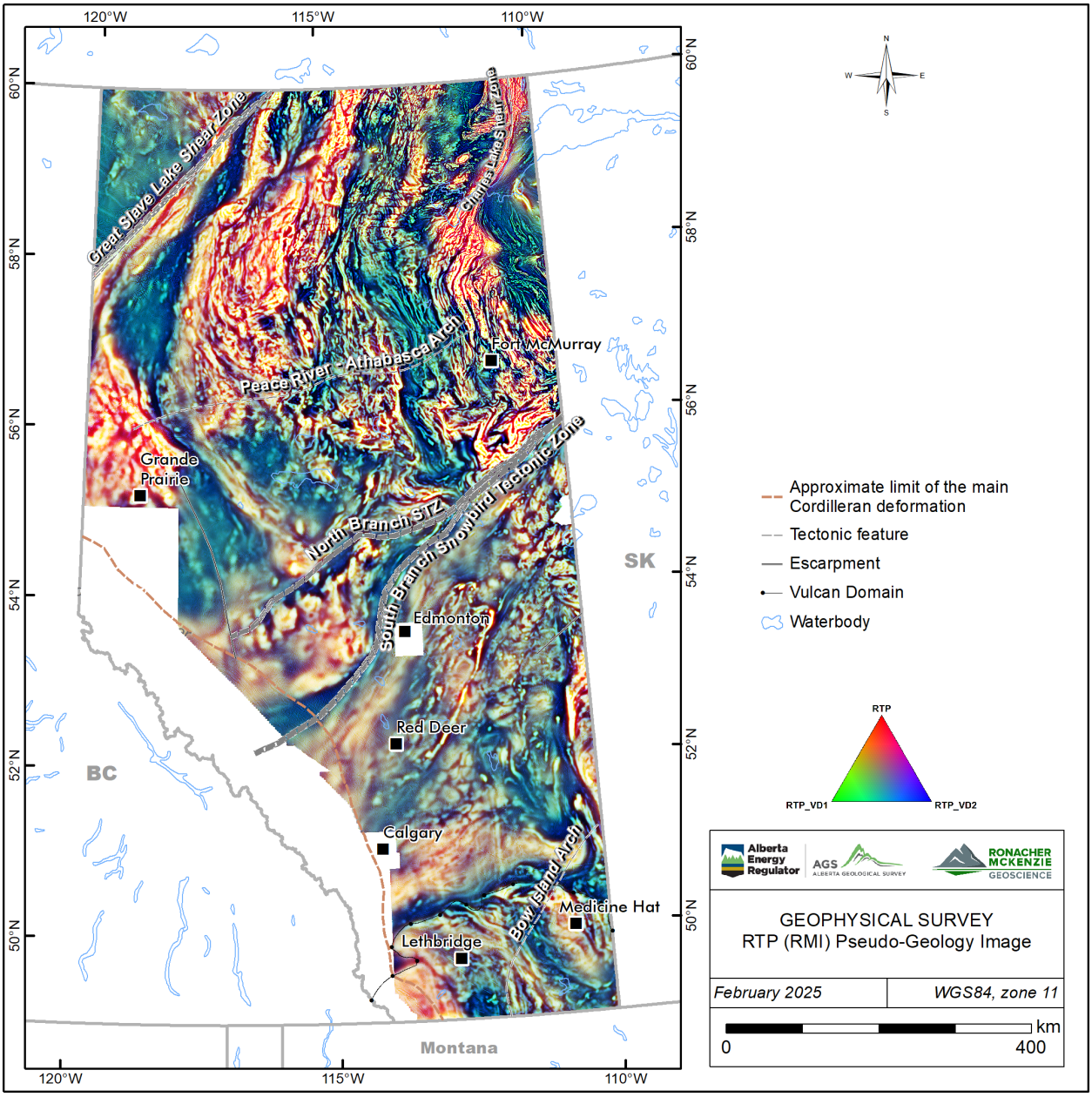

Figure 5-9. RMI, reduced to pole, pseudo-geology ternary image. Selected structural lineaments from Pană et al. (2021).

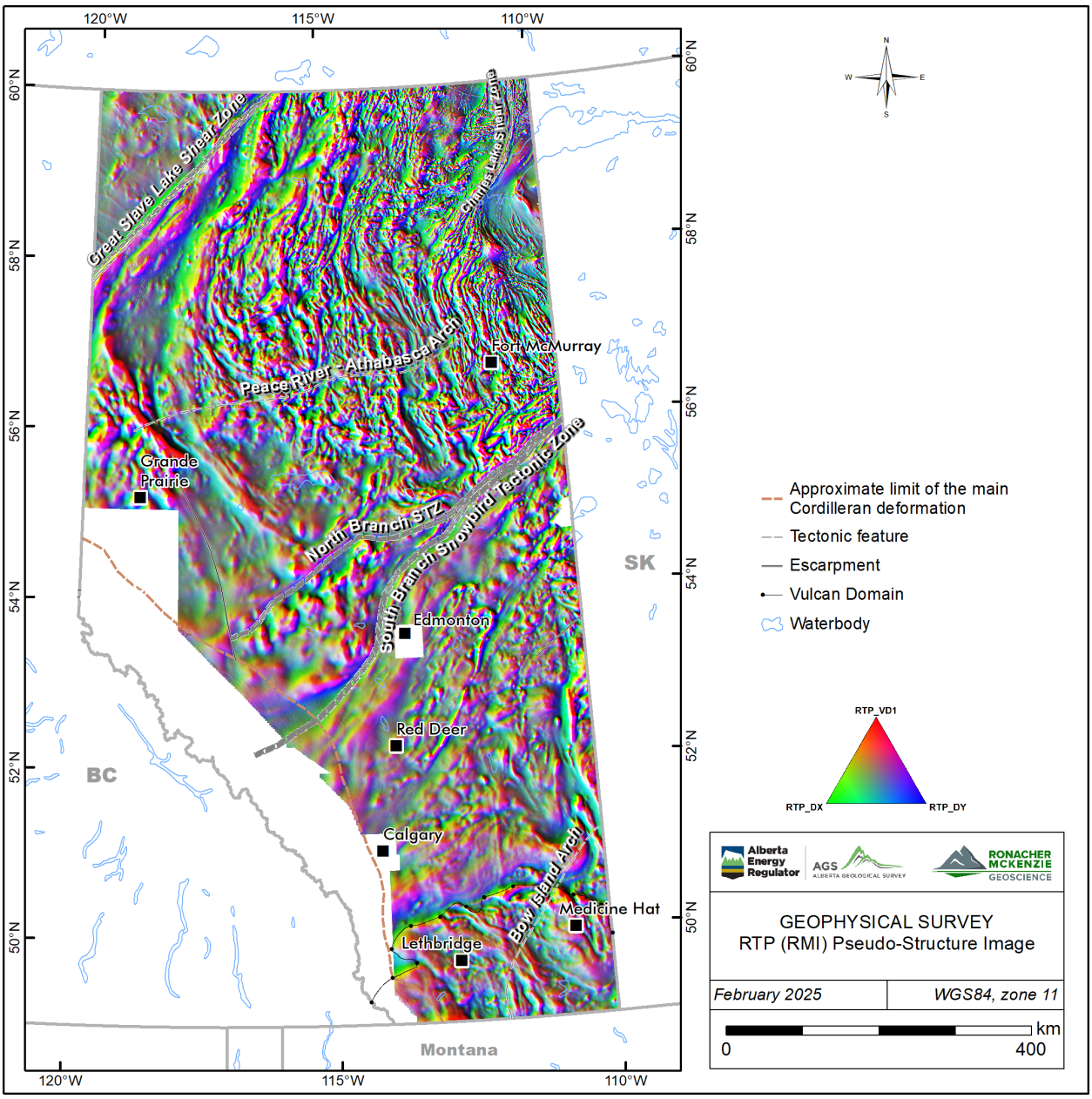

Figure 5-10. RMI, reduced to pole, pseudo-structure ternary image. Selected structural lineaments from Pană et al. (2021).

Differential upward continuation grids were created to extract information from selected approximate depths. Differential grids show information from an approximate depth range equal to half of the upward continuation distances (e.g., the 3000-5000 m differential grid will show information from approximately 1500 to 2500 m depth). Selected differential maps are presented in Figure 5-11 and Figure 5-12.

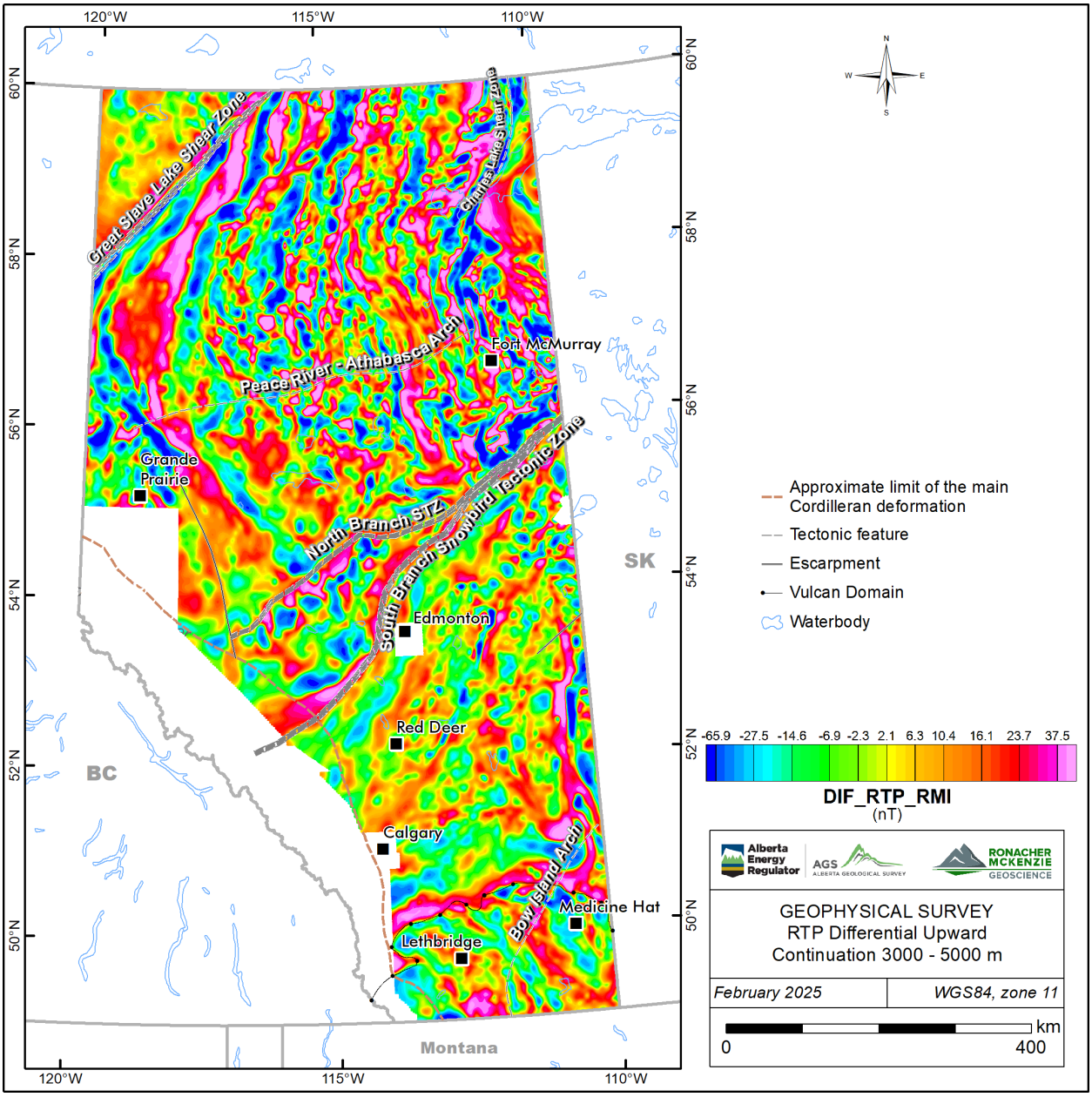

Figure 5-11. Differential upward continuation, 3000-5000 m (1500-2500 m approximate depth). Selected structural lineaments (grey) from Pană et al. (2021).

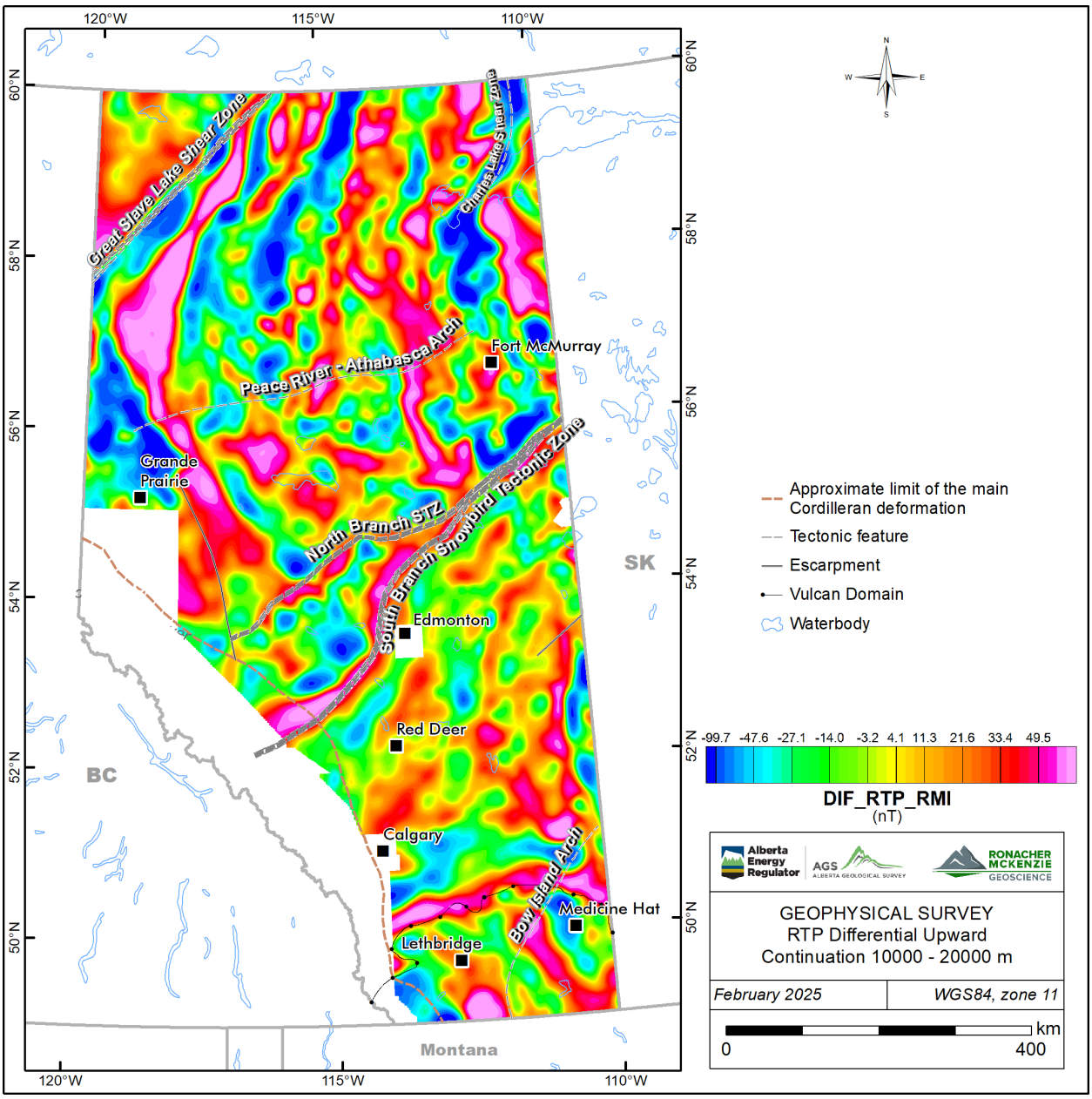

Figure 5-12. Differential upward continuation, 10000-20000 m (5000-10000 m approximate depth). Selected structural lineaments from Pană et al. (2021).

The gridded magnetic data are also displayed using alternate colour distributions to aid in data interpretation (Table 5-2). Different colour distributions are used to help identify structures in the interpretation process. For example, greyscale maps are useful for highlighting high and low areas while minimizing the effects of local amplitudes, and isoluminant palettes (e.g., CET i1 described in Kovesi 2015) mitigate artificial highlighting caused by perceived brighter colours in commonly used rainbow palettes, particularly in the yellow and green ranges.

Table 5-2. Colour palettes applied to geophysical datasets.

Colour Distribution	Abbreviation	Description
Rainbow	(none)	Standard blue through purple colour palette.
Greyscale	BW	Black to white colour range, often easier to see structures.
Centre for Exploration Targeting (I1)	CET	Isoluminant colour range developed by University of Western Australia. No 'bright spots' in the spectrum to artificially attract the eye.

Selected examples of alternate colour distributions are shown in Figure 5-13 through Figure 5-15.

A complete set of georeferenced gridded data including alternate colour distributions is included in the Digital Appendix B.

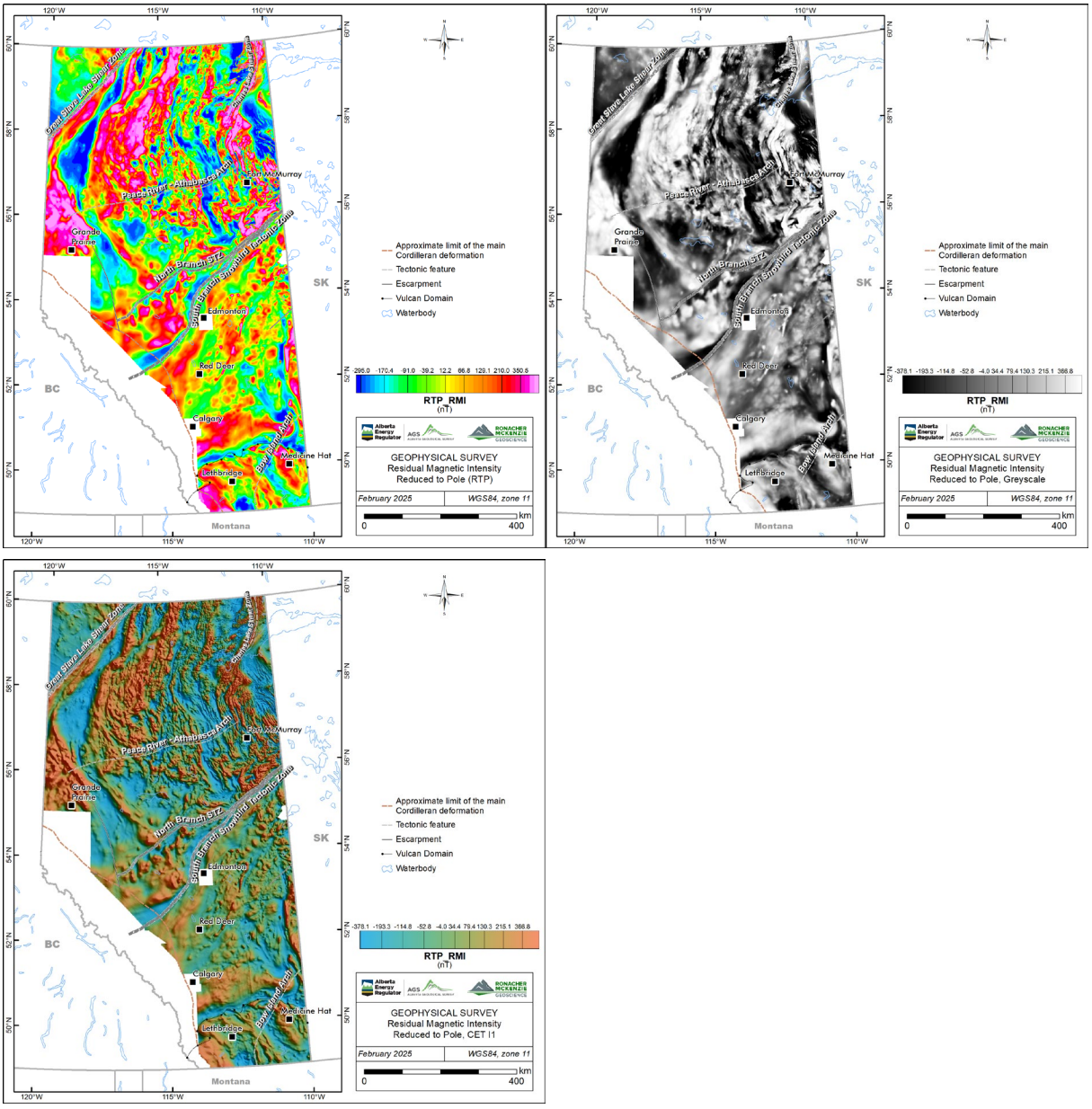

Figure 5-13. RMI, reduced to pole, standard rainbow (upper left), greyscale (upper right), and CET i1 isoluminant (lower left) colour distributions. Selected structural lineaments from Pană et al. (2021).

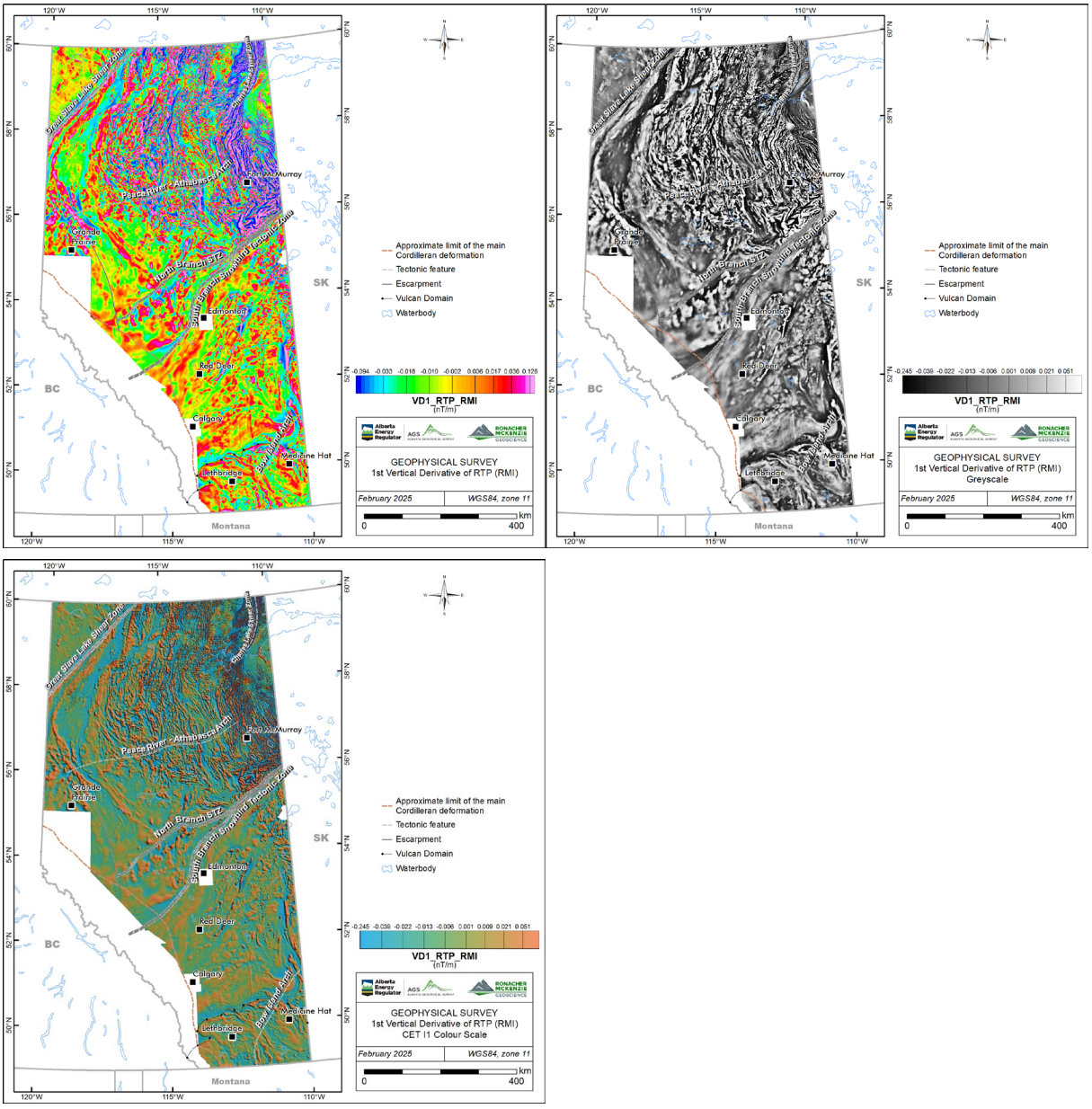

Figure 5-14. 1st vertical derivative (RTP), standard rainbow (upper left), greyscale (upper right), and CET i1 isoluminant (lower left) colour distributions. Selected structural lineaments from Pană et al. (2021).

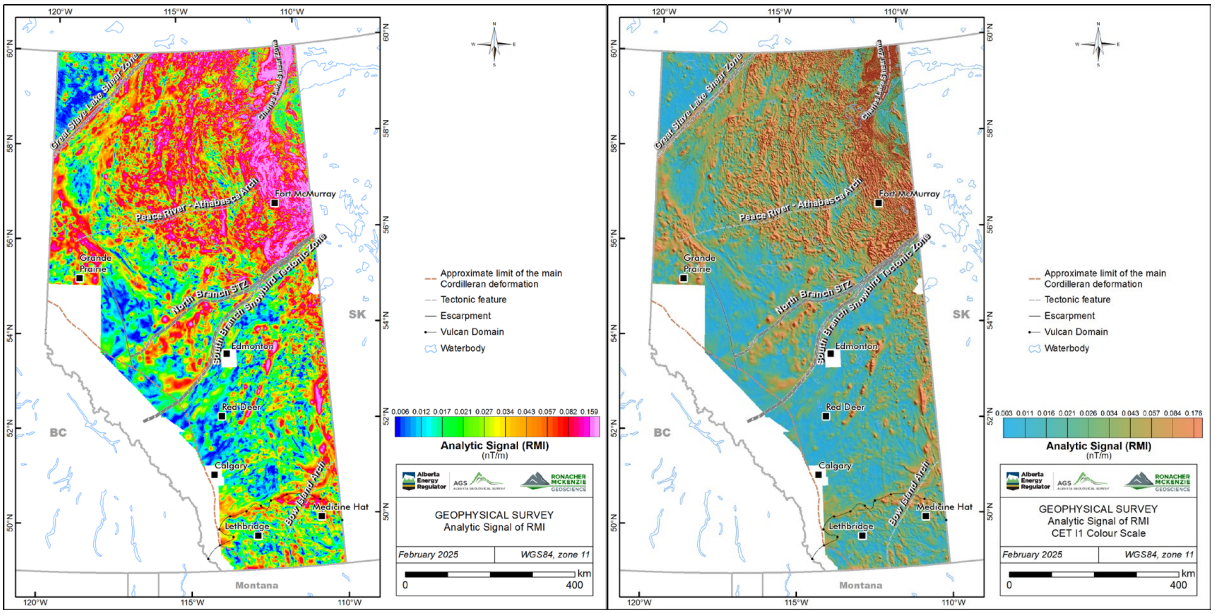

Figure 5-15. RMI, Analytic Signal, standard rainbow (left) and CET i1 isoluminant (right) colour distributions. Selected structural lineaments from Pană et al. (2021).

5.3 Automatic Structure Detection

RMG collaborated with Fathom Geophysics to perform automatic structure detection and to generate additional magnetic products to assist with the geological interpretation of the magnetic basement. Automatic detection was applied to the merged gridded magnetic data for all of Alberta, with the exception of depth to basement, which was applied separately to the individual northern, central and southern Alberta grids.

The processing included application of standard filters as well as Fathom Geophysics' structure detection, radial symmetry, fabric orientation, and depth to basement filters. Fathom Geophysics' report is available in Appendix 1. Final digital vector and image products are available in the Digital Appendix C.

The additional filter and image processing products created by Fathom Geophysics are listed in Table 5-3. An example of an image processing product, a ternary image of 1VD (1st vertical derivative), tilt angle (tilt derivative), and horizontal gradient magnitude ("HGM"), is shown in Figure 5-16.

Automatic structure detection is a linear feature detection algorithm used to highlight ridges, valleys, or edges in gridded data. Automated structure detection is a multi-scale phase congruency algorithm in which features are highlighted either in areas of low or high magnetic contrast, irrespective of amplitude. The method also allows inference of the estimated depth of structures between 0.5 and 1 times the filter wavelength, assuming shorter wavelengths are related to shallow structures and longer wavelengths are related to deeper structures (which may not always be the case). Structure detection products are listed in Table 5-4.

Radial symmetry is a filtering process that identifies equant discrete features in the data. The algorithm seeks locations around which data values either decrease or increase in all directions. These features may be related to stocks, batholiths, cupolas, alteration haloes, kimberlites, diatremes, steeply plunging mineralized zones, and breccia pipes. Radial symmetry products were calculated using wavelengths from 250-16,000 m, starting from a number of different residuals. Radial symmetry products are listed in Table 5-5.

Table 5-3. Additional filter and image products.

Product	Abbreviation	Description
Filter Products		
Automatic Gain Control (standard deviation = 30)	AGC30	Evens anomaly amplitudes to make subtle features more visible, longer wavelengths are suppressed.
Pseudogravity	PGrav	Useful for highlighting large scale features.
Pseudogravity residual	PGravRes	Difference between 0-2000 m upward continued pseudogravity. Longest wavelength features suppressed to highlight intermediate scale features.
Horizontal gradient of PGravRes	PGravResHGM	Highlights edges of intermediate scale features.
Small-scale residual	Res500_2000	Differential upward continuation residual, 500-2000 m. Highlights sources at 250-1000 m depth.
Medium-scale residual	Res2000_5000	Differential upward continuation residual, 2000-5000 m. Highlights sources at 1000-2500 m depth.
Large-scale residual	Res5000_10000	Differential upward continuation residual, 5000-10000 m. Highlights sources at 2500-5000 m depth.
Vertical derivative minus horizontal derivative	VDMHGM	Accentuates contrast in 1st vertical derivative, aids in highlighting shallow features.
Vertical integral	VINT	Vertical integral of total field.
Analytic signal of vertical integral.	VIAS	Produces a result with similar amplitudes and wavelengths to total field, with reduced effects of magnetization direction and remanence.
Image Products		
Ternary of directional derivatives	X_Y_Z	Ternary images (CMY+RGB) of 1st X, Y, and vertical derivatives.
Ternary of 1VD, Tilt, HGM	1VD_Tilt_HGM	Ternary images (CMY+RGB) of 1VD, tilt angle, horizontal gradient.
Ternary of residuals	SmRes_MedRes_LgRes	Ternary images (CMY+RGB) of small, medium, large-scale residuals.
Ternary of RTP, VIAS, Asig	RTP_vias_asig	Ternary images (CMY+RGB) of RTP, analytic signal of vertical integral, and analytic signal. Helps identify remanent zones.

Product	Abbreviation	Description
Ternary of pseudogravity	Prav_PGravRes_PGravRes HGM	Ternary images (CMY+RGB) of Pseudogravity, pseudogravity residual, and horizontal gradient of pseudogravity residual.

Table 5-4. Structure detection products.

Product	Abbreviation	Description
Fabric Orientation (RTP and AGC)	Fabric_Orientation	Reflects the orientation of long-wavelength features.
Total Structure (RTP and AGC)	StructX_Total	Total structure detected. X = filter wavelength (100 to 3200 m).
Oriented Structural Domains	StructX_OriDom_Th	Total structure (X = filter wavelength), thresholded into orientation domains.
Vectorized Structure	StructX_Total_Vec	Vectorized total structure (X = filter wavelength).
Belt-parallel structure	StructX_Para	Structure parallel to major belts (X = filter length).
Vectorized belt-parallel structure	StructX_Para_Vec	Vectorized structure parallel to major belts (X = filter length).
Belt-crossing structure	StructX_Cross	Structure crossing major belts (X = filter length).
Vectorized belt-crossing structure	StructX_Cross_Vec	Vectorized structure crossing major belts (X = filter length).

Table 5-5. Radial Symmetry products

Product	Code	Description
Radial Symmetry Lows	Res_X_Y_RSymZ_mi_Lows	Magnitude-independent radial symmetry at wavelength Z from X to Y residual, lows. Also vectorized.
Radial Symmetry Highs	Res_X_Y_RSymZ_mi_Highs	Magnitude-independent radial symmetry at wavelength Z from X to Y residual, highs. Also vectorized.
Radial Symmetry Highs and Lows	Res_X_Y_RSymZ_mi_Highs_and_Lows	Magnitude-independent radial symmetry at wavelength Z from X to Y residual, highs and lows. Also vectorized.

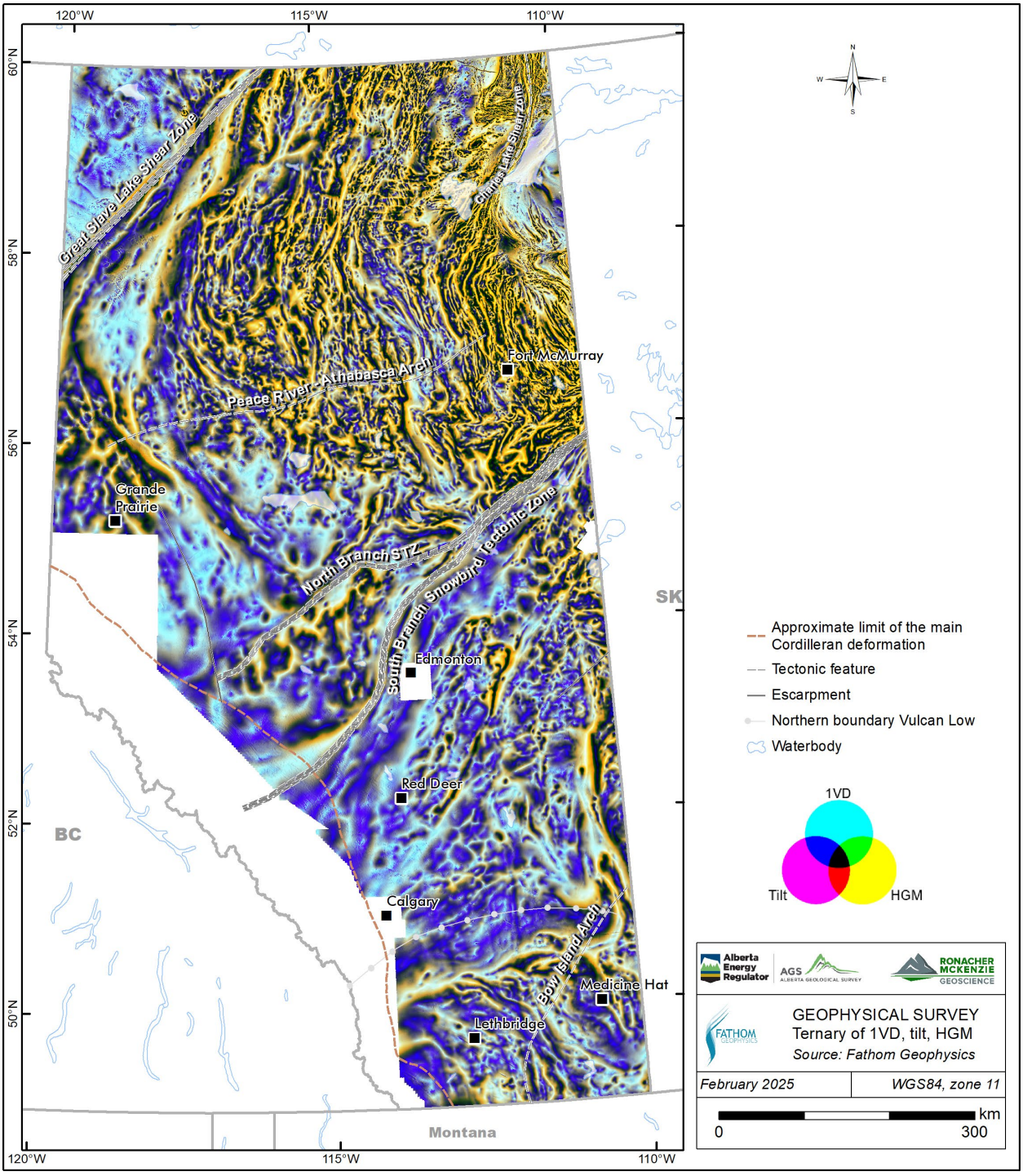

Figure 5-16. CMY ternary image displaying the 1VD, tilt angle, and HGM results from the RTP. Selected structural lineaments from Pană et al. (2021).

6.0 INTERPRETATION METHODOLOGY

6.1 Overview

The airborne magnetic derivative and filter products of the merged grid (Section 5.0) allowed RMG to merge the GIS files of previous geological interpretations conducted by RMG in 2024 and 2025 (Lopez et al., 2024a, 2024b; Brem et al., 2024; Lopez et al., 2025) into continuous observations and interpretation files for the entire province; RMG interpreted the merged files, which resulted in modifications of previous interpretations and new observations. Integration of anomalies with existing geological data allows for new insights in the subsurface in the region, which can steer structural interpretations, tectonic models, and subsurface exploration activities.

6.2 Workflow

The analysis follows the methodology developed by Isles and Rankin (2013), where the interpretation of the magnetic data is completed in three stages: observations, integration, and interpretation. This method is also employed in the reports on the individual areas (Lopez et al., 2024a, 2024b; Brem et al., 2024; Lopez et al., 2025).

The observation stage is focused on observing features directly from the magnetic filter products (Digital Appendix B) and automatic detection results (Digital Appendix C). The interpreter records magnetic ridges and linear trends as form line features, and magnetic domains from the anomalies that cause them as polygons. Form lines may represent either stratigraphic or structural trends, and line breaks or juxtapositions may represent structural elements (e.g., faults, shear zones, unconformities or intrusive contacts). This stage also includes the definition of domains that outline magnetic characteristics of different regions based on combined form lines and magnetic rock unit observations.

The first step for the merging and integration of the interpretation GIS files for the Shield, northern, central and southern Alberta survey areas was to use GIS software to merge all observation stages recorded in GIS vector files into new GIS files covering the entire province. This initial merging was followed by correcting form lines across survey boundaries and mapping new form lines to standardize observations throughout all areas. Thus, form line observations were combined and compiled into a single vector file, “form lines”, which is provided in Digital Appendix A.

The integration stage combines observations with existing geological and other types of data. This stage includes identification of discontinuities and definition of structural elements, magnetic domains, and changes or disruptions in domains with coherent structural or form line trends. Cross-referencing of the observations with other datasets, including Lithoprobe seismic (e.g., Ross et al., 1995; Ross and Eaton, 2002), gravity surveys (Edwards et al., 1998), geology (e.g., Pană, 2003a, 2010; Pană and Elgr 2013; Prior et al., 2013), geochronology (Ross et al., 1991; Villeneuve et al., 1993; Burwash et al., 1994; Burwash et al., 2000a; and Pană, 2010), and structural lineament compilations (e.g., Pană et al., 2001; Pană and Waters, 2016; Pană et al., 2021; Alberta Geological Survey 2021b) is completed in this stage.

The interpretation stage involves the revision or creation of a structural framework that includes inferences of structural and lithotectonic history. This is the final step in generating an integrated geological and geophysical interpretation of an area to present a final geological interpretation map. The domains and structure layers are the basis of the structural framework interpretation.

6.3 Domains and Subdomains

We started our interpretation by recognizing and delineating tectonic basement domains previously defined by Villeneuve et al. (1993), Ross et al. (1994) and Pilkington et al. (2000). Following delineation of known basement domains, new domains were delineated based on magnetic character. In this work, we use the term domain to indicate regions of similar magnetic character, although some inferences regarding a tectonic meaning is sometimes offered. Further integration with historical and newly acquired geochronological data, isotope data, and additional geophysical studies is required to conclude that new domains defined herein can be interpreted as tectonic domains involved in the assembly and evolution of western Laurentia.

The reduced to pole residual magnetic intensity, analytic signal, vertical integral of analytic signal, first vertical derivative, total horizontal derivative, and ternary magnetic images that highlight geological affinity (e.g., pseudo-geology, pseudo-gravity), are used as the first step to outline domains and subdomains.

Increasing sediment thickness of the WCSB towards the west attenuates and widens anomalies observed in various magnetic filter products. The tilt angle (derivative) (Figure 5-8) and structure detection products (Appendix 1) are used for interpretation where the magnetic signal appears attenuated by the sedimentary cover because these products remove information about the amplitude of the magnetic signal facilitating the interpretation of subtle features.

Basement domains have distinct magnetic signatures, which include distinct orientations, and amplitudes and wavelengths of magnetic features. Domain boundaries are usually marked by sharp magnetic ridges representing either major contact zones or shear zones. Magnetic intensity and fabric orientation usually changes significantly across domain boundaries.

Domains may be divided into subdomains based on contrasting magnetic character within certain domains, however, boundaries are weakly defined or fuzzy. Subdomains may be related to a primary heterogeneous magnetic fabric or secondary geological processes that created, introduced, or destroyed magnetic minerals. Boundaries between subdomains are not necessarily tectonic in nature as they may represent an internal magnetic variant or an intrusion within a known domain.

6.4 Intrusions

Analytic signal products are used to identify equant round features (as opposed to linear features) in the data allowing to locate anomalies that can be interpreted as intrusive bodies, pipes or discrete alteration zones. The horizontal gradient derivative product is useful to map the outline of round features. However, manual detection is challenging when the contrasts in magnetic intensity in an area are low. Automatic detection radial symmetry is better at identifying round features particularly when used in magnitude-independent mode

(Appendix 1). This report uses a combination of manual detection conducted by RMG and automatic detection conducted by Fathom Geophysics to select possible intrusions. Manual detection of round features is conducted first, followed by review of radial symmetry results to confirm selection and identify additional round features.

6.5 Lineaments

Filters such as vertical and horizontal derivatives and the tilt angle filter combined with results from the structure detection for parallel structures (Section 5.3) were used to identify deeper basement structures and shear zones. The wavelength separation results, particularly the separation of long wavelengths, allows for the delineation of potential deeper structures. Furthermore, differential upward continuation magnetic products were useful for discriminating deeper from shallower structures (Figure 5-11 and Figure 5-12).

Shear zones are usually characterized by the following:

- broad zones of anastomosing surfaces, with curvilinear margins
- bending of magnetic units or contacts into the shear zone
- magnetic mineral alteration that may be destructive, additive, or both; or
- offsets of units associated with deflection or thinning of magnetic markers as they enter the shear zone

High-pass filter products such as the second derivative, tilt, and automatic gain control (AGC), and the results for short wavelengths from automatic structure detection for cross structures were used to emphasize shallow and detailed brittle structures in the project area. Criteria to identify brittle structures included the following:

- juxtaposition of different form line orientations
- linear features with angular margins
- angular fault jogs or steps
- short subtle curvilinear linear features (for sub-horizontal sedimentary strata)
- narrow zones of demagnetization (due to low temperature oxidation of magnetic minerals)
- discrete offsets of magnetic units

Offsets and sense of movement were recorded in the accompanying GIS vector files where possible. Because of the 2D plan nature of the magnetic data, interpreted offsets are apparent offsets.

Other possible lineaments are domain boundaries, contacts, stratigraphic bedding and edges, unconformities, folds, fractures, and dikes.

The interpretation of lineaments is also supported by the structure detection conducted by Fathom Geophysics, particularly by fabric-parallel and fabric-crossing products. Fabric-parallel and fabric-crossing structures are different structure types and may have different timing. The fabric-parallel features tend to be contacts or belt-parallel shear zones. The cross structures are more likely to be faults. Any sense of motion is

possible on the cross structures. If clear lateral offset of the units is present, the faults are likely strike-slip faults. Normal and reverse faults are often represented by a change in amplitude or frequency content of the magnetic data (Appendix 1).

7.0 INTERPRETATION AND RESULTS

7.1 Cultural Artefacts

Alberta's widely distributed oil and gas infrastructure and urban areas are noticeable in the magnetic products. The survey contractor applied filtering and manual editing to attenuate the effects of culture in the data, but residual cultural artefacts are still present throughout the survey area. The following cultural features were evaluated against the aeromagnetic images: (1) municipal areas, (2) railways, (3) pipelines, and (4) oil and gas related infrastructure. As these features are all near surface, expected signatures include high frequency linear and circular anomalies and/or distortion of larger magnetic anomalies (Figure 7-1). The infrastructure layers were always consulted before mapping features such lineaments or intrusions.

Identification of larger pipelines do not represent a major challenge in the interpretation of the magnetic images, because they present as distinct shallow straight lines and can be easily correlated with infrastructure maps. However, most smaller pipelines do not display a clear magnetic signature at this survey resolution and clusters of pipelines creating a broad magnetic response are difficult to discern from a natural source. Overall, the impact of pipelines on the magnetic image is high and therefore, calibration of lineaments with AER's pipeline information and imagery is highly recommended.

Numerous small (< 5 km^2) rounded anomalies are present throughout the project area that are cultural in nature (e.g., gathering stations, processing plants, power stations). Examples of culture mapped are not exhaustive (Figure 7-1). High-frequency anomalies could also represent small intrusions or kimberlites. RMG's interpretation focused on larger-scale items (> 5 km^2). It is recommended that smaller rounded magnetic anomalies are carefully evaluated and calibrated against cultural data on a case-by-case basis before assigning a geological meaning.

The regional railroad and powerline networks do not exhibit a distinct signature in the magnetic filter products; therefore, the impact of these cultural components is considered negligible.

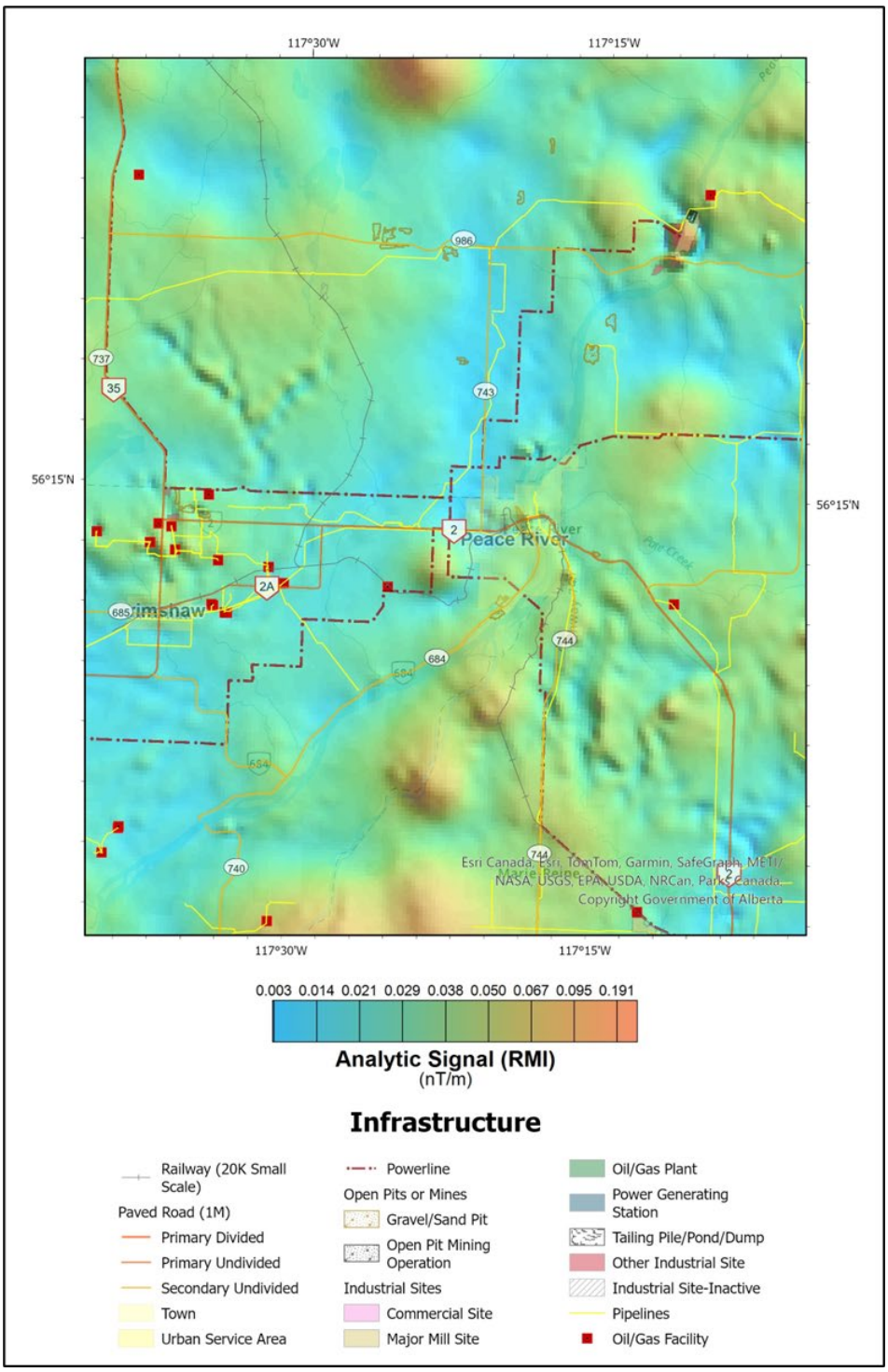

Figure 7-1. Impacts of infrastructure (urban, utility, access, pipelines, and industrial facilities) of the Peace River area on magnetic data. The area displays a circular anomaly (magnetic high) related to an industrial site and faint straight lineaments related to pipelines.

7.2 Domains and Subdomains

The interpretation of the magnetic filter products for the four project areas (Canadian Shield, northern, central and southern Alberta survey) resulted in the modification of published basement domain boundaries (Lopez et al., 2024a, 2024b; Brem et al., 2024; Lopez et al., 2025). Classification followed known basement domains definitions by previous authors wherever possible. Many modifications were minor adjustments to the original domain boundaries. Due to the higher quality of the new magnetic data some domain modifications were significant and involved a major relocation of a domain boundary, reintroduction of abandoned domain definitions, or definition of new domains and subdomains.

The merging of interpretation GIS files from the four survey areas revealed inconsistencies across survey boundaries that required revision and modification of domain and subdomains files. Existing basement domain interpretations by Villeneuve et al. (1993), Ross et al. (1994) and Pilkington et al. (2000) are used to calibrate and modify interpreted domains in this step. During the reinterpretation across magnetic survey boundaries, several domain and subdomain boundaries were readjusted and standardized to create a continuous and consistent interpretation basement domain layer of Alberta. The attribute table related to domains and subdomains was edited to reflect enhancements to the newer interpretation (Digital Appendix A).

Domains identified herein are shown in Figure 7-2 and Figure 7-3, and subdomains are shown on Figure 7-4 to Figure 7-6.

The main geophysical characteristics of domains are presented below, organized from northwest to northeast, followed by west-central to southeast. These domains are also summarized and tabulated in Table 7-1. Petrological and chronological data is taken from unpublished compilations provided by the AGS from Ross et al. (1991), Villeneuve et al. (1993) and Burwash et al. (1994).

7.2.1 Hottah Domain

The Hottah domain in northern Alberta corresponds to the Hottah Terrane defined by Villeneuve et al. (1993) and Ross et al. (1994), and the Hottah domain of Pilkington et al. (2000). This domain is characterized by a magnetic low locally containing irregular-shaped magnetic highs. This domain presents northwest-trending straight linear magnetic trends of moderate to low amplitude and long wavelengths that are regularly spaced between 10 to 30 km apart. These linear trends are overprinted by various short wavelength squiggly ENE-trending lineaments that resemble dikes. Well intersections correspond to 1.85 to 1.94 Ga granitic rocks, however the dominant magnetic low throughout the domain suggests that demagnetization may have occurred. This domain is bounded to the east by the Great Slave Lake shear zone and a contrasting magnetic high related to Nova domain.

7.2.2 Great Bear Domain

The Great Bear domain in northern Alberta corresponds to the Great Bear continental magmatic arc of Ross et al. (1994), the Great Bear Arc of Villeneuve et al. (1993), and the Great Bear basement domain of Pilkington et al. (2000). In this work, the Great Bear domain is subdivided into two subdomains, the Great Bear and

Hottah/Great Bear subdomains (Figure 7-4 to Figure 7-6). The Great Bear subdomain is characterized by a variable magnetic signature dominated by magnetic highs in the northeast and south corners. Internal fabric trends are variable from NW to NNE. The Hottah/Great Bear subdomain is located between the Hottah domain and the Great Bear subdomain and presents overlapping characteristics of these two magnetic rock units. It is suspected that the magnetic character of the Great Bear magmatic arc domain overprints the Hottah domain in this region. Five historic core samples of granite, tonalite and monzonite from Ross et al. (1991) suggest that the Hottah/Great Bear subdomain is part of the Great Bear magmatic arc domain.

7.2.3 Nova Domain

The small Nova domain in northern Alberta corresponds to the Nova Domain of Villeneuve et al. (1993) and the Nova domain of Pilkington et al. (2000). Only minor adjustments to the previously defined domain boundary were made. This domain consists of a narrow northeast-trending magnetic high between the Hottah and Kiskatinaw domains (Figure 7-2 and 7-3) and is bounded by the Great Slave Lake shear zone. It is considered to represent a slice of Slave Province (Pană et al., 2021).

7.2.4 Kiskatinaw Domain

The Kiskatinaw domain in northern Alberta corresponds to the Kiskatinaw Low defined by Villeneuve et al. (1993) and the Kiskatinaw domain of Pilkington et al. (2000). Only minor adjustments to the previously defined domain boundary were made. This domain consists of a narrow (<15 km) northeast-trending magnetic low between the Nova and Ksituan domains. This magnetic low may be related to a deformed portion of the Ksituan domain as suggested by Villeneuve et al. (1993) or to demagnetization due to activity related to the Great Slave Lake shear zone or during accretion as suggested by Pilkington et al. (2000).

7.2.5 Ksituan Domain

The Ksituan domain in northern Alberta corresponds to the Ksituan High of Villeneuve et al. (1993), the Ksituan continental magmatic arc defined in Ross et al. (1994) and the Ksituan basement domain of Pilkington et al. (2000). Only minor adjustments to the previously defined domain boundary were made. In this work, the Ksituan domain is subdivided into two subdomains, the Ksituan High and Ksituan South subdomains (Figure 7-4 to Figure 7-6). The Ksituan High subdomain consists of a prominent 15-30 km wide NNW to NE-trending curvilinear magnetic high between the Kiskatinaw and Chinchaga domains. The Ksituan South subdomain displays NW-trends and subcircular anomalies resembling those seen in weakly deformed plutonic belts. Historical core samples from the Ksituan domain consist of granitic gneiss, monzonite, and syenogranite (Ross et al., 1989) consistent with the interpretation of a magmatic arc.

7.2.6 Chinchaga Domain

The Chinchaga domain in northern Alberta corresponds to the Chinchaga Low of Villeneuve et al. (1993), the Chinchaga Terrane of Ross et al. (1994), and the Chinchaga domain of Pilkington et al. (2000). It is generally characterized by a magnetic low. In central Alberta, close to the contact with the Wabamun domain, the Chinchaga domain displays a localized magnetic high that is possibly related to magnetization along the north

branch of the Snowbird tectonic zone (Figure 7-2 to Figure 7-6). The magnetic character of the Chinchaga domain is consistent with metasedimentary or volcanic rocks (Lopez et al., 2024), also suggested by previous authors (Villeneuve et al., 1993; Ross et al., 1994).

7.2.7 Buffalo Head Megadomain

The Buffalo Head domain herein is a megadomain in northern Alberta that corresponds to the Buffalo Head Terrane of Villeneuve et al. (1993), the Buffalo Head accreted terrane of Ross et al. (1994), and to the Buffalo Head's High and Utikuma basement domains of Pilkington et al. (2000). The Buffalo megadomain is subdivided herein into three main domains based on contrasting variations in magnetic amplitude, general trend, and internal character in relation to the surrounding units. The Buffalo Head domains defined in this work are Buffalo Arch, Buffalo High, and Buffalo Utikuma (Table 7-1).

Buffalo Arch Domain

The newly defined Buffalo Arch domain in northern Alberta corresponds to the westernmost part of the Buffalo Head domain of Villeneuve et al. (1993) and Ross et al. (1994), and the westernmost part of Buffalo High domain of Pilkington et al. (2000). The Buffalo Arch domain is a 15-30 km wide magnetic high belt similar in magnitude to the Ksituan domain. Historical core samples indicate that this domain consists of quartz diorite, monzonite, granite, leucogranite, and lesser granitic gneisses and metavolcanic rocks, ranging in age between 2.16 and 1.99 Ga (Ross et al., 1989). The arcuate shape of the domain, magnetic signature, and occurrence of granitoids suggest that the Buffalo Arch may represent a magmatic arc along the margin of the Buffalo Head terrane.

Buffalo High Domain

The Buffalo High domain in northern Alberta, following the definition by Pilkington et al. (2000), corresponds to the western part of the Buffalo Head Terrane of Villeneuve et al. (1993) and Ross et al. (1994), except the Buffalo Arch domain defined in this work. Variations in magnetic signature allow the interpretation of three contrasting subdomains: Buffalo Caribou in the north, Buffalo High in the centre, and Buffalo Low in the south (Figure 7-2 to Figure 7-6). The Buffalo Caribou subdomain is characterized by a magnetic low bisected by a linear N-trending magnetic high. The Buffalo High subdomain is characterized by NNW to NE magnetic high linear trends. Historical samples from the Buffalo High subdomain include quartz monzonite, monzonite gneiss and pegmatite with ages ranging from 2.17 to 1.97 Ga (Ross et al., 1989). Near the contact with the Buffalo Utikuma domain, the Buffalo High subdomain hosts 25 kimberlites of the Buffalo Head Hill kimberlite field. The Buffalo Low subdomain is characterized by a magnetic low and variable magnetic trends. Historical core samples consist of diorite and quartz monzonite with one age available of 2.324 Ga (Ross et al., 1989). The Buffalo Low subdomain may be related to demagnetization along the Snowbird tectonic zone shear zone during collision between the Hearne and Rae provinces.

Buffalo Utikuma Domain

The Buffalo Utikuma domain in northern Alberta, following the definition by Pilkington et al. (2000), corresponds to the eastern part of the Buffalo Head domain of Villeneuve et al. (1993) and Ross et al. (1994).

The Buffalo Utikuma domain is subdivided herein into the Buffalo Central and Buffalo Utikuma subdomains. The Buffalo Central subdomain is a major north-trending unit that separates the Buffalo High domain to the west from the Buffalo Utikuma subdomain to the east. Buffalo Central is characterized by structural or irregular contacts and shows evidence of magnetic remanence throughout (Figure 7-2 to Figure 7-6). Historical core samples consist of granodiorite, granite porphyry and syenogranite gneiss, with one available age of 1.995 Ga (Ross et al., 1989). The Buffalo Central subdomain coincides with the known N-trending Trout Mountain gravity low (e.g., Eccles et al., 2002). and the location of 27 kimberlites of the Buffalo Head Hills kimberlite field (the other 14 kimberlites of this field intrude the eastern boundary of Buffalo High subdomain).

7.2.8 Taltson Megadomain

The Taltson domain herein is a megadomain in northern Alberta that corresponds to the Taltson Arc of Villeneuve et al. (1993), the Taltson continental magmatic arch of Ross et al. (1994), and to the Taltson basement domain of Pilkington et al. (2000). The Taltson megadomain is subdivided herein into three main domains and nine subdomains based on contrasting variations in magnetic amplitude, general trend, and internal character in relation to the surrounding units. The Taltson domains defined in this work are the Taltson Slave – Birch, Taltson Charles Lake – Athabasca, and Taltson South domains (Table 7-1).

Taltson Slave – Birch Domain

The Taltson Slave – Birch domain consists of a 50-100 km wide north-trending zone encompassing four subdomains of contrasting magnetic signature: the Taltson Slave, Taltson High, Talson Wood Buffalo, and Taltson Birch subdomains (Figure 7-4 to Figure 7-6). In the north, the Taltson Slave subdomain is characterized by a general magnetic low without fabric trends and containing smaller rounded magnetic highs slightly trending to the east-northeast. These magnetic highs are interpreted to represent intrusions. The Taltson High subdomain is a 20 km wide by 60 km long magnetic high located between the Taltson Slave subdomain and the Taltson Charles Lake – Athabasca domain (Figure 7-4 to Figure 7-6). The Taltson High subdomain is interpreted here as a single intrusion. The Taltson High subdomain is a small magnetic high anomaly between the Taltson Slave and Taltson Wood Buffalo subdomains. The magnetic signature of the Taltson Slave and Taltson High subdomains resembles intrusive domains which might be related to anorogenic magmatism associated with the extensional features shown in the Taltson Birch and Taltson Wood Buffalo subdomains.

The Wood Buffalo subdomain consists of a magnetic low that displays weakly defined wide linear north trends, and it is distinctly affected by E- to ENE-trending brittle faults (Figure 7-4 to Figure 7-6). The internal fabric resembles an extensional structure system, with a general north-trending central magnetic low zone, and perpendicular faults or fracture zones. The central magnetic low zone displays evidence of remanent magnetization (Figure 7-6). This extensional structure may represent a remnant rift basin. The Taltson Birch subdomain consists of a magnetic low with a distinct linear internal fabric (Figure 7-4 to Figure 7-6). It is characterized by parallel moderately magnetic NNW-trending ridges displaced by NW- and NE-trending faults. The southernmost end of the Taltson Birch subdomain is displaced, possibly affected by a tectonic escape wedge related to the Snowbird tectonic zone (“STZ”).

Overall, the four subdomains may represent different structural levels of a rift system in which the Taltson Birch subdomain represents the upper level and the Taltson Slave subdomain is the deeper anorogenic magmatic component. However, this interpretation is only based on magnetic signature, geometries and spatial relationships, therefore further studies are needed to confirm this hypothesis.

Taltson Charles Lake – Athabasca Domain

The Taltson Charles Lake – Athabasca domain consists of a north- to northeast-trending zone characterized by a regional magnetic high. This domain is divided into four subdomains: the Taltson Arch Lake, Taltson Charles Lake, Taltson Rae, and Taltson Athabasca subdomains.

The Taltson Charles Lake subdomain correspond to the narrow zone (5-35 km) of anastomosing magnetic linear trends in the north of the Taltson Charles Lake – Athabasca domain and includes the known Charles Lake shear zone (Figure 7-4 to Figure 7-6). The Taltson Athabasca subdomain corresponds to the fan-like zone of magnetic linear trends that extend from the Charles Lake subdomain to the Taltson South subdomain and widens to about 130 km in the south near the contact with the Taltson South domain. The Beatty River shear zone separates the Taltson Athabasca subdomain from the Charles Lake subdomain.

The Taltson Arch Lake subdomain corresponds to the area containing the known Arch Lake granitoids. This subdomain is characterized by strong linear fabrics, trending N and NE parallel to the Charles Lake and Leland Lakes shear zones, and strong E-trending linear magnetic fabric in the south of the subdomain (Figure 7-4 to Figure 7-6). The centre of the subdomain displays weaker fabrics in variable orientations. The Taltson Arch Lake subdomain contains 1.960–1.934 Ga, collision-related, peraluminous (S-type), monzo-syenogranite complexes (see Taltson granitoid descriptions in Pană, 2010 and references therein).

The Taltson Rae subdomain lacks linear trends, except at the boundary with the Rae domain, and presents characteristics of both the Taltson and the Rae domains (Figure 7-4 to Figure 7-6), such as the low magnetic intensity of the Rae domain and internal fabric of the Taltson domain intrusive complexes. The Taltson Rae subdomain located to the east of the Charles Lake shear zone contain 1.974–1.959 Ga, subduction-related, weakly peraluminous to metaluminous (I-type) intrusive complexes (see Taltson granitoid descriptions in Pană, 2010 and references therein).

Taltson South Domain

The Taltson South domain displays a dominant ENE-trending refolding fabric (Figure 7-2 to 7-6), is bound by a major E-trending shear zone in the north, and the Thorsby domain and the STZ in the south. Either the Taltson South subdomain is a refolded part of the Taltson Charles Lake – Athabasca domain affected by the collision between the Hearne and Rae provinces along the STZ or it belongs to an older (Archean) terrain.

7.2.9 Rae Domain

The Rae domain in northern Alberta corresponds to the Archean Rae Province defined in Ross et al. (1994) and the Rae domain of Pilkington et al. (2000). This domain is characterized generally by a magnetic low,

strong NNW- to NE-trending linear fabrics, a local linear magnetic high to the north of the Beatty River shear zone (see section 7.4.4), and an ample folded fabric (Figure 7-2 to Figure 7-6) to the south of the Beatty River shear zone. The mapped trends of the Archean-Proterozoic Taltson basement complex (Pană, 2010a) in the Canadian Shield in Alberta are consistent with the magnetic fabric observed in magnetic products, whereas magnetic linear trends in the Athabasca Basin area are colinear with the boundaries of mapped units of the Athabasca Group suggesting either a basement control on disposition of the Athabasca Group or influence of the Athabasca Group on the magnetic signal.

7.2.10 Wabamun Domain

The Wabamun domain in central Alberta corresponds to the Wabamun High defined in Villeneuve et al. (1993) and the Wabamun domain of Pilkington et al. (2000). The Wabamun domain was interpreted as a tectonic escape wedge formed during collisions along the STZ (Ross, 2002).

Internally, this domain is a magnetic high bounded in the northwest by a linear magnetic low related to the north branch of the Snowbird tectonic zone and in the southeast by a magnetic low related to the Thorsby domain and southern branch of the STZ. In the southeast, the boundary between the Wabamun and the Thorsby domains is a distinct curvilinear magnetic high. Only minor adjustments were made to the previously defined domain boundary. This domain is subdivided into two subdomains based on subtle differences in magnetic trends and subcircular features seen on the pseudo-structure ternary image (Figure 5-10) and structure detection products (Digital Appendix C): the Wabamun Lake and the Wabamun West subdomains. The Wabamun domain presents evidence of magnetic remanence in the northwest corner (Figure 7-6).

The Wabamun Lake subdomain (Figure 7-4 to Figure 7-6) is an elongate NE-trending region bounded by rounded features resembling plutons and anastomosing, relatively higher frequency NNW and NE internal magnetic trends. The Wabamun West subdomain (Figure 7-4 to Figure 7-6) presents rounded features resembling zoned plutons. Historical core samples in this subdomain include quartz diorite and tonalite (Ross et al., 1989) with ages ranging from 2.322 to 2.294 Ga (Villeneuve et al., 1993). Internally, the Wabamun West subdomain is characterized by large subrounded magnetic highs bounded by linear magnetic lows with variable orientations. The fabric of both subdomains resembles that seen in weakly deformed plutonic belts.

7.2.11 Thorsby Domain

The Thorsby domain in central Alberta follows the Thorsby Low defined by previous authors (Villeneuve et al., 1993; Ross et al., 1994; Pilkington et al., 2000). This domain is herein subdivided into two distinct subdomains: Thorsby Low and Thorsby High (Figure 7-4 to Figure 7-6). The Thorsby Low subdomain has a homogenous low magnetic signature. The Thorsby High subdomain is identified between the Thorsby Low and Rimbey domains as a small high amplitude crescent-shaped north-trending magnetic ridge and a trough along the western edge of the Rimbey domain. The Thorsby domain may be the result of demagnetization due to deformation and metamorphism during terrane collision as suggested as well by Pilkington et al. (2000).

7.2.12 Rimbey Domain

The northeast-trending Rimbey domain in central Alberta consists of a prominent northeast-trending curvilinear magnetic high between the Thorsby and Lacombe domains. It corresponds to the Rimbey continental magmatic arc defined in Ross et al. (1994), the Rimbey High of Villeneuve et al. (1993), and the Rimbey domain of Pilkington et al. (2000). The Rimbey domain was interpreted as a magmatic arc related to the southeastward subduction of the Thorsby domain (Ross et al., 1991).

In our work, only minor adjustments to the previously defined domain boundary were made. The eastern part of the domain is characterized by a NE-trending high amplitude magnetic signature, whereas the west margin presents a penetrative higher frequency, NE- to NNE-trending and moderate-amplitude magnetic fabric, possibly due to deformation (Figure 7-4). The magnetic fabric resembles that seen in deformed plutonic belts. Historical core samples within this domain include quartz diorite, monzogranite and leucogranite with ages ranging from 1.856 to 1.798 Ga (Ross et al., 1989; Villeneuve et al., 1993) which are consistent with the previous magmatic arc interpretation.

7.2.13 Lacombe Domain

The Lacombe domain in central Alberta is an indistinct, approximately 80 km wide, northeast-trending zone that has a generally moderate magnetic intensity, but high magnetic variation. The Lacombe domain is bounded to the east by a narrow magnetic high (Red Deer trend: Section 7.4.9) and to the west by the Rimbey domain. Only minor adjustments to the previously defined domain boundary of Pilkington et al. (2000) were made. The boundary between the Lacombe and Rimbey domains is well defined on magnetic filter products, but locally fuzzy where crosscut by other lineaments. To the south, the Lacombe domain ends at the confluence of the Red Deer trend and the Rimbey domain. Internally, the Lacombe domain presents a NNE-trending magnetic fabric, but in the northeast corner it presents a local subrounded magnetic low with a magnetic high rim (Figure 7-6). Legacy data from well samples report low-grade metavolcanic samples from the Red Deer trend that could not be dated (Villeneuve et al. 1993).

7.2.14 Loverna Domain

The Loverna domain in central Alberta corresponds to the Loverna Block defined by Villeneuve et al. (1993) and the Loverna domain of Pilkington et al. (2000). This domain is the magnetically indistinct region between the Lacombe and Rimbey domains in the west, the Matzhiwin domain in the south, and the Vulcan Low North domain in the east. Major boundary modifications to the Loverna domain are made here, particularly to the eastern side. Previous authors had defined the eastern edge of the Loverna domain in contact with the Eyehill domain. However, a distinct magnetic low similar to the Vulcan Low domain of southern Alberta separates the Loverna domain from the Eyehill domain (Figure 7-2 to Figure 7-6).

The Loverna domain is characterized by high variation of magnetic signature and magnetic fabric. This domain is subdivided into two main subdomains: the Loverna High and the Loverna Low subdomains (Figure 7-4 to Figure 7-6). The Loverna High subdomain presents a moderate magnetic amplitude and subtle linear to no internal fabric orientation, except along the western edge where strong linear trends of magnetic ridges

demonstrate shearing related to the Red Deer trend (section 7.4.9). The Loverna Low subdomain presents generally as a magnetic low with a NNW-trending fabric with local, broad, rounded magnetic highs. The edges of the Loverna Low subdomain are fuzzy and it is unclear whether this subdomain relates to the adjacent northern extent of the Vulcan Low North feature or if it is a separate entity within the Loverna domain that has been affected by secondary processes. The only sample available from the NW corner of this subdomain is a gneissic biotite-quartz diorite. The Loverna High subdomain displays a NE-trending central discontinuity and attenuation of the magnetic amplitude to the east, whereas the Loverna Low displays parallel N-trending magnetic lineaments also at the centre of the subdomain (Figure 7-5 and Figure 7-6). Both the Loverna High and Low subdomains display high magnetic variability; more small internal features could be delineated.

7.2.15 Vulcan Low North Domain

The newly defined Vulcan Low North domain in central Alberta is a distinct narrow north-trending magnetic low lying between the Loverna and Eyehill domains and forms the extension of the Vulcan Low domain (Figure 7-2 to Figure 7-6). This domain displays a linear NNW- to NNE-trending internal fabric more clearly seen on the pseudo-structure ternary image (Figure 5-10), various derivative products (Digital Appendix B) and structure detection products (Digital Appendix C). This feature is 15 to 30 km wide and appears to merge into the major east-trending Vulcan Low of southern Alberta (Brem et al., 2024). This merge was also observed by Villeneuve et al. (1993) based on older aeromagnetic data. The Vulcan Low North domain laterally displaces a section of the Matzhiwin domain towards the major east-trending Vulcan Low structure in southern Alberta (see magnetic products in Brem et al., 2024). Sharp edges along the boundary with the Eyehill domain and contrasting internal magnetic intensity and fabric in relation to both the Eyehill and the Loverna domains suggest tectonic boundaries for this domain. Therefore, the Vulcan Low North domain is considered in this work as a distinct tectonic domain similar in magnetic character to the Vulcan Low domain (Figure 7-2 to Figure 7-6).

7.2.16 Eyehill Domain

The Eyehill domain in central Alberta is a magnetic high region located in the east near the Alberta-Saskatchewan provincial boundary. It corresponds to the Eyehill High defined by Villeneuve et al. (1993) and the Eyehill domain of Pilkington et al. (2000). The western edge of the Eyehill domain is a curvilinear NNW- to N-trending magnetic high, whereas the internal magnetic fabric displays northeast trends that bend towards the south along (or into) the western curvilinear edge (Figure 7-2 to Figure 7-6). Only minor adjustments to the previously defined domain boundary were made.

7.2.17 Matzhiwin Domain

The Matzhiwin domain in southern Alberta is a moderately high magnetic zone that corresponds to the Matzhiwin High defined by Villeneuve et al. (1993) and the Matzhiwin domain of Pilkington et al. (2000). The magnetic amplitude is similar to the Rimbey domain and presents a general NE-trending internal fabric. In the eastern part of the domain the fabric is superposed by a second fabric of N-trending magnetic ridges more clearly seen on pseudo-geology and pseudo-structure ternary images (Figure 7-4 and Figure 5-9). Only minor adjustments to the previously defined domain boundary were made (Figure 7-4). An alternative published

interpretation of this domain is that it is the magnetic high portion of the remanently magnetized Vulcan Low domain (Hope and Eaton, 2002).

7.2.18 Vulcan Low Domain

The Vulcan Low domain in southern Alberta is a distinct E-trending magnetic low flanked to the north by the Matzhiwin domain and to the south by the Medicine Hat domain. This domain corresponds to the Vulcan Low defined by Hoffman (1988) and Villeneuve et al. (1993), Vulcan structure of Hope and Eaton (2002), and the Vulcan domain of Pilkington et al. (2000). It is characterized by curvilinear boundaries and NE- to ENE-trending curvilinear fabric. The boundaries of the Vulcan Low domain were adjusted herein, based on differences in character and fabric orientation between the Medicine Hat and Matzhiwin domains. The ternary of RTP, analytic signal of the vertical integral, and analytic signal (Figure 7-6) implies the presence of remanent magnetization, which aligns with Hope and Eaton (2002).

The Vulcan Low domain coincides with a Bouguer gravity low, which implies its importance as a crustal-scale boundary (Villeneuve et al., 1993). Differences in the positioning of the Vulcan Low domain boundaries exist in published reports and there are various tectonic models discussing the structural evolution of the Vulcan Low domain, including rift basin, collision zone, and suture zone (Pană et al., 2021).

7.2.19 Medicine Hat Domain

The Medicine Hat domain in southern Alberta corresponds to the Medicine Hat Block defined in Villeneuve et al. (1993) and Ross et al. (1994), and the Medicine Hat domain of Pilkington et al. (2000). This domain is characterized by a high variation of magnetic signature, with dominant NW- to N-trending, low to high amplitudes of magnetic anomalies. This domain was originally subdivided into three subdomains by Brem et al. (2024), each represented by a different magnetic character. To maintain consistency with interpretations in central and northern Alberta, two additional subdomains are defined for the Medicine Hat domain herein, Medicine Hat South and Medicine Hat Low (Figure 7-4 to Figure 7-6). The boundaries may not necessarily follow a distinct magnetic lineament and there is lateral uncertainty on the locations of these boundaries due to the potentially shallowly dipping nature of these domain contacts.

The Medicine Hat High subdomain underlies the foothills and is characterized by a homogeneous, high magnetic response. The small Medicine Hat South subdomain is characterized by a large round magnetic low. The Medicine Hat Central subdomain is characterized by a low-to-moderate magnetic amplitude, wide NNW- and NW-trending linear magnetic lows and highs that locally appear to be overlapping. The Medicine Hat South subdomain is a rounded 50 km wide magnetic low located south of the Medicine Hat Central subdomain. The Medicine Hat Low subdomain is characterized by a NNW-trending 20-25 km wide magnetic low possibly due to demagnetization related to the N-trending structure separating the Medicine Hat Central and East subdomains (Grand Forks Fault; Burwash et al., 2000). The Medicine Hat East subdomain is characterized by a dominant magnetic high, and NW- to N-trending linear magnetic highs.

7.2.20 Unknown Domains

Four magnetic domains of uncertain association to defined domains occur in northern Alberta.

In the northwest, a narrow 5-15 km wide north-trending domain of distinct fabric is interpreted between the Chinchaga and Buffalo Head domains. This domain is bounded in the south by the High Level shear zone (section 7.4.6) and could represent an internal variation within the Chinchaga domain, or a separate rigid terrane between the Chinchaga and Buffalo Arch domains. In the west, the Chinchaga domain displays a small second variation along the contact with the Buffalo Arch domain distinct from the overall character of this domain, which may consist of an intrusion in the Chinchaga domain or belong to the Buffalo Arch domain.

The “uncertain” domain defined by Pilkington et al. (2000) was redrawn and converted into two smaller domains based on contrasting magnetic amplitude, general trend, and internal character in relation to the surrounding units. These two domains display different orientations of magnetic fabric suggesting block rotations; the western block presents NNE trends and the eastern block presents ENE to WNW trends. These domains were all labeled as unknown, and they appear to represent broken deformed pieces of adjacent domains, possibly from the Buffalo Head megadomain and the Wabamun domain.

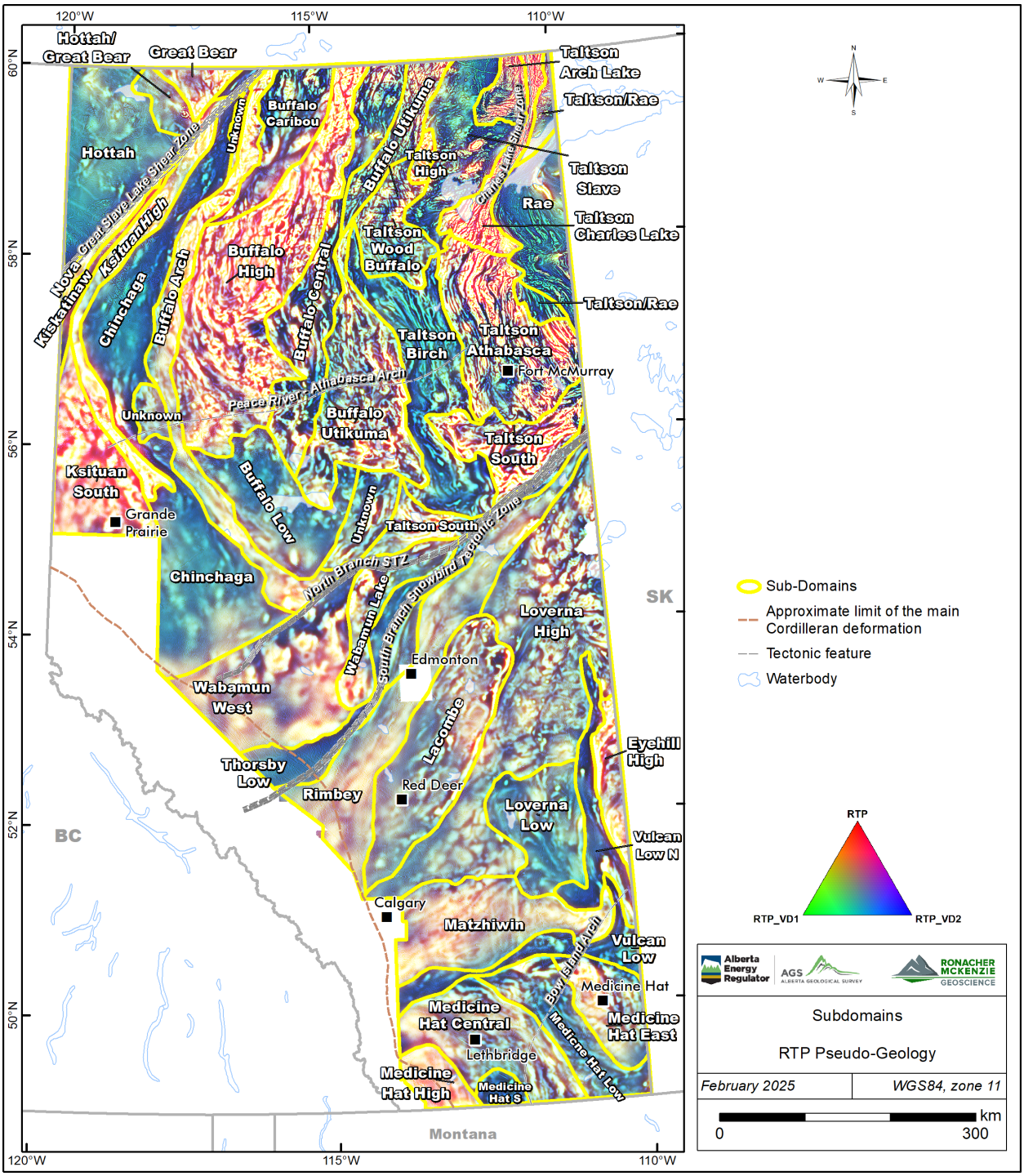

Figure 7-4. Interpreted subdomain boundaries in Alberta defined by this study. Background image: pseudo-geology ternary.

and

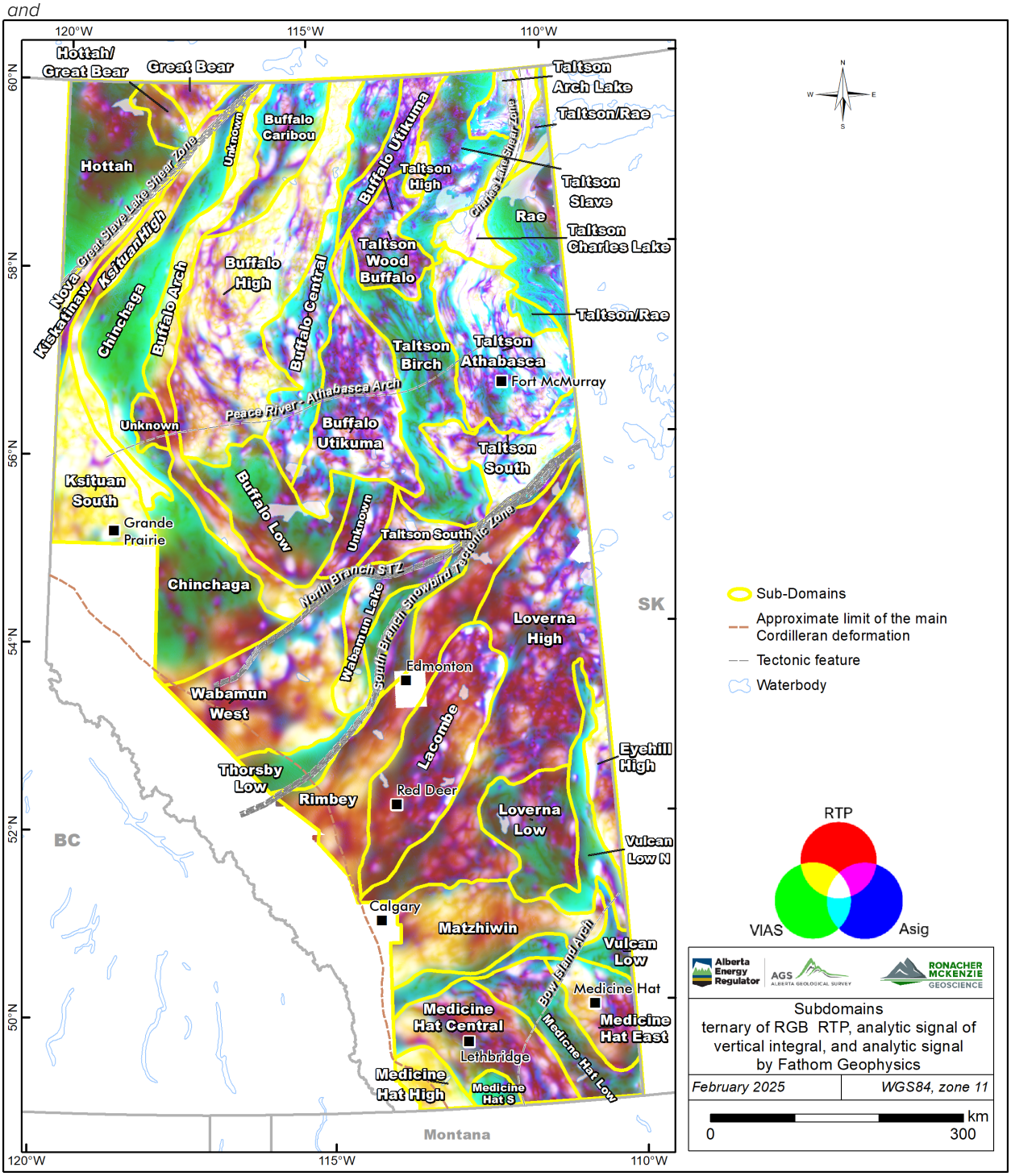

Figure 7-5. Interpreted subdomain boundaries in Alberta defined by this study. Background image: ternary of RGB RTP, analytic signal of vertical integral, and analytic signal by Fathom Geophysics.

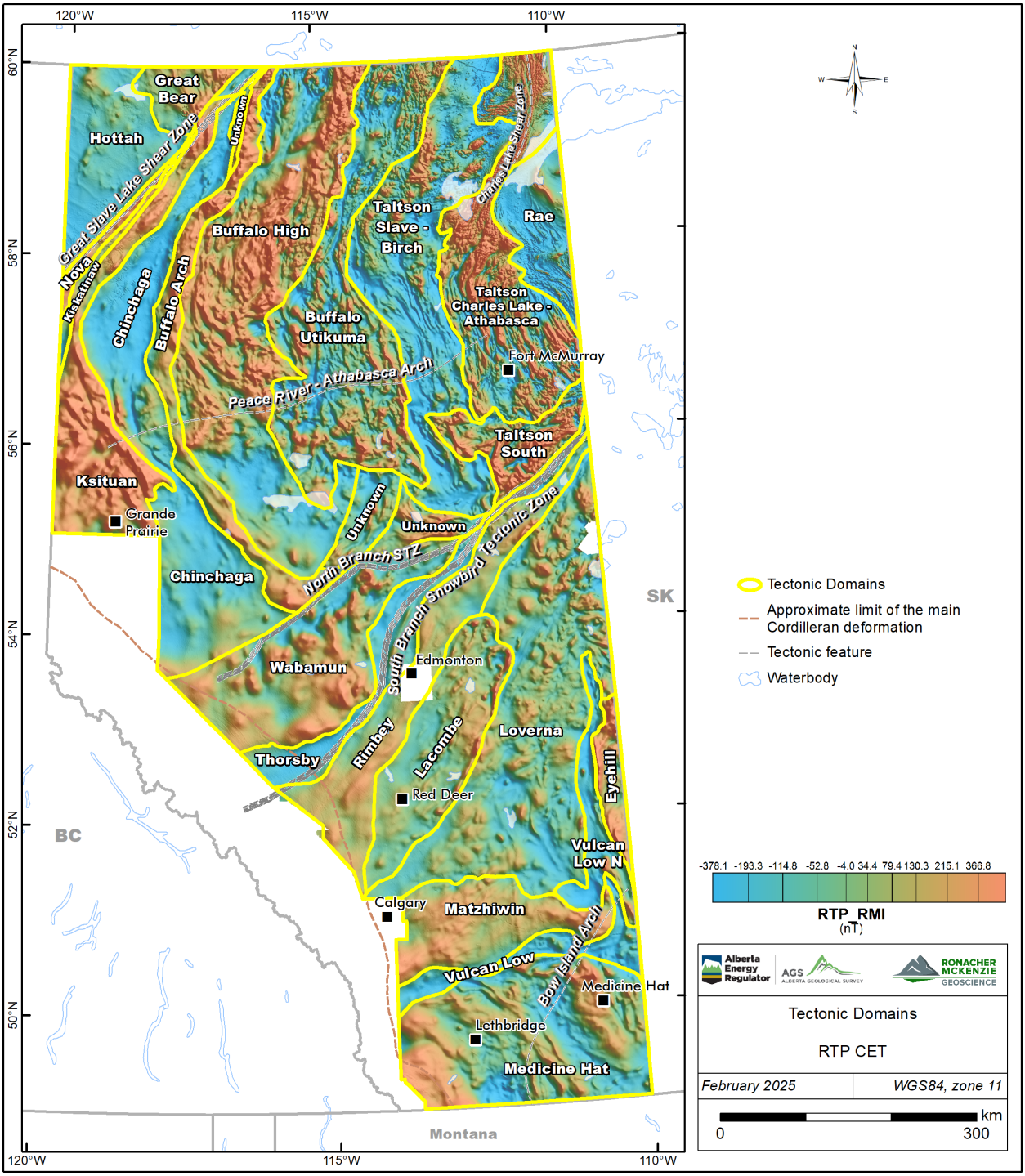

Figure 7-2. Interpreted domain boundaries in Alberta modified from Pilkington et al. (2000). Selected structural lineaments (grey) are from Pană et al. (2021). Background image: RMI reduced to pole, CET.

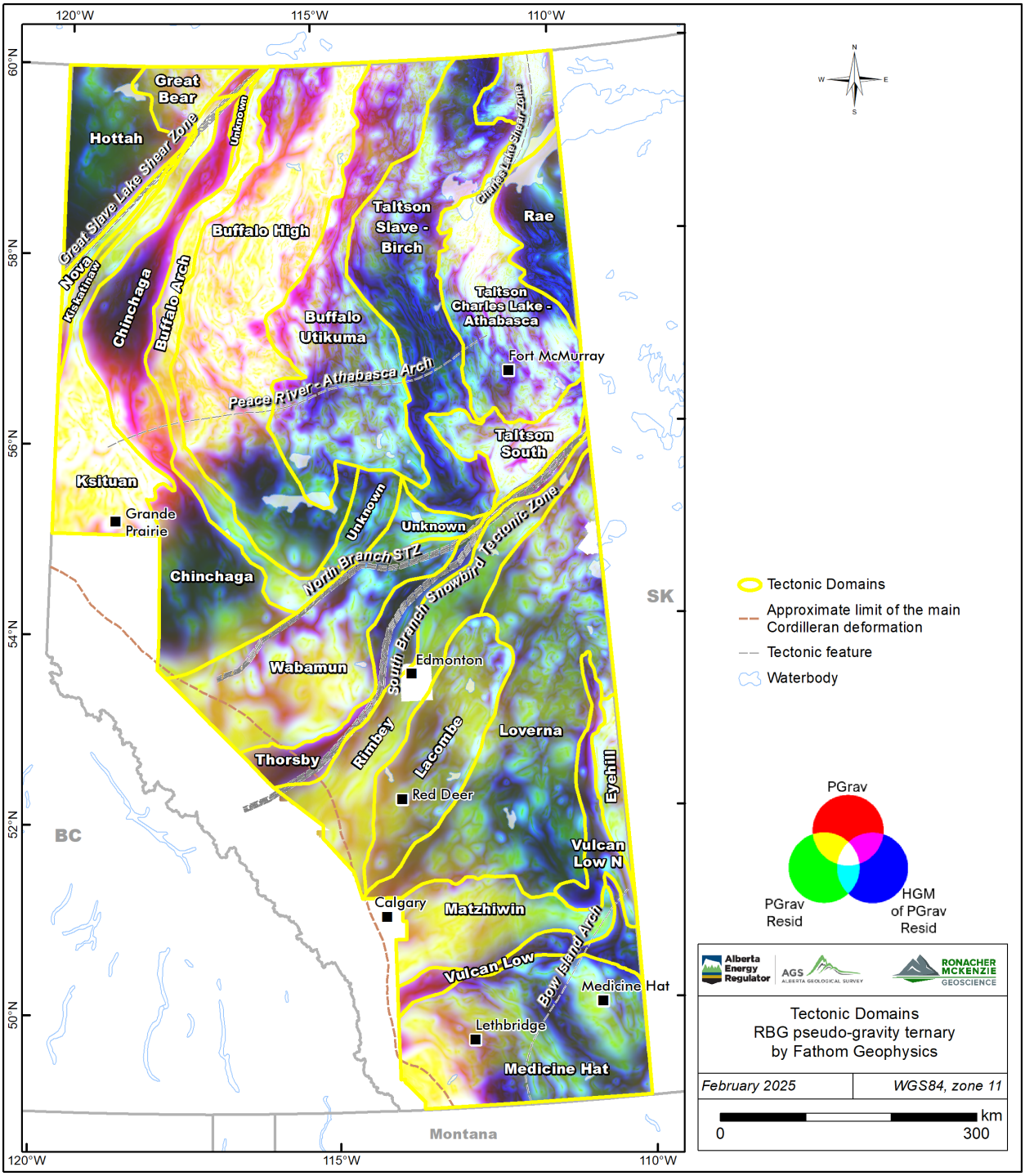

Figure 7-3. Interpreted domain boundaries in Alberta modified from Pilkington et al. (2000). Selected structural lineaments (grey) are from Pană et al. (2021). Background image: HGM of residual of pseudogravity ternary by Fathom Geophysics.

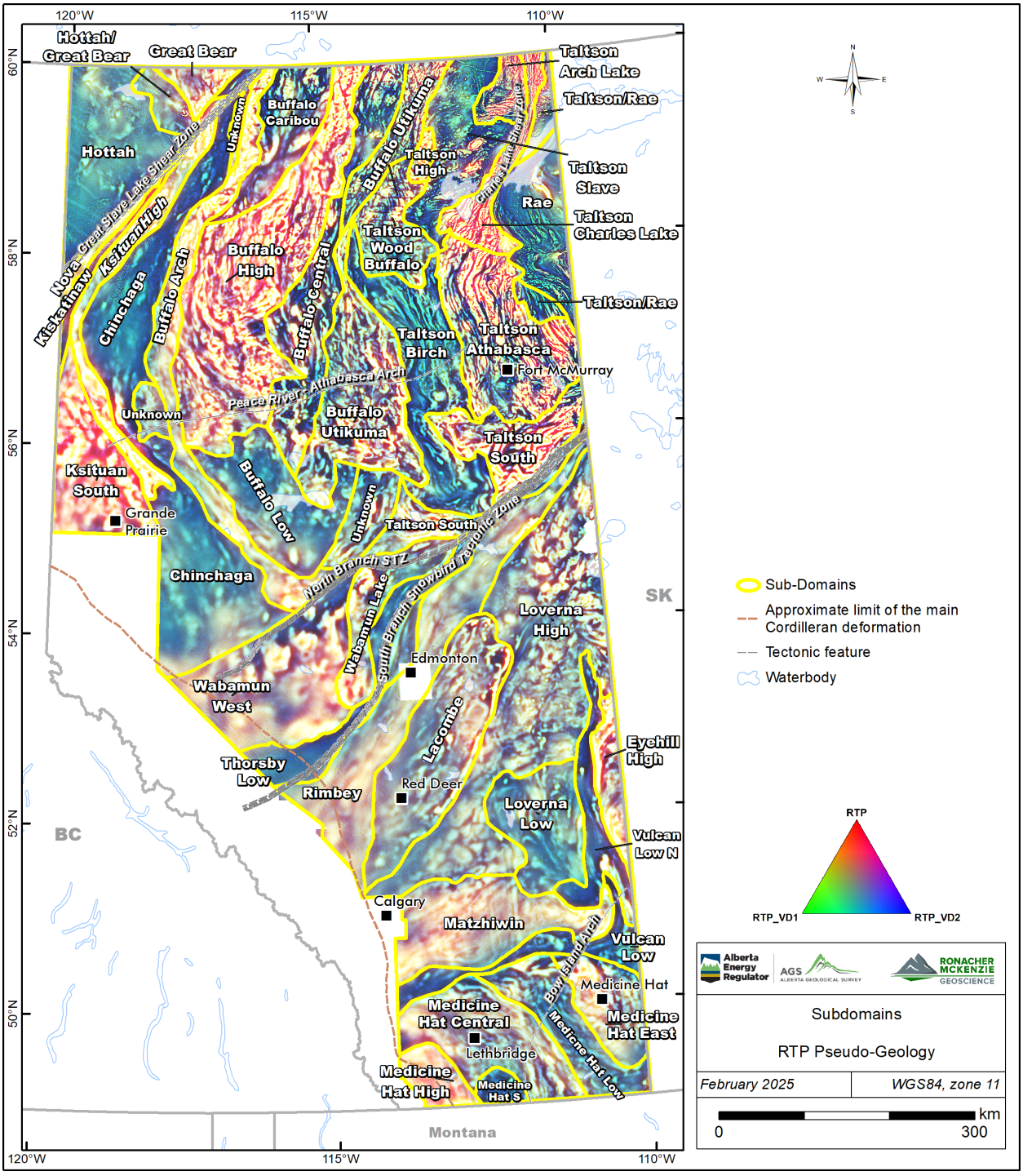

Figure 7-4. Interpreted subdomain boundaries in Alberta defined by this study. Background image: pseudo-geology ternary.

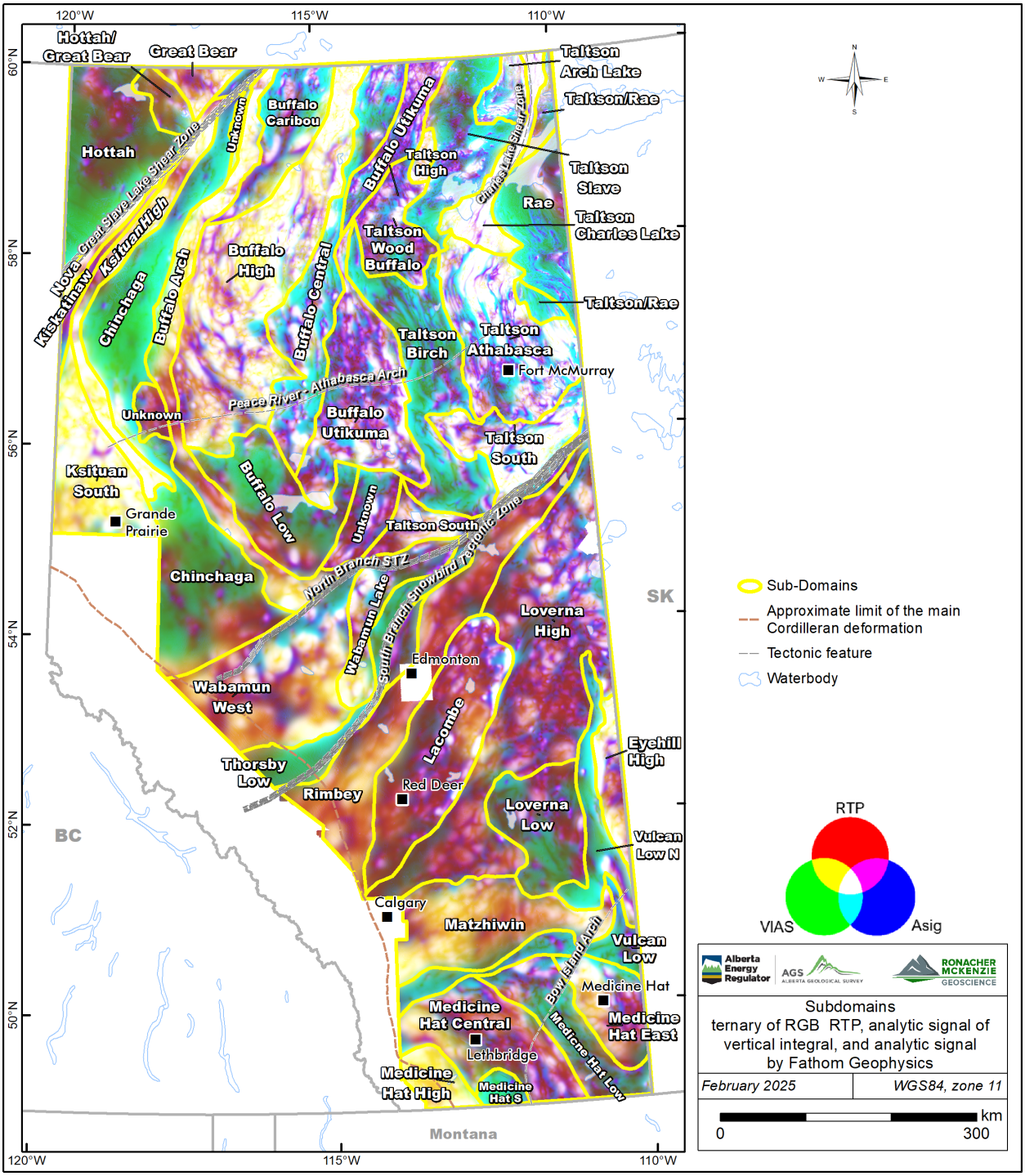

Figure 7-5. Interpreted subdomain boundaries in Alberta defined by this study. Background image: ternary of RGB RTP, analytic signal of vertical integral, and analytic signal by Fathom Geophysics.

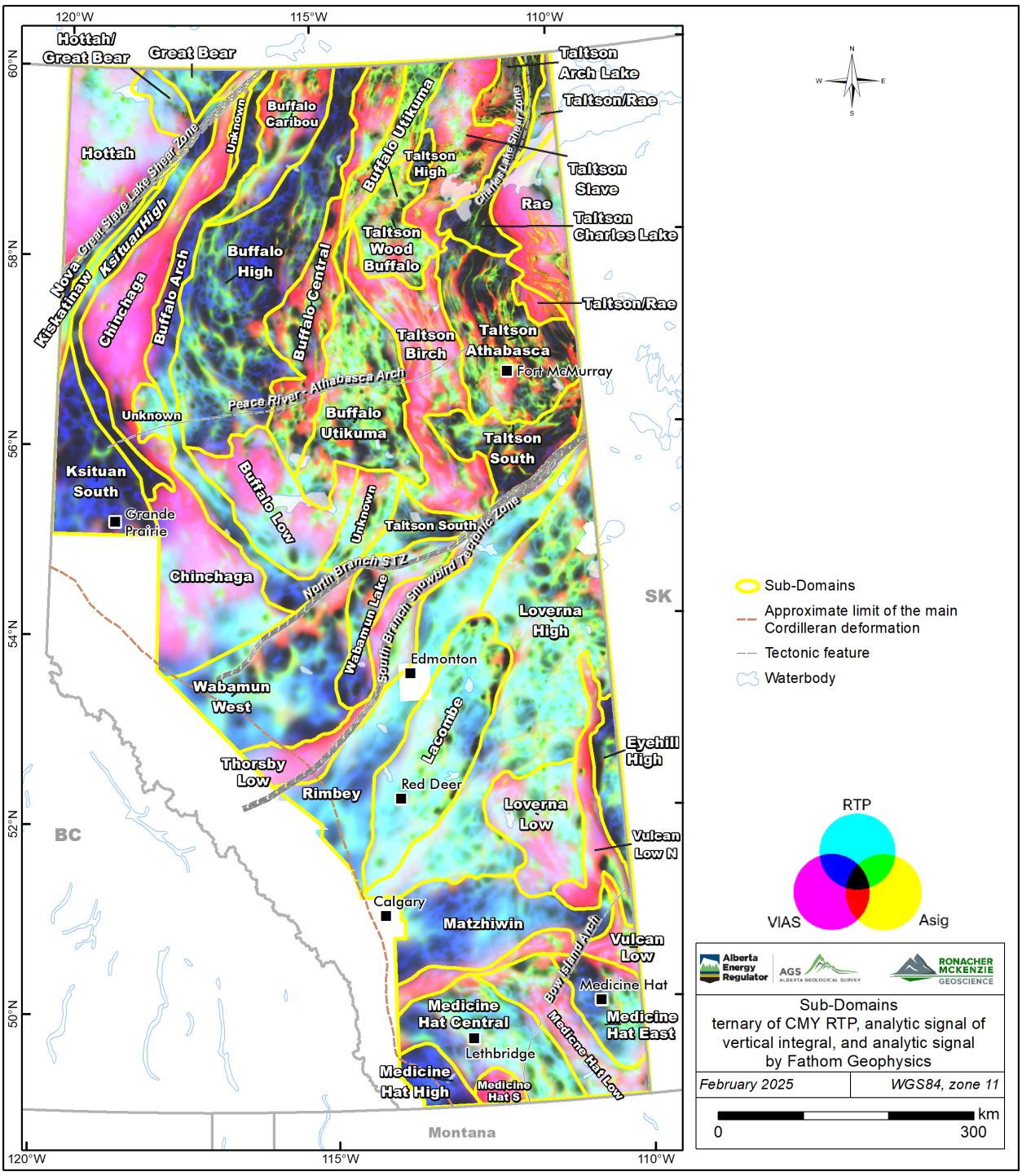

Figure 7-6. Interpreted subdomain boundaries in Alberta defined by this study Background image: ternary of CMY RTP, analytic signal of vertical integral, and analytic signal by Fathom Geophysics. Darkest red colour in Buffalo Caribou, Buffalo Central, Taltson Athabasca, Wabamun, and Vulcan Low domains indicate areas possibly affected by magnetic remanence.

Table 7-1. Characteristics of basement domains and subdomains.

Domain by previous authors[1]	Domain defined in this study[2]	Subdomain defined by this study[2]	Age (Ga)[3]	Type[4]	Magnetic amplitude[2]	General Trend[2]	Magnetic character[2]
Hottah	Hottah		1.8–1.9	Proterozoic accreted terrane	Moderate	NW	Few broad subcircular anomalies, locally grainy with high frequency subcircular moderate anomalies. High frequency broadly spaced NW linear trends.
Great Bear	Great Bear	Great Bear		Continental magmatic arc	Variable, moderate to low	NNW	Broad NNW trends.
		Hottah/Great Bear		Hottah overprinted by Great Bear	Moderate	NW and NNW	Broad NNW and NW trends, grainy with high frequency subcircular moderate anomalies.
Nova	Nova		2.0–2.8	Archean	High	NE	Elongate NNE trends.
Kiskatinaw	Kiskatinaw		1.9–2.0	?	Low	None	Few broad subcircular to oblate anomalies, locally grainy.
Ksituan	Ksituan	Ksituan High	1.9–2.0	Continental magmatic arc	High	NW to NE	N to NE trends in north, broad amplitude NW trend in the south.
		Ksituan South	1.9–2.0	Continental magmatic arc	Variable, high to low	NW and NE	Subcircular and NW elongate anomalies.
Chinchaga	Chinchaga		2.1–2.2	Proterozoic accreted terrane	Variable, moderate to low	NW to NNE	NW to NNE low-amplitude trends.
Buffalo High (western part of Buffalo Head)	Buffalo Arch		2.0–2.2	Magmatic arc	High	NW to NNE	Broad NW to NNE trends and locally without linear trends.
	Buffalo High	Buffalo Caribou	2.0–2.3	Subdomain of Proterozoic accreted terrane	Variable, moderate to low	NNW to NNE	Variable amplitude and frequency signature. N to NNW linear high frequency trends.
		Buffalo High[1]	2.0–2.7	Subdomain of Proterozoic accreted terrane	High	NW to NNE	Three subregions: NW linear trends in the southwest, blocky N-NNW trends in the center, subangular NNE trends in the east with E-trending brittle faults.
Buffalo High	Buffalo High	Buffalo Low	2.3–2.8	Subdomain of Proterozoic accreted terrane	Variable, moderate to low	None	Subcircular anomalies and few NW trends near boundaries.
Buffalo Utikuma (eastern part of Buffalo Head)	Buffalo Utikuma	Buffalo Central	2.0–2.6	Subdomain of Proterozoic accreted terrane	Variable, high to low	NNW to NNE	Variable grain. NW to NNW trends in the south, NW to NNE trends in the north. Some subcircular and oblate anomalies. Several zones of remanence.
		Buffalo Utikuma			Variable, high to moderate	None, NNW	Variable grain; weakly elongate NNW trends in

Domain by previous authors[1]	Domain defined in this study[2]	Subdomain defined by this study[2]	Age (Ga)[3]	Type[4]	Magnetic amplitude[2]	General Trend[2]	Magnetic character[2]
							south, lineated NNE trends in the north.
Taltson		Taltson Arch Lake	1.9	Continental magmatic arc	Variable, very high to low	EW and NNE	Oblate to linear EW trends in the south, and N to NNE linear trends in the north and edges.
	Taltson Charles Lake - Athabasca	Taltson Charles Lake		Continental magmatic arc	Variable, very high to low	NE to NNE	Strong anastomosing NE to NNE linear trends.
		Taltson Athabasca	1.9-2.7	Continental magmatic arc	Variable, high to low	NNW to NE	Strong curvilinear high-amplitude and anastomosing NNW to NNE linear trends.
		Taltson/Rae	1.9	Continental magmatic arc	Low to moderate	None	Grainy with subcircular moderate anomalies, and broad NE trends at boundary with the Rae domain.
	Taltson South		1.9-2.8	Continental magmatic arc	Variable, very high to low	ENE to NNE	Refolded fabric with folds trending from ENE to NE.
	Taltson Slave - Birch	Taltson Slave	1.9	Continental magmatic arc	Variable, moderate to low	None	Strong and significant number of subcircular anomalies in the south. Fewer subcircular anomalies and local N linear trends.
		Taltson Wood Buffalo		Continental magmatic arc	Variable, high to low	NNW	Broad NNW to N linear trends, crosscut by E-trending brittle faults. Better defined NNW trends in the north.
		Taltson High		Continental magmatic arc	High	None	Broad anomaly. No linear trends.
Taltson	Taltson Slave-Birch	Taltson Birch	1.9-2.7	Continental magmatic arc	Variable, high to low	NNW	Strong curvilinear low-amplitude and anastomosing NW- N - NNW linear trends. Zones of remanence.
		Taltson/Rae	1.9	Continental magmatic arc	Low to moderate	None	Grainy with subcircular moderate anomalies, and broad NE trends at boundary with the Rae domain.
Rae	Rae			Archean	Variable, high to low	NW to NE	Strong parallel high frequency linear trends, two subregions: tight folded in the south with fold trending NW and linear trends curving from NW to NNE trends in the north.
Wabamun	Wabamun	Wabamun Lake	2.3	Proterozoic accreted terrane	Variable, high to low	NNW & NE	NE-trending elongate subdomain with rounded boundaries and internal anastomosing linear trends
		Wabamun West				None	Strong large subcircular anomalies bounded

Domain by previous authors[1]	Domain defined in this study[2]	Subdomain defined by this study[2]	Age (Ga)[3]	Type[4]	Magnetic amplitude[2]	General Trend[2]	Magnetic character[2]
							magnetically by low linear trends.
Thorsby	Thorsby	Thorsby Low	1.9–2.4	Remnant of Proterozoic oceanic lithosphere Trough[2] (?)	Low	NNE to none	Strong parallel NE trends curving to the NNE in south boundaries.
		Thorsby High			High	NNE	Crescent-shaped magnetic high trending to the NNE.
Rimbey	Rimbey		1.8	Continental magmatic arc	Variable, high to moderate	NNE	Subcircular anomalies and few NE trends at boundaries.
Lacombe	Lacombe			Proterozoic metavolcanic rocks sequence	Variable, high to moderate, locally low	NNE to NE	Moderate to low intensity, NNE to NE internal fabric, bounded in the east by a narrow magnetic high ridge.
Loverna	Loverna	Loverna High	1.8–2.7	Archean block of Hearne Province	Variable, high to low	NE to ENE	Broad subcircular moderate anomalies and NE trends along western margin.
		Loverna Low			Low	NNW to NNE	Dominantly low magnetic signature with sparse NNW to NNE magnetic high trends, and circular magnetic highs in the north.
Matzhiwin	Matzhiwin		2.6	Magmatic arc[5]	High	ENE	Moderate-intensity, high magnetic signature with little internal fabric.
Vulcan Low	Vulcan Low		2.6		Low	ENE	Northern component of Vulcan Low. Dominantly low magnetic signature, and sparse N-trending magnetic high ridges
	Vulcan Low North[2]				Low	NW to N	Northern component of Vulcan Low. Dominantly low magnetic signature, and sparse N-trending magnetic high ridges
Eyehill	Eyehill		2.6	Archean block of Hearne Province	High	NE	Internally high to moderate magnetic intensity with NE trends. Western edge is a NNW to N-trending magnetic high ridge.
Medicine Hat	Medicine Hat	Medicine Hat High	1.8–2.7	Archean block of Hearne Province	High	None	A homogeneous, high magnetic response.
		Medicine Hat South			Low	None	A large round magnetic low.
		Medicine hat Central			Variable, high to low	NW to NNW	Moderate magnetic signature, ample NNW- and NW-trending magnetic fabrics at various intensities that occasionally appear to be overlapping.
		Medicine Hat Low			Low	NW, N and NE	NNW-trending low magnetic signature.

Domain by previous authors[1]	Domain defined in this study[2]	Subdomain defined by this study [2]	Age (Ga)[3]	Type[4]	Magnetic amplitude[2]	General Trend[2]	Magnetic character[2]
		Medicine Hat East			Variable, high to low	NNW to NNE	High magnetic signature. Locally, north-trending fabrics that deviate into W-trending fabrics are visible.

1. *Domain name according to Villeneuve et al. (1993) Ross et al. (1994) and/or Pilkington et al. (2000)*
2. *This study*
3. *Ages by Ross et al. (1991), Villeneuve et al. (1993), Burwash et al. (1994)*
4. *Type of tectonic domain from structural elements compilation by Pană et al. (2021)*
5. *Type of tectonic domain suggested by Villeneuve et al. (1993)*

The most relevant changes to domain boundaries and characteristics include:

- Redefinition of the Buffalo Head and the Taltson basement domains defined by previous studies as megadomains; redefinition of their boundaries, and new subdivisions within both megadomains.
- Major modifications of the outline and extensive subdivision are proposed for the Buffalo Head megadomain including changes to the Buffalo High and Buffalo Utikuma domains of Pilkington et al. (2000). Identification of the Buffalo Arch domain as a potential magmatic arc, the Buffalo High domain subdivision into three different subdomains, and the Buffalo Central subdomain as a N-trending zone with evidence of remanence separating the Buffalo High from the Buffalo Utikuma domains.
- Major modifications to the outline and extensive subdivision are proposed for the Taltson megadomain into three distinct basement domains, the Taltson Slave-Birch, Taltson Charles Lake – Athabasca, and Taltson South domains as potentially representing three different tectonic settings.
- Introduction of the north-trending component of the Vulcan Low structure as a separate domain (named here as Vulcan Low North domain) between the Loverna and Eyehill domains, possibly linked to the Vulcan Low domain.
- Major boundary modifications to the Loverna domain, particularly to its eastern side, and subdivision of the Loverna domain into the Loverna High and Loverna Low subdomains.

Other changes to domains domain boundaries and characteristics include:

- Subdivision of the Wabamun domain into two subdomains that resemble large intrusions.
- Subdivision of the Thorsby domain into Thorsby Low and Thorsby High subdomains.
- Minor adjustments were made to the following domain boundaries: Hottah, Great Bear, Nova, Kiskatinaw, Chinchaga, Rae, Wabamun, Thorsby, Rimbey, Lacombe, Matzhiwin, and Eyehill domains.
- Definition of four small domains labeled as unknown, two adjacent to the STZ and two between the Chinchaga and Buffalo Arch domains.

- Definition of subdomains with overlapping magnetic signals from adjacent domains, such as the subdomain between the Hottah and Great Bear domains, and between the Rae and Taltson Charles Lake- Athabasca domains.

The higher quality of the 2021-2024 magnetic survey data and derived products allow for the definition of subdomains within known tectonic domains. Decreasing the uncertainties associated with the domain boundaries to refine the interpretation of the architecture of the crystalline basement will require further integration with available geological, petrological, chronological, and magnetic susceptibility data.

The GIS files containing the outlines and details of the new interpreted lithotectonic domains and subdomains are included in the Digital Appendix A.

7.3 Regional Fabric Orientation

The orientation of the magnetic fabric throughout the survey area was determined by Fathom Geophysics (Section 5.3; Appendix 1). The resulting orientations were interpolated and smoothed (Figure 7-7). On Figure 7-7, green areas are dominated by WNW to ENE trends; blue and cyan areas are dominated by NE trends; yellow areas are dominated by NW trends, red and orange areas are dominated by NNW to N trends and magenta indicates N to NNE trends and.

The magnetic fabric orientation unveils five main NE-trending regions and one southernmost area with different internal fabric orientations.

- Zama – Steen River: dominant WNW to ENE trends
- High Level – Wood Buffalo: dominant NNW to NNE trends
- Peace River – Athabasca: dominant WNW to NW trends
- Red Deer – Cold Lake: dominant N to NNE trends, locally variable
- High River - Provost: variable trends
- Lethbridge - Medicine Hat: dominant WNW to ENE trends

The Peace River – Athabasca area is coincident with the axis of the Peace River Athabasca-Arch, which is also coincident with the curvature change (from NW to NE) of the crystalline basement fabric implying that the well-documented Peace River – Athabasca Arch uplift was superimposed upon a pre-existing Precambrian basement geology.

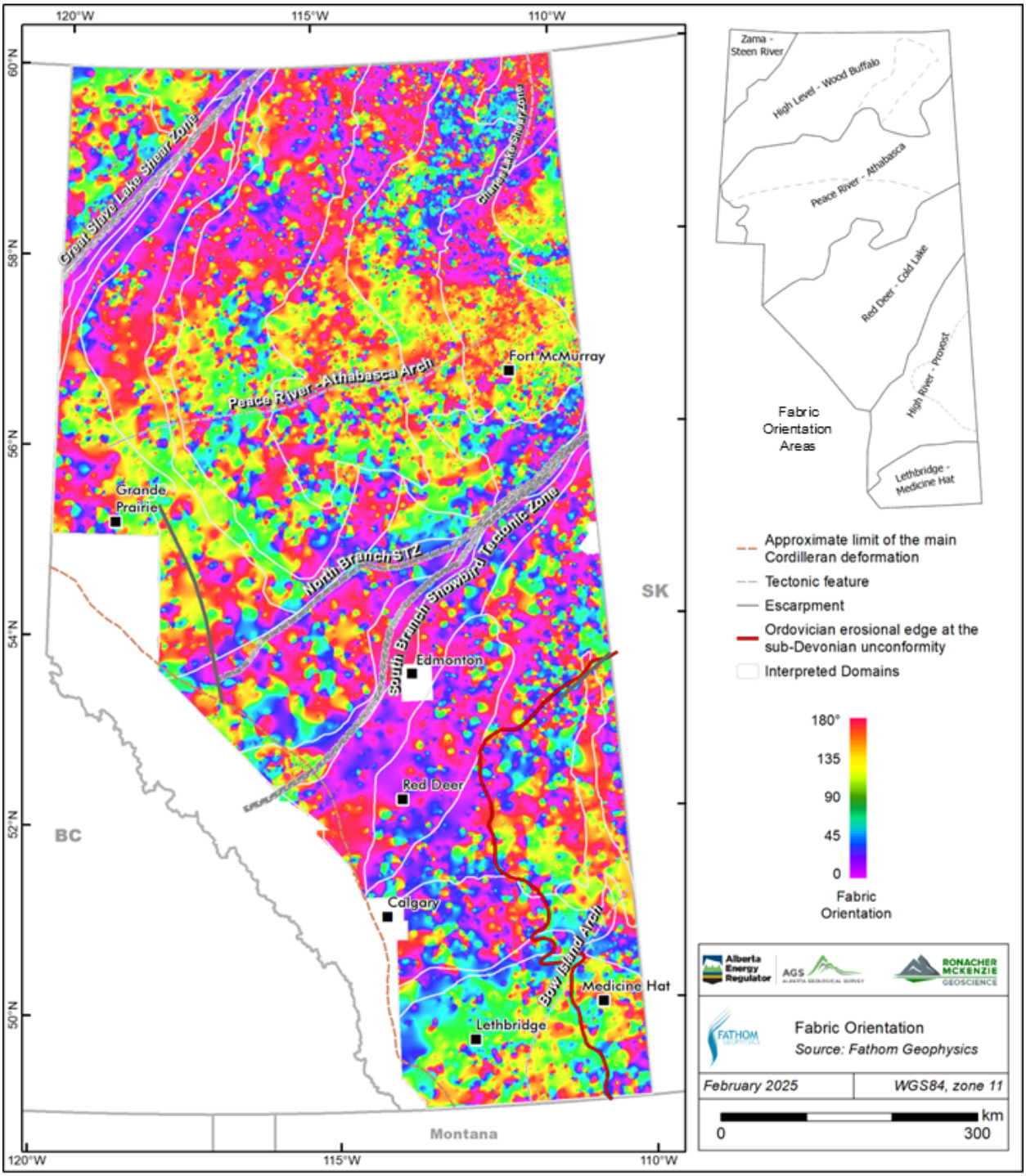

Figure 7-7. Magnetic fabric orientation for Alberta.

7.4 Lineaments

The geological interpretation of magnetic lineaments for the four project areas (Shield, northern, central and southern Alberta) resulted in four separate GIS files containing various types of lineaments with attached additional information in their attribute tables (Lopez et al., 2024a; Lopez et al., 2024b; Brem et al., 2024; Lopez et al., 2025). The merge of interpretation files from these four reports revealed inconsistencies across survey boundaries that required revision and adjustments to various lineaments elsewhere using the new merged grid. Like with the domains, reviewing the data for the entire province rather than for individual areas made the relevance and extension of many features significantly more obvious.

For each survey area, numerous lineaments had been identified and a selection of them had been correlated with the subsurface lineament compilation (Alberta Geological Survey, 2021b). During the merging and reinterpretation across magnetic survey boundaries, lineaments were readjusted and standardized to create a smooth, continuous and consistent interpretation layer of Alberta. The merged attribute table related to lineaments was also standardized across survey areas.

Lineaments were interpreted as ductile shear zones, brittle faults, thrusts, boundaries, contacts, fractures, faults (when unclear whether ductile/brittle nature), unconformities, erosional edges, dikes and lineaments (or structural trend). The GIS files containing the interpretation of lineaments and relation to documented structures are included in the Digital Appendix A.

Classification followed known structural elements defined by previous authors wherever possible, whereas many lineaments are defined here for the first time.

Basement faults and structures can impact the sedimentation of the overlying basin. Therefore, RMG attempted to establish whether faults can be delineated in the WCSB using magnetic data and/or whether the magnetic lineaments attributed to basement structures have affected the WCSB sedimentary rocks. The interpretation of faults from magnetic data required the search for lateral offsets in magnetic ridges, changes of form line trends across a lineament, changes in amplitude or frequency across a lineament, and attenuation of magnetic signature to infer uplifted and down-dropped blocks. In addition, the fabric-parallel and fabric-crossing structure detection products by Fathom Geophysics (Digital Appendix C) were used to support lineament interpretations. The fabric-parallel features tend to be contacts or shear zones, whereas the cross structures are more likely faults. Whether these faults occur in the basement or the WCSB is challenging to determine. Faults interpreted from upward continued products can help to determine the structural level, however the best method to determine their existence is the correlation with additional information from seismic, structural contours, stratigraphic, and morphological data.

Key interpreted lineaments were also correlated at a high-level with available results from Lithoprobe seismic studies, stratigraphic thickness changes, erosional edges of WCSB modelled units from the AGS 3D geological model (Alberta Geological Survey 2021a), and other studies (e.g., Burwash et al., 2000b)

The most relevant interpreted lineaments identified are described in the subsections below (Figure 7-8 and Figure 7-9). Other interpreted lineaments can be found in the GIS files enclosed with this report (Digital Appendix A).

7.4.1 Charles Lake Shear Zone

The Charles Lake shear zone in northeastern Alberta (McDonough et al., 2000; Figure 7-8 and Figure 7-9) consists of a NNE-trending anastomosing system of sheared rocks overprinted by parallel brittle faults. Deformation zones include mostly broad areas of demagnetization due to magnetite destruction possibly related to low-grade metamorphism or alteration, and some narrow areas of magnetization due to magnetite addition possibly related to contact metamorphism or magnetite mineralization. In the southern end of the project area, sheared rocks of the Charles Lake shear zone curve towards the south-southeast following the edge of the Athabasca Basin where it dips to the east, and to the south and southwest into the Taltson Athabasca domain where branches of the shear zone open, resembling horse-tail splays. Further description about this shear zone is found in Lopez et al. (2024a, 2024b).

7.4.2 Leland Lake Shear Zone

The Leland Lake shear zone is a continuous NNE-trending magnetic high curved lineament separating the Arch Lake and Slave granitoids of the Taltson domain in northwestern Alberta. This lineament is a known shear zone (McDonough et al., 2000) and the new magnetic data provides more detail about its geometry. The magnetic data indicates that this shear zone dips towards the west. Further description of this shear zone is found in Lopez et al. (2024a).

7.4.3 Andrew Lake Shear Zone

In the Andrew Lake area in northern Alberta, a continuous linear feature, is characterized by a magnetic low that separates the Rutledge River complex in the west from the Andrew Lake granitoids in the east. The automatic detection results indicate that the Charles Lake shear zone splits into two branches and the dominant eastern branch extends into the Andrew Lake area. Structure detection results for longer wavelengths indicates that this zone is possibly a major boundary. Further description of this shear zone is found in Lopez et al. (2024a).

7.4.4 Beatty River Fault

The Alberta extension of the Beatty River Fault (“BRF”) in Saskatchewan is mentioned in at least one report (e.g., Ramaekers, 2004) but not included in more recent structural compilations (e.g., Pană et al., 2021; Alberta Geological Survey 2021b). In the magnetic products, the BRF is a complex system of E-, WSW- and NW-trending lineaments at the southern edge of the Athabasca Basin (Figure 7-8 and Figure 7-9). The E-trending lineament is interpreted as a major shear zone that runs parallel to the southern edge of the Athabasca Basin. This E-trending structure dextrally offsets the splays of the Charles Lake shear zone. The NW-trending lineaments abut the E-trending shear zone and the eastern branch of the Charles Lake shear zone. Further description of this shear zone is found in Lopez et al. (2024b).

7.4.5 Great Slave Lake Shear Zone and McDonald -Hay River Fault

The Great Slave Lake shear zone ("GSLSZ") in northwest Alberta presents as a NE-trending magnetic high with subsidiary lineaments with an estimated width of up to 30 km from the northern branch that separates the Hottah and Nova domains, to the southwest boundary of the magnetic low that defines the Kiskatinaw domain (Figure 7-8 and Figure 7-9). Several N060E-oriented lineaments are present on either side of the GSLSZ. Lineaments with this orientation have been reported and are commonly interpreted as normal faults in the sedimentary stack and at basement level (Pană et al., 2021). Eaton and Hope (2003) postulated that the gravity high anomaly along this lineament represents either uplifted deeper crustal material within the shear zone, or the protolith is different from surrounding wall rocks. In our work, we interpreted the broad magnetic high anomaly as the Nova domain (see section 7.2.3) as uplifted and affected by this shear zone. Further description of this shear zone is found in Lopez et al. (2024b). The new gravity products display a gravity lineament colinear with the GSLSZ which is interpreted here as the McDonald – Hay River Fault.

7.4.6 High Level Shear Zone

The newly defined High Level shear zone is a 250 km lineament in northwest Alberta (Lopez et al., 2024b; Figure 7-8 and Figure 7-9). A dextral sense of shear with 40 km of dextral offset is interpreted by correlating distinct magnetic signatures across the lineament. The High Level shear zone is bound to the west by uninterrupted magnetic lineaments that are associated with the Great Slave Lake shear zone. To the east, the shear zone cannot be confidently traced into the Taltson megadomain.

On a regional scale, the High Level shear zone does not offset Phanerozoic bedrock geology nor is there a distinct spatial correlation with any of the 3D modeled horizons (Alberta Geological Survey, 2019), suggesting that this prominent shear zone is restricted to the crystalline basement. However, further studies are needed to understand this shear zone. Further description about this shear zone is found in Lopez et al. (2024b).

7.4.7 Utikuma Trend

The newly defined Utikuma Trend is a ENE-trending lineament in northern Alberta crosscutting the Chinchaga domain, Buffalo Head megadomain, and Taltson Slave – Birch domain (Figure 7-8 and Figure 7-9). This lineament coincides with the boundary between subdomains such as Buffalo High and Buffalo Low. The lineament is evident in various magnetic products particularly ternary images and cross-structure products suggesting a brittle structure. Magnetic amplitude is either attenuated to the south of this lineament or demagnetization has occurred possibly related to the STZ.

7.4.8 Snowbird Tectonic Zone (STZ)

Across central Alberta, the magnetic products exhibit the STZ as a NE-trending narrow zone or belt of parallel linear features within the Thorsby domain (Figure 7-8 and Figure 7-9). A northern branch of the STZ separates the Wabamun domain from the Chinchaga domain (Figure 7-2 to Figure 7-7). The STZ separates the refolded Taltson South domain and unknown domains in the north from NE-trending domains in the south suggesting

the STZ as a collision feature responsible for the deformation of Taltson megadomain between the Hearne and Rae provinces which is consistent with the interpretation of Berman et al. (2007).

7.4.9 Red Deer Trend

The Red Deer trend corresponds to the Red Deer Trend of Villeneuve et al. (1993) and the Red Deer High of Hope and Eaton (2002). The Red Deer trend is a NE-trending narrow positive magnetic ridge marking the boundary between the Lacombe and Loverna domains (Figure 7-8 and Figure 7-9). To the northeast, the magnetic high that represents the Red Deer trend ends, however, the trend possibly extends as a fault that runs through the Loverna High subdomain. To the southwest it also ends but it appears to continue as a fault that merges with the Rimbey domain. In this work the Red Deer trend is interpreted as a ductile thrust zone with a dextral component. Further description about this shear zone is found in Lopez et al. (2025).

7.4.10 Eyehill Trend

The Eyehill trend is a curvilinear NNW- to N-trending continuous magnetic high flanking the western part of the Eyehill domain (Figure 7-8 and Figure 7-9). This lineament corresponds to the margin of the Eyehill High domain of Villeneuve et al. (1993) and the Eyehill High magnetic high of Hope and Eaton (2002). The internal magnetic fabric trends in the Eyehill domain are oblique to the Eyehill trend and bend into the Eyehill trend magnetic high Figure 7-8 and Figure 7-9. The magnetic characteristics of the Eyehill trend are consistent with the interpretation of a shear zone modelled by Hope and Eaton (2002). The 3D inversion conducted by RMG resolves this feature as continuing to depth, vertical or dipping to the east at high angle (Lopez et al., 2025).

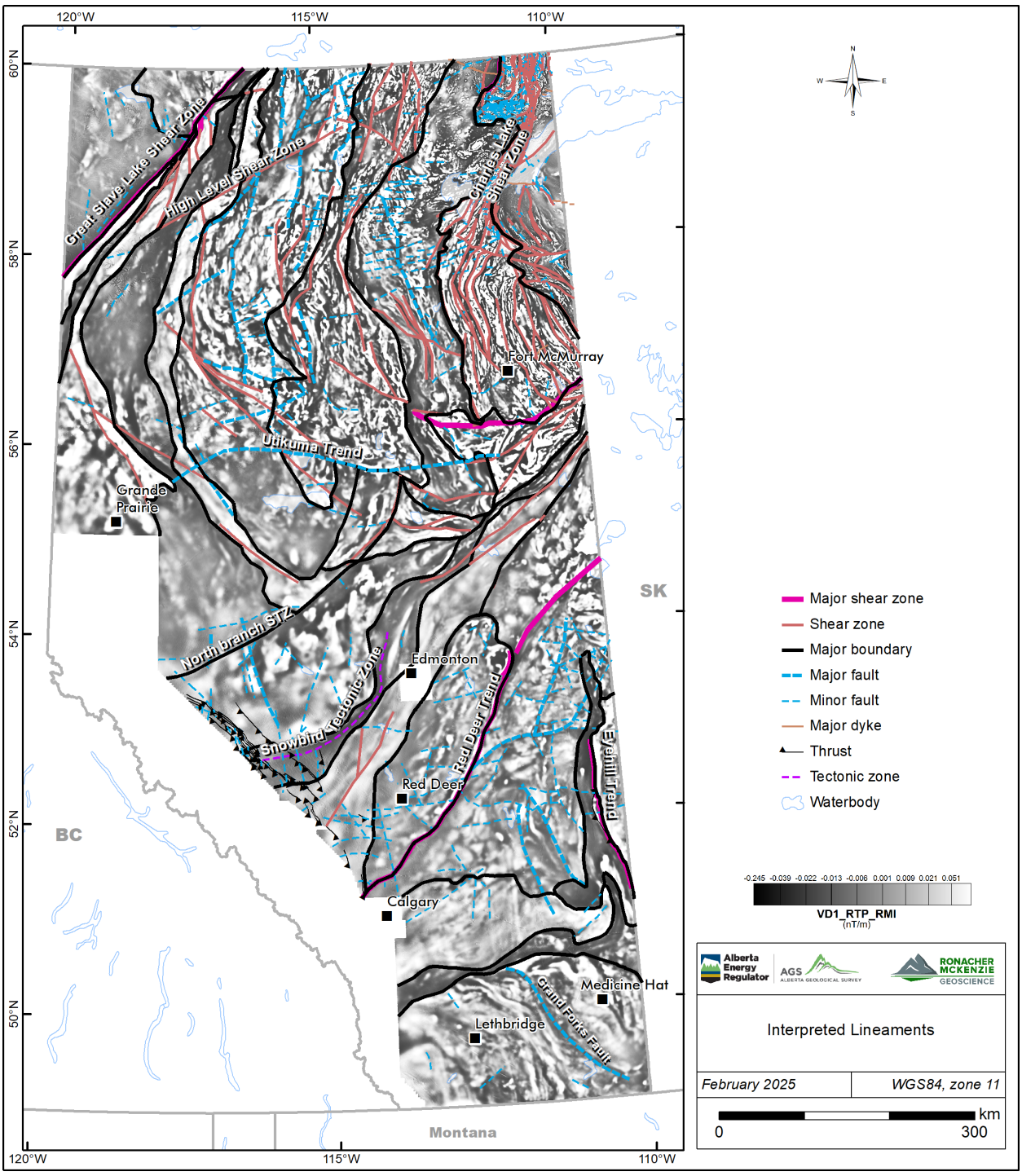

Figure 7-8. Interpreted linear features, including lineaments, faults and shear zones, in Alberta. Background image: first vertical derivative in black and white colour scheme.

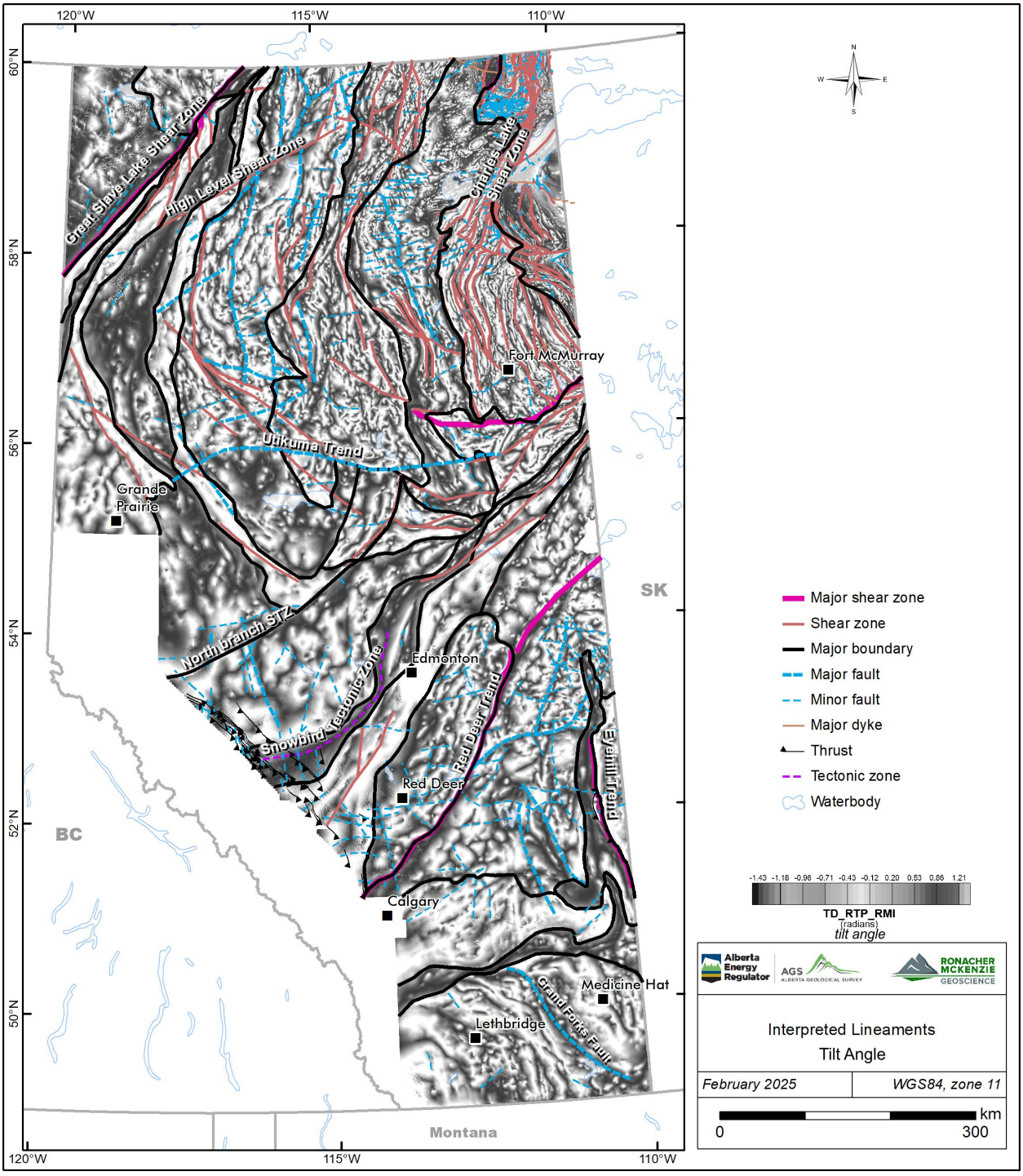

Figure 7-9. Interpreted linear features, including lineaments, faults and shear zones. Background image: tilt angle in black and white colour scheme.

7.5 Intrusions

Intrusion detection was conducted in the project area using a combination of manual examination and automatic radial symmetry detection (Figure 7-10; Section 6.4). Small and rounded magnetic anomalies were identified that can be interpreted as probable intrusive bodies including stocks, cupolas, kimberlites, diatremes, or breccia pipes among other possible interpretations. These anomalies are noted to be circular magnetic highs and lows. Following automatic detection, a manual examination was conducted that included calibration with culture such as urban sites and industry infrastructure, and calibration with the known geology. None of these rounded anomalies had been identified by previous studies.

Anomalies interpreted to be intrusions display the following character:

- single lobe small circular, semi-circular or oblate magnetic anomalies;
- isolated to poorly isolated high frequency smaller (< 5 km^2) circular or asymmetric anomalies;
- larger rounded multi-lobe anomalies;
- larger bodies with rims or concentric zonation patterns; and
- broad anomalies with rounded boundaries and distinct internal texture.

Some new intrusions were recognized along the margins of the merged surveys, however, no new major intrusions were identified.

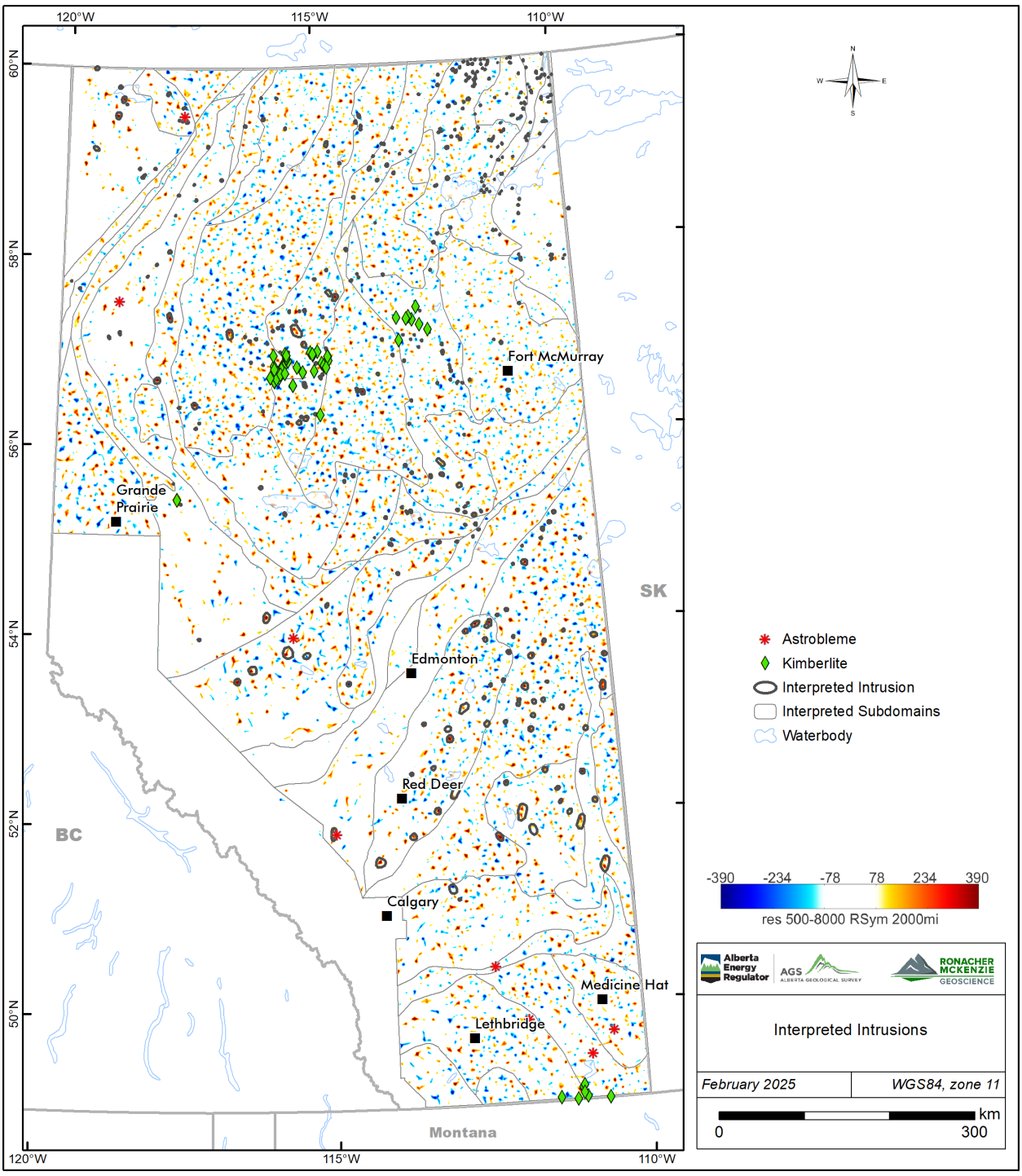

Figure 7-10. Intrusion detection results of the automatic radial symmetry analyses for 2000 m magnitude independent wavelength by Fathom Geophysics (red represents rounded magnetic highs, blue represents rounded magnetic lows, and the colour bar represents radial symmetry (i.e., how radially symmetric is a high or low).

Three of the round anomalies detected correspond to astroblemes. All magnetic filter products show a rounded feature related to the location of the Steen River impact crater in northwest Alberta. The structure is

about 10 km in diameter with a higher amplitude central anomaly and complex internal structure. The outside of the circular structure displays magnetic anomalies in the NW and SE corners. (Lopez et al., 2024b)

The Bow City astrobleme (located southeast of Calgary) is only noted in some of the magnetic filter products as a faint circular ~1 km diameter anomaly that is spatially associated with the Bow City structure location found in Alberta Geological Survey (2021). The Eagle Butte astrobleme (located south of Medicine Hat) has a circular magnetic signature of about 2 km diameter observed on several magnetic filter products. Further descriptions on these two astrobleme-related magnetic anomalies are found in Brem et al. (2024).

8.0 MINERAL POTENTIAL

The exploration for mineral deposits requires thoughtful conceptual targeting that involves the understanding of genetic models in a way that considers mineralization processes in a hierarchical manner from geodynamic setting to deposit-scale (Groves et al., 2022). Knowledge of the tectonic history of Alberta's basement provides the first step towards the identification of prospective settings for mineral deposits.

Each tectonic domain has the potential for hosting particular types of mineral deposits during certain stages of the basement's geodynamic history if certain conditions were met. In addition to a suitable geodynamic setting, a fertile ore-component, a favourable architecture as migration pathway that connects the source to a final trap in the upper crust, and preservation are key requirements to the formation of ore deposits (Kelley et al., 2021).

In this section we propose areas at a regional scale for further mineral prospectivity analyses. This section is speculative, knowledge-based, and created without the assistance of a formal quantitative prospectivity analysis. It intends to highlight the first step of conceptual targeting at a lithospheric scale when applying the mineral systems approach.

The following are some selected commodities that are documented as anomalous in Alberta and that might be associated with a particular basement domain and geodynamic setting.

8.1.1 Helium

Oil and gas fields in Alberta have economic (>0.3%) concentrations of helium (Lyster et al., 2022). Geological models that describe the generation, migration and trapping of radiogenic helium (^{4}He) follow a similar workflow as oil and gas accumulations and require: (1) a source of radioactive uranium-238, uranium-235 and thorium-232 in the crust such as granitic basement rocks, (2) time to accumulate such as in old basement rocks (3) heat and/or deformation event that releases helium from minerals and nitrogen to transport it (primary migration) (4) buoyancy or solution in water and the presence of fracture and/or fault systems that serve as migration pathways for gas and/or fluids (secondary migration), (6) gas accumulation, and (7) trap integrity (Danabalan et al., 2022). A helium accumulation may not necessarily overlie the radioactive source that initially released it.

In Alberta, Archean granitic domains have great potential for generating helium through radioactive decay because of their age. Cordilleran orogenesis may have triggered the release of helium from its granitic source rocks; major basement boundaries, major faults and second order structures may have channeled helium into the upper levels of the crust and from there into supracrustal rocks. Once in the WCSB several migration pathways and sites for accumulation exist that are also pathways for natural gas.

Helium potential in Alberta is in natural gas plays where anomalous and sometimes economic amounts are found. However, significant amounts of helium may still be trapped in the basement or at the base of the WCSB, possibly closer to a major structural pathway above a major Archean granitic terrane (Figure 8-1). Major structures to consider are domain boundaries and internal domain structures linking Archean granitic suites to

a trap at the base of the WCSB. Possible sites for helium accumulation would be Cambrian rocks above the Medicine Hat and Eyehill domains above or near subdomain boundaries and basement faults, and major structures in Proterozoic extensional and wrench settings linking uranium endowed source rocks below with a trap at the base of the WCSB, such as the Taltson Charles Lake-Athabasca domain under the WCSB.

8.1.2 Lithium

Oilfield brines in Alberta have anomalous concentrations of lithium (>50 mg/L), particularly in pools within Devonian strata. The origin of lithium in these brines is still debated but chemical data collected and interpreted by the AGS suggested some of these brines in west-central Alberta formed by the dissolution of halite and mixing with Li-enriched basement- or Cambrian-derived fluids (Huff, 2019). Convergence and collisional orogens might be potential sources of lithium in the basement if they contain synorogenic to late-orogenic granitoids which are prospective source rocks for lithium-cesium-tantalum (LCT) pegmatites. Major basement boundaries and faults, particularly along the Snowbird tectonic zone and the Charles Lake shear zone may have provided pathways for LCT pegmatite emplacement (Figure 8-1).

8.1.3 Uranium

Alberta has the potential for uranium deposits in the Athabasca Basin in the northeast of the province (Figure 8-1) near basement shear zones and unconformities. The southern edge of the Athabasca Basin where the Charles Lake shear zone meets the Beatty River shear zone exhibits structural complexity with several locations where jogs and bends intersect the basal strata and the unconformity of the Athabasca Group; these locations may be conduits for mineralizing fluids (Figure 8-1).

8.1.4 Rare Earth Elements

Niobium-yttrium-fluorine (NYF) pegmatites are characterized by enrichment in Nb, Ti, Y, rare earth elements (REE), Zr, U, Th and F; these pegmatites are considered to be typically associated with metaluminous to peralkaline granitic bodies. NYF pegmatites form in extensional settings from depleted-crust or mantle-derived magmas, highly evolved and fractionated, and are typically emplaced in the roof zone of larger granitic intrusions. The Taltson Slave and Taltson High domains in northeast Alberta are spatially related to extensional features to the south, suggesting these domains may host intrusions related to extension (Figure 8-1). Further tectonic characterization of these domains through basement samples is needed to determine if these domains have the potential to host NYF pegmatites and REE mineralization. Rare earth element anomalies in Slave granitoids suggests potential exist in northeastern Alberta.

8.1.5 Lead and Zinc

The Pine Point district in the Northwest Territories hosts carbonate-hosted lead-zinc Mississippi Valley Type (“MVT”) deposits. It is located along the GSLSZ with individual deposits distributed in linear trends in Paleozoic platform carbonate sequences of the WCSB above basement fault scarps. In northwestern Alberta, lead and zinc mineral occurrences are documented in Devonian platform carbonates proximal to the GSLSZ (Pană, 2003b). Our work demonstrates that the GSLSZ is structurally complex in its middle section, between the High

Level and Steen River shear zones; it has bends and subsidiary faults that may have controlled potential epigenetic Pb-Zn mineralization in brecciated and hydrothermally dolomitized Devonian carbonates during possible GSLSZ reactivation and formation of fault-related scarps during the Mesozoic – Cenozoic Cordilleran orogenesis and foreland basin development. Alternatively, MVT deposits may have formed areas above major reactivated structures of central Alberta where Paleozoic reef complexes also developed (Figure 8-1).

In addition, the potential presence of a rifted arc setting in the Taltson domain opens the potential for clastic-dominated sediment-hosted lead-zinc ("SEDEX") and volcanic massive sulphide ("VMS") lead-zinc deposits. Clastic-dominated sediment-hosted lead-zinc deposits (SEDEX) formed in intracontinental or failed rifts and rifted continental margins. VMS lead-zinc deposits, which are the result of submarine hydrothermal systems, usually formed in extensional zones via the circulation of seawater through the subsurface driven by the heat from underlying magmatism.

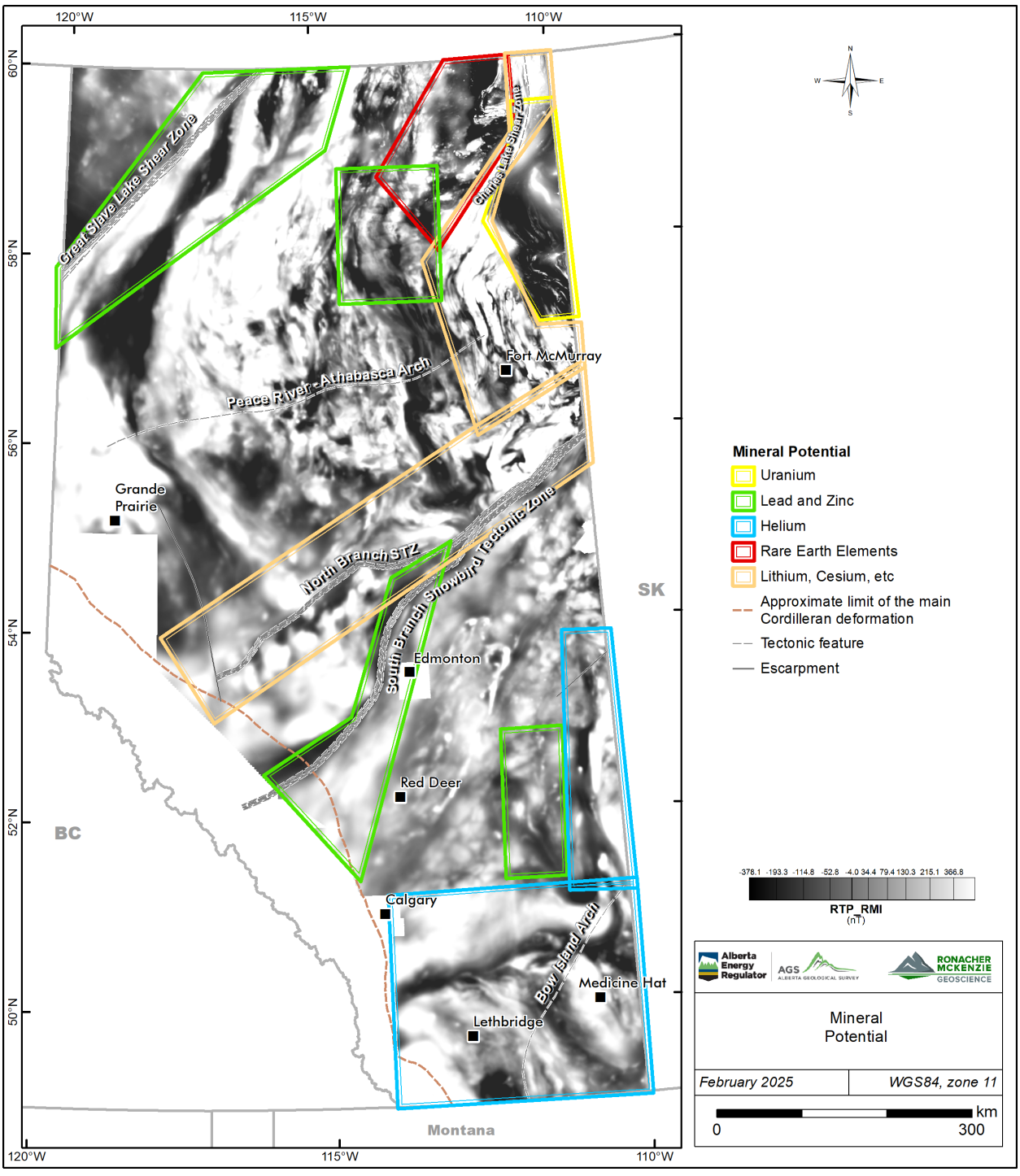

Figure 8-1. Selected areas with critical mineral potential in Alberta.

9.0 CONCLUSIONS

The magnetic filter products and images as well as the automatic detection products derived from the 2021 - 2024 airborne magnetic survey provide new insights into the basement in Alberta and overlying sedimentary sequence. The geological interpretation involved a high-level integration with tectonic elements documented in publications.

Care was taken to recognize cultural artefacts (predominantly oil and gas infrastructure) during the interpretation stage.

Domains in this report refer to areas of distinct magnetic signature and well-defined magnetic boundaries. Subdomains refer to areas of contrasting magnetic signature, but with unclear boundaries. Further integration with historical and newly acquired geochronological data, isotope data, and additional geophysical studies is required to conclude that the magnetic domains herein can be interpreted as tectonic domains involved in the assembly and evolution of western Laurentia.

The following conclusions can be made:

- Modifications to basement domains were made by editing the tectonic domain boundaries of Ross et al. (1994) and Pilkington et al. (2000) and by dividing known domains into subdomains. The higher resolution of the new magnetic data allows for further subdivision of subdomains in the crystalline basement based on variations of internal magnetic fabrics.

- Round anomalies were delineated. These range from small single lobe circular anomalies to larger multi-lobe rounded asymmetrical anomalies and may represent potential intrusions emplaced either in the basement or the WCSB.

- Known ductile structures were recognized, and new regional-scale ductile structures were identified.

- New brittle faults were delineated. Few faults of the WCSB reported in literature display a spatial correlation with the magnetic and gravity lineaments.

- The axis of the Peace River-Athabasca Arch coincides with changes in magnetic fabric orientation from NW to NE observed in most subdomains. This change in fabric orientation possibly relates to the original geometry of the continental margin. Therefore, the rise of the Peace River Arch appears to be related to a basement feature.

- The Snowbird tectonic zone spatially correlates with extensive deformation in the northern block resembling collisional features.

- A number of known kimberlites can be positively identified in the magnetic data as high-frequency circular anomalies. Given the small size of Alberta kimberlites and abundant cultural footprint in the

region, a higher resolution magnetic survey and correlation with infrastructure and imagery are needed to effectively conduct kimberlite detection.

Local interpretations of the magnetic data are required to resolve remaining uncertainties in the geometry of basement structure and gain insights into the shallower structure. In addition, further integration with existing and new petrological, geochronological and rock property data, and integration with regional seismic and magnetotelluric data can improve the interpretation of the nature and architecture of the basement geology.

The interpretation of the new high-quality aeromagnetic data for Alberta corroborated previously defined tectonic domains and identified new structural elements that may help to refine current tectonic models.

10.0 RECOMMENDATIONS

The high quality of the 2021-2024 aeromagnetic data for Alberta allows for improved and detailed interpretations of: the basement geology, structure, paleotopography, and influence of sedimentation patterns and structure in the overlying sedimentary sequence. The magnetic products generated for this work are abundant and suitable for local or case studies to resolve structural uncertainties and better understand both the basement and basin architecture by integrating them with additional information (e.g., seismic data, isopach studies, petrology, lithogeochemistry, geochronology). The following are recommendations to help with the interpretation and correlation with existing geological data:

- Perform localized interpretation studies, or alternatively acquire closer spacing aeromagnetic surveys, to resolve the structural setting within a particular area.
- Reprocess historical gravity products and integrate the findings with the observations from the new magnetic data.
- Integrate with newly acquired geochronological, isotope geochemistry, and additional geophysical studies to conclude that the magnetic domains and subdomains may be interpreted as tectonic domains involved in the assembly and evolution of western Laurentia.
- Conduct local 3D inversions across lineaments of interest to help resolve the 3D architecture of an area. In particular, RMG advises conducting local inversions where additional data exists to better constrain the inversion.
- Create mineral prospectivity maps by deposit type, instead of commodity, that use artificial intelligence algorithms (e.g., machine learning) and the mineral systems approach (favourable geodynamics, architecture, and fertility) to generate risk (or confidence) maps of areas with potential of having generated and preserved mineral deposits.

11.0 REFERENCES

Alberta Geological Survey. 2019. *3D provincial geological framework model of Alberta, Version 2.* Alberta Energy Regulator / Alberta Geological Survey AER/AGS Model 2018-02.

—. 2023. "Alberta Aeromagnetic and Gravity Survey, Southern Alberta, Northern Alberta and Gap + Shield Surveys." (https://geology-ags-aer.opendata.arcgis.com/pages/aeromag-gravity-survey).

Alberta Geological Survey. 2021a. *Geological Framework of Alberta, Version 3 (interactive app and map, methodology, model, dataset, StoryMaps, web maps).* ;Alberta Energy Regulator / Alberta Geological Survey, AER/AGS Interactive Application. <https://gfa-v3-ags-aer.hub.arcgis.com> [January 2025].

Alberta Geological Survey. 2024. *High quality regional airborne geophysical surveys in Alberta, version 3 (data, multiple formats); Alberta Energy Regulator / Alberta Geological Survey.*

Alberta Geological Survey. 2021b. "Structural Elements in the Alberta Plains (interactive app and map)." Alberta Energy Regulator / Alberta Geological Survey, AER/AGS Interactive Application, Interactive App and Map 011, <https://ags.aer.ca/publications/all-publications/iam-011>.

Atkinson, L.A., S.M. Pawley, L.D. Andriashek, G.M.D. Hartman, D.J. Utting, and N. Atkinson. 2020. *Sediment thickness of Alberta, version 2 (gridded data, ASCII format).* AER/AGS Digital Data 2020-0023, Alberta Energy Regulator / Alberta Geological Survey.

Banas, A., D.R. Eccles, and M.B. Dufresne. 2016. "Diamond potential in Alberta: distribution of kimberlite and kimberlite indicator mineral clusters ." Alberta Energy Regulator. AER/AGS Special Report 103, 50 p. .

Berman, R. G., W. J. Davis, and S. Pehrsson. 2007. "Collisional Snowbird tectonic zone resurrected: Growth of Laurentia during the 1.9 Ga accretionary phase of the Hudsonian orogeny." *Geology, v. 35 (10):, p. 911–914.*

Brem, A., G. Lopez, D. McGill, and J. McKenzie. 2024. *Airborne geophysics data analysis and Interpretation, southern Alberta.* Special Report 120, Alberta Energy Regulator / Alberta Geological Survey, AER/AGS, 106 p.

Burwash, R.A., J. Krupička, and J.R. Wijbrans. 2000a. "Metamorphic evolution of the Precambrian basement of Alberta." *The Canadian Mineralogist* 38: p. 423–434.

Burwash, R.A., McGregor, C.R., Wilson, J.A. and O'Connell, S.C. 1994. "Chapter 5: Precambrian Basement." In *Geological Atlas of the Western Canada Sedimentary Basin*, by G.D. Mossop and I. Shetsen (comp.), p. 48-56. Canadian Society of Petroleum Geologists and Alberta Research Council. https://ags.aer.ca/atlas-the-western-canada-sedimentary-basin/chapter-5-precambrian-basement.

Burwash, R.A., T. Chacko, K. Muehlenbachs, and Y. Bouzidi. 2000b. "Oxygen isotope systematics of the Precambrian basement of Alberta: implications for Paleoproterozoic and Phanerozoic tectonics in northwestern Alberta." *Canadian Journal of Earth Sciences* 37: p.1611-1628.

Danabalan, D., J.G. Gluyas, C.G. Macpherson, T.H. Abraham-James, J.J. Bluett, P.H. Barry, and C.J. Ballentine. 2022. "The principles of helium exploration." *Petroleum Geoscience, v. 28, Issue 2. petgeo2021-029* 13 p.

Dufresne, M.B., D.R. Eccles, B. . McKinstry, D.R. Schmitt, M. Fenton, J.G. Pawlowicz, and W.A.D. Edwards. 1996. "The diamond potential of Alberta." Alberta Energy, AE/AGS Bulletin 63, 164 p.

Eaton, D.W., and J. Hope. 2003. "Structure of the crust and upper mantle of the Great Slave Lake shear zone, northwestern Canada, from teleseismic analysis and gravity modeling ." *Canadian Journal of Earth Sciences, v. 40,* p. 1203–1218.

Eaton, D.W., B. Milkereit, G.M. Ross, E.R. Kanasewich, W. Geis, D.J. Edwards, L. Kelch, and J. Varsek. 1995. "Lithoprobe basin-scale profiling in central Alberta: influence of basement on the sedimentary cover." *Bulletin of Canadian Petroleum Geology* 43: p. 65-77.

Eaton, D.W., G.M. Ross, and J. Hope. 1999. "The rise and fall of a cratonic arch: a regional perspective on the Peace River Arch, Alberta." *Bulletin of Canadian Petroleum Geology* 47 (No. 4): p. 346–361.

Eccles, D. R., E. C. Grunsky, M. Grobe, and Weiss. J. A. 2002. *Structural-emplacement model for kimberlitic diatremes in northern Alberta.* Alberta Energy and Utilities Board, ARC/AGS, Earth Sciences Report 2000-01, 114 p.

Eccles, D.R. 2011. "Northern Alberta kimberlite province: the first 20 years. ." Energy Resources Conservation Board, ERCB/AGS Bulletin 65, 119 p.

Edwards, D.J., and J.R. Brown. 1999. "Understanding the influence of Precambrian crystalline basement on Upper Devonian carbonates in central Alberta from a geophysical perspective." *Bulletin of Canadian Petroleum Geology, v. 47, 4,* p. 412-438.

Edwards, D.J., H.V. Lyatsky, and R.J. Broten. 1998. "Regional interpretation of steep faults in the Alberta Basin from public-domain gravity andmagnetic data: an update." *CSEG Recorder* 23, No.1.

Groves, D.I., M. Santosh, D. Müller, L. Zhang, J. Jun Deng, L-Q. Yang, and Q-F. Wang. 2022. "Mineral systems: Their advantages in terms of developing holistic genetic models and for target generation in global mineral exploration." *Geosystems and Geoenvironment, v. 1(1),* p. 2772-8838.

Hoffman, P.F. 1989. "Precambrian geology and tectonic history of North America; in The geology of North America–an overview." *A.W. Bally and A.R. Palmer (ed.), Geological Society of America v. A,* p. 447–512.

Hoffman, P.F. 1988. "United plates of America, the birth of a craton, Early Proterozoic assembly and growth of Laurentia." *Annual Review of Earth and Planetary Science Letters* 16: p. 543–603.

Hope, J., and D. Eaton. 2002. "Crustal structure beneath the Western Canada Sedimentary Basin: constraints from gravity and magnetic modelling; ." *Canadian Journal of Earth Sciences, v. 39,* p. 291– 312.

Hope, J., D.W. Eaton, and G.M. Ross. 1999. "Lithoprobe seismic transect of the Alberta Basin: Compilation and overview." *Bulletin of Canadian Petroleum Geology* 47, No. 4: p. 331-345.

Huff, G.F. 2019. "Origin and Li-enrichment of selected oilfield brines in the Alberta Basin, Canada. ." Alberta Geological Survey / Alberta Energy Regulator, AER/AGS Open File Report 2019-01, 29 p. .

Isles, D. J., and L. R. Rankin. 2013. *Geological interpretation of aeromagnetic data.* Australian Society of Exploration Geophysicists, 365 p.

Kelley, K.D., D.L. Huston, and J.M. Peter. 2021. "Toward an effective global green economy: the Critical Minerals Mapping Initiative (CMMI)." *SGA News, 8* p. 1-5.

Kovesi, P. 2015. *Good Colour Maps: How to Design Them (colorcet.com).* Accompanying Document, Crawley, Western Australia: Centre for Exploration Targeting, The University of Western Australia. (https://colorcet.com/).

Lemieux, S., Ross, G.M. and Cook, F.A. 2000. "Crustal geometry and tectonic evolution of the Archean crystalline basement beneath the southern Alberta Plains, from new seismic reflection and potential field studies." *Canadian Journal of Earth Sciences, v. 37* p. 1473–1491.

Lopez, G., D. McGill, and J. McKenzie. 2024a. *Airborne geophysics data analysis and interpretation, Canadian Shield, northeastern Alberta.* Special Report 119, Alberta Energy Regulator / Alberta Geological Survey, AER/AGS, 111 p.

Lopez, G.P., A. Brem, D. McGill, and J. McKenzie. 2024b. *Airborne geophysics data analysis and interpretation, northern Alberta.* Special Report 122, Alberta Energy Regulator / Alberta Geological Survey, AER/AGS, 153 p.

Lopez, G.P., D. McGill, A. Brem, and J. McKenzie. (2025, in preparation). *Airborne geophysics data analysis and interpretation, central Alberta.* Special Report, Alberta Energy Regulator / Alberta Geological Survey, AER/AGS.

Lyatsky, H.V., D.I. Pană, and M. Grobe. 2005. "Basement structure in central and southern Alberta; insights from gravity and magnetic maps." Alberta Energies and Utilities Board/Alberta Geological Survey, Special Report 72, 83 p.

Lyster, S., G.P. Lopez, and S. Poulette. 2022. "Geochemistry data of lithium-bearing groundwater in the Alberta Basin compiled from multiple sources (tabular data, tab-delimited format)." Alberta Energy Regulator / Alberta Geological Survey Digital Data 2021-0021.

Mazur, M.J. 1999. "Seismic characterization of meteorite impact craters." M.Sc. Thesis, University of Calgary, 176 p.

McDonough, M.R., V.J. McNicoll, E.M. Schetselaar, and T.W. Grover. 2000. "Geochronological and kinematic constraints on crustal shortening and escape in a two-sided oblique-slip collisional and magmatic orogen, Paleoproterozoic Taltson magmatic zone, northeastern Alberta ." *Canadian Journal of Earth Sciences v. 37, no. 11,* p. 1549–1573.

McGregor, M., E., E. Walton, C. Mcfarlane, and J. Spray. 2020. "Multiphase U-Pb geochronology of sintered breccias from the Steen River impact structure, Canada: Mixed target considerations for a Jurassic-Cretaceous boundary event." *Geochimica et Cosmochimica, v. 274,* p. 136-156.

Misra, K.S., V.R. Slaney, D. Graham, and J. Harris. 1991. "Mapping of basement and other tectonic features using SEASAT and Thematic Mapper in hydrocarbon-producing areas of the Western Sedimentary Basin of Canada." *Canadian Journal of Remote Sensing v. 17, 2,* p.137-151.

Molak, B., S.A. Balzer, R.A. Olson, and E.J. Waters. 2001. "Petrographic, mineralogical and lithogeochemical study of core from three drillholes into the Steen River structure, northern Alberta;. Earth Sciences Report 2001-04." Earth Sciences Report 2001-04, Alberta Energy and Utilities Board, EUB/AGS, 89 p.

Mossop, G.D., and I. Shetsen. 1994. "Geological Atlas of the Western Canada Sedimentary Basin." *Alberta Geological Survey.* Canadian Society of Petroleum Geologists and Alberta Research Council. Accessed October 30, 2023. https://ags.aer.ca/reports/atlas-western-canada-sedimentary-basin.

O'Connell, S.C. 1994. "Geological history of the Peace River Arch." In *Geological Atlas of the Western Canada Sedimentary Basin, G.D. Mossop and I. Shetsen (comp.).* Canadian Society of Petroleum Geologists and Alberta Research Council, URL https://ags.aer.ca/publications/atlas-the-western-canada-sedimentary-basin/chapter-28-geological-history-the-peace-river-arch , [November 2024].

Pană, D. I. 2010. *Precambrian geology of notheastern Alberta (NTS 74M, 74L and part of 74E).* Energy Resources Conservation Board, ERCB/AGS Map 537.

Pană, D.I. 2003a. "Precambrian basement of the Western Canada Sedimentary Basin in northern Alberta. ." Alberta Energy and Utilities Board, EUB/AGS Earth Sciences Report 2002-02, 39 p.

Pană, D.I. 2003b. "Structural control of lead-zinc mineralization in carbonate sequences of northern Alberta: a contribution to the carbonate-hosted Pb-Zn (MVT) targeted geoscience initiative." Alberta Energy and Utilities Board EUB/AGS Geo-Note 2002-15, 39 p.

Pană, D.I., and E. J. Waters. 2016. *GIS compilation of structural elements in Alberta, version 3.0 (GIS data, line features).* Digital Data 2003-0012, Alberta Energy Regulator/Alberta Geological Survey.

Pană, D.I., and R. Elgr. 2013. *Geology of the Alberta Rocky Mountains and Foothills.* Map 560, Alberta Energy Regulator / Alberta Geological Survey.

Pană, D.I., R. Elgr, E.J. Waters, J.A. Warren, G.P. Lopez, and J.G. Pawlowicz. 2021. "Structural elements in the Alberta Plains." Alberta Energy Regulator/Alberta Geological Survey, AER/AGS Open File Report 2021-01, 33 p.

Pană, D.I., Waters, J., and Grobe, M. 2001. "GIS compilation of structural elements in northern Alberta, release 1.0." Alberta Energy and Utilities Board, EUB/AGS Earth Sciences Report 2001-01, 60 p.

Pilkington, M., W.F. Miles, G.M. Ross, and W.R. Roest. 2000. "Potential-field signatures of buried Precambrian basement in the Western Canada Sedimentary Basin." *Canadian Journal of Earth Sciences* 37: p. 1453-1471.

Prior, G.J., B. Hathaway, P. Glombick, D.I. Pană, C.J. Banks, D.C. Hay, C.L. Schneider, M. Grobe, R. Elgr, and J.A. Weiss. 2013. "Bedrock geology of Alberta." Alberta Energy Regulator / Alberta Geological Survey, AER/AGS Map 600.

Ramaekers, P. 2004. *Development, stratigraphy and summary diagenetic history of the Athabasca Basin, Early Proterozoic of Alberta and its relation to uranium potential.* EUB/AGS Special Report 62, 84 p., Alberta Energy and Utilities Board, .

Ramaekers, P., C. W. Jefferson, G. M. Yeo, B. Collier, D. G.F. Long, O. Catuneanu, S. Bernier, et al. 2007. *Revised geological map and stratigraphy of the Athabasca Group, Saskatchewan and Alberta.* Bulletin of the Geological Survey of Canada 588, p. 155-191., in EXTECH IV geology and uranium EXploration TECHnology of the Proterozoic Athabasca Basin.

Ross, G.M. 2002. "Evolution of Precambrian continental lithosphere in Western Canada: results from LITHOPROBE studies in Alberta and beyond ." *Canadian Journal of Earth Sciences, v. 39,* p. 413–437.

Ross, G.M., and D.W. Eaton. 2002. "Proterozoic tectonic accretion and growth of western Laurentia: results from Lithoprobe studies in northern Alberta." *Canadian Journal of Earth Sciences* 39: p. 313-329.

Ross, G.M., B. Milkereit, D Eaton, White, D., E.R. Kanasewich, and M.J.A. and Burianyk. 1995. "Paleoproterozoic collisional orogen beneath the western Canada sedimentary basin imaged by Lithoprobe crustal seismic-reflection data." *Geology* 23: p. 195-199.

Ross, G.M., J. Broome, and W. Miles. 1994. "Chapter 4: Potential fields and basement structure." In *Geological Atlas of the Western Canada Sedimentary Basin*, by G.D. Mossop and I. Shetsen (comp.), p. 41–47. Canadian Society of Petroleum Geologists and Alberta Research Council.

Ross, G.M., R.R Parrish, M.E. Villeneuve, and S.A. Bowring. 1989. "Tectonic subdivision and U-Pb geochronology of the crystalline basement of the Alberta Basin, western Canada; Geological Survey of Canada." Open File 2103.

Ross, G.M., R.R. Parrish, M.E. Villeneuve, and S.A. Bowring. 1991. "Geophysics and geochronology of the crystalline basement of the Alberta Basin, western Canada." *Canadian Journal of Earth Sciences* 28: p. 512–522.

Rukhlov, A.S., and J.G. Pawlowicz. 2012. "Eocene potassic magmatism of the Milk River Area, southern Alberta (NTS 72E) and Sweet Grass Hills, northern Montana: overview and new data on mineralogy geochemistry, petrology and economic potential." Energy Resources Conservation Board/AGS Open File Report 2012-01, 88 p.

Villeneuve, M.E., G.M. Ross, R.J. Thériault, W. Miles, R.R. Parrish, and J. Broome. 1993. "Tectonic subdivision and U-Pb geochronology of the crystalline basement of the Alberta Basin, western Canada." Geological Survey of Canada Bulletin 447, 95 p.

Walton, E., A., E. A. Hughes, E. MacLagan, C. Herd, and M. Dence. 2017. "A previously unrecognized high-temperature impactite from the Steen River impact structure, Alberta, Canada." *Geology, v. 45 (4),* p. 291–294.

Appendix 1 – Automatic detection - Fathom Geophysics Report

Processing of the Alberta Merged magnetic survey for Ronacher McKenzie Geoscience

January 2025

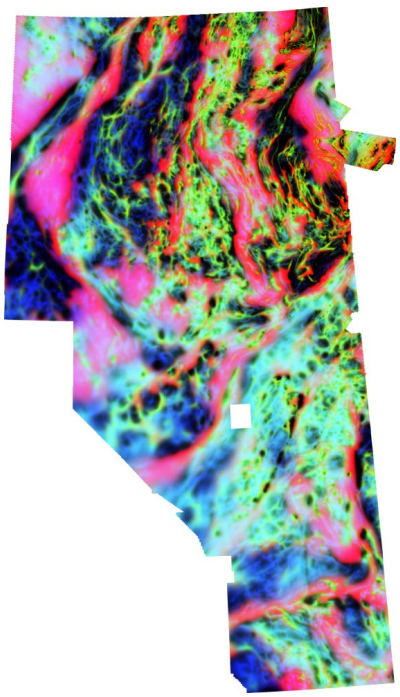

by Dan Core†, Eric Core, and Lisa Lombardi
Fathom Geophysics

†Corresponding author: dan@fathomgeophysics.com

Introduction

The location of the project area is shown in **Figure 1**. The goal of this work is to filter the magnetic dataset over the area to highlight structural features, lithologies, and possible intrusive rocks.

Most of the processing has been applied to a merged grid as indicated by the blue outline on **Figure 1**. The red outline indicates the magnetic survey for Central Alberta. It was processed on its own for the depth-to-source calculation.

The merged grid was provided to Fathom Geophysics by Ronacher-McKenzie Geoscience. The surveys incorporated into the merged grid are the Shield, Southern Alberta, Northern Alberta, and Central Alberta grids. All of these except Central Alberta have been processed individually as part of other projects.

The Central Alberta magnetic data are from a survey flown in 2023 and 2024 by EON Geosciences Inc on behalf of the Alberta Energy Regulator. Gridded data provided with the survey were good quality with some relatively minor cultural artifacts in the western part of the dataset**.** Survey data have 800m line-spacing. All gridded products use a cell size of 200m.

The merged grid also has a grid cell size of 200m (**Figure 2**). This is the native resolution of all the datasets except the Shield dataset. It was down-sampled when it was stitched with the other data.

The merged and Central Alberta grids were supplied to us with coordinates in WGS84 UTM Zone 11N. This coordinate system was used for all our outputs.

The processing completed includes differential reduction to the pole, application of a suite of standard filters and application of Fathom Geophysics' structure detection and radial symmetry filters to the Merged Alberta dataset. Depth-to-source processing was applied to the Central Alberta dataset.

Processing summary — Magnetic data

Differential reduction to the pole

RTP processing produces a magnetic field that is equivalent to what would be generated if the data were collected at the magnetic north pole. This shifts magnetic highs to be directly over their sources and creates symmetric anomalies over the top of symmetric magnetic sources.

We applied a differential RTP (DRTP) filter for this project. The filter uses the appropriate inclination and declination at each point in the project area as apposed to using the mean RTP parameters like a standard RTP would.

The DRTP filter for these data has a median inclination of 76.0° and a median declination of 14.4° (**Figure 3**).

Note that in general RTP processing is not valid for remanent bodies unless the remanence is directly opposed to the present-day field. The dataset almost certainly contains some remanent bodies that will not be corrected properly using the RTP filter. However, it is worthwhile applying the filter because most of the anomalies in the area are normally magnetized or reversely magnetized with relatively few anomalies possessing an apparent magnetization direction at a high angle to the present-day field.

Magnetic standard filtering

The RTP grid was filtered with a suite of standard geophysical filters including the analytic signal and vertical derivative. These grids were imaged using our in-house software to produce shaded images with the sunlight coming from the northwest (NW in the filename) and northeast (NE in the filename). Unshaded images were also produced so that the geographic location of pertinent features in the data can be readily defined (because shaded images can ‘fool the eye’ in this respect).

Figures 4 to 22 show images of most of the standard filtering results supplied. Standard filtering results have been included in this report because of their capacity to help the reader who might be new to the delivered processing results files to quickly grasp the project area’s overall magnetic susceptibility changes/contrasts.

Processing summary — Magnetic data (continued)

Magnetic total structure detection

Structure detection was applied to highlight edges in the RTP magnetic data and the AGC of the RTP data. Edges in potential field data are locales that are more likely to be faults, contacts or other structures. The structure detection algorithm and processing are described in more detail in **Appendix 1**.

Representative images of the total structure detection filtering are shown in **Figure 23** and **Figure 26**. Further results files were delivered in addition to those visualized within this report, and we urge the reader to explore the entire series of results files to ensure full familiarity with the results of total structure detection processing and their possible exploration ramifications.

Total-structure detection filtering was applied to the RTP grid at minimum wavelengths of 250m, 500m, 1000m, 2000m, 4000m, and 8000m. Structure intersection images were supplied alongside structure images.

This filtering was also applied to the AGC grid at minimum wavelengths of 250m, 500m, 1000m, 2000m, 4000m, and 8000m. Structure intersection images were supplied alongside structure images.

The results show that different orientations of structure are dominant in different parts of the area. The N has dominantly N-S features with ENE being the most prominent cross structure orientation. A relatively sharp break separates this fabric from the NE-trending fabric in the central part of the area. The central cross structures are mainly W to NW-trending.

The south has a less pronounced dominant structural orientation. The major structural orientation in the far south appear to be NW to NNW-trending. These structures end at an ENE-trending break in the data. North of this break, the NE-trending fabric of the central area begins.

Processing summary — Magnetic data (continued)

Magnetic belt-parallel and belt-crossing structure detection

In many heavily deformed belts, the fabric-parallel and fabric-crossing structures can be different structure types and may have different timing. The fabric-parallel features tend to be contacts or belt-parallel shear zones. The cross structures are usually not contacts and are more likely to be faults. Any sense of motion is possible on the cross structures. If clear lateral offset of the units is present, the faults are likely strike-slip faults. Normal and reverse faults are often represented by a change in amplitude or frequency content of the magnetic data.

The first step in extracting fabric-parallel and fabric-crossing structures is to extract the fabric orientation. The AGC was used for determining the fabric orientation because it was better at delineating the different structural domains than the RTP did (**Figure 27**).

The results show several domains in the area with different orientations. Most of the far north is dominated by a NNE trend. This orientation bends around to a NNW trend to the south. In the central part of the area, there is an abrupt change to a NE trend. The far south of the dataset is complex and shows several different orientations.

Representative images of the results of parallel and cross structure detection are shown in **Figures 28 to 31**. Further results files were delivered in addition to those visualized within this report, and we urge the reader to explore the entire series of results files to ensure full familiarity with the results of belt-parallel and belt-crossing structure detection processing and their possible exploration ramifications.

The fabric parallel features highlighted by this method are typically either lithological contacts or fabric-parallel shear zones. The AGC results appear to be very good for highlighting lithological boundaries. The RTP results are better for highlighting longer-wavelength features and those are more likely to be major faults.

The fabric-crossing features are more likely to be faults than the fabric-parallel features, but they are also more affected by noise in the data. The most reliable results will come from moderate to long-wavelength results on the RTP data.

It can often be useful to display relatively high-frequency fabric-parallel features with lower-frequency fabric-crossing features. This can be done using the vector outputs for each product.

Processing summary — Magnetic data (continued)

Magnetic radial symmetry

The radial symmetry detection filter can highlight discrete, equant magnetic features with different radii. Radial symmetry detection was completed on the RTP data. The radial symmetry algorithm is described in greater detail in **Appendix 2** of this report.

Representative images of the radial symmetry results are shown in **Figure 32**. Further results files were delivered in addition to those visualized within this report, and we urge the reader to explore the entire series of results files to ensure full familiarity with the results of radial symmetry analysis processing and their possible exploration ramifications.

When applied to the RTP grid, radial symmetry detection processing was applied in magnitude-independent mode at minimum-radius runs of 1000m, 2000m, 4000m, 8000m, and 16000m. Radii greater than these did not appear to be useful on this particular data grid. Both magnetic highs and magnetic lows represent meaningful/useable results and therefore are presented in images.

The radial symmetry results show high-frequency features concentrated in the NE of the area. This is to be expected as that area has less cover, so more high-frequency information is in the data.

The moderate frequencies show a large concentration of features in the north with a gap in the middle of the dataset in an area dominated by very linear features. The south has a significant number of moderate wavelength features as well.

The long-wavelength features are roughly evenly distributed throughout the area. These features have the most uncertainty as far as whether they are intrusions. The causative bodies for the anomalies could be quite deep making ground truthing difficult even if there was outcrop present.

Processing summary — Magnetic data (continued)

Depth to magnetic source

Many algorithms can be used to estimate the depth to magnetic sources. Most are based on at least second order derivatives making them significantly influenced by any kind of noise in the data. This dataset presents some significant challenges for these algorithms due to high frequency noise that occurs where cultural features are present in the data. These features are mostly due to oil and gas infrastructure in the area. While the airborne contractor took steps to mitigate the noise caused by these features, the effects were not completely removed. These features are most abundant in the western part of the dataset.

In order to smooth out these features, a localized Gaussian filter was applied only where the high-frequency noise was a problem. This had to be done rather than using a global filter because a global filter would have smoothed out real detail in the east.

The method that was used for the depth to source is that of Cooper (2014). It involves looking at the derivative of the tilt angle to estimate the depth of contacts in the dataset. The resulting depths were then interpolated to generate a continuous distance to magnetic source grid. The average altitude of the aircraft was subtracted off to generate a depth to magnetic basement grid.

The results of the depth to magnetic source processing are shown in **Figure 45**. The smoother parts of the dataset show greater depth to source as is expected. The results show that the basement surface gets deeper to the west and shallower in the east. The basement does not appear to be exposed anywhere.

The average depths observed in the depth to source processing are similar to those observed in wells that have pierced the basement in parts of the area. The correlation between the well depths and the calculated basement depths are reasonably good indicating that the depth to source appears to be a good estimate. The results correlate well with depth to source completed on the Alberta North grid but have significant mismatches with the results for the Alberta South grid. The Alberta South results are probably incorrect due to insufficient suppression of cultural noise. That dataset could be revisited to improve the results.

The depth to magnetic source grid was subtracted from the topography data to generate a top of magnetic basement surface (**Figure 46**)**.** The magnetic basement surface looks almost like an inverse of the depth to source grid. This is expected given the relatively small amount of topographic variation in much of the area.

**Cooper (2014) The automatic determination of the location, depth, and dip of contacts from aeromagnetic data. Geophysics, v79, pp J35-J41. https://library.seg.org/doi/10.1190/geo2013-0181.1*

File formats and image types delivered

The grids for this work have been delivered in ER Mapper ERS format. All images have been provided in GeoTIFF format with associated MapInfo TAB files and ESRI world files. Vectors have been delivered in ESRI shapefile format.

Structure detection results have been supplied as grids, images (GeoTIFF), and polylines (vectorization of the gridded results). The polylines have been attributed with the values from the structure detection grid and the orientation of the structure calculated based on the vectorized result.

Structure images were made in an unshaded fashion using a warm color bar (yellows through to reds) and a linear color stretch. Dominant orientation images use a wraparound colorbar palette that produces the same color for 0 and 180 with a rainbow distribution for colors in between. Those orientation images that have been thresholded display only significant features and are white in locales that essentially lack structure.

Radial symmetry ‘lows and highs’ images were made using a blue-and-red color bar possessing no intermediate colors. Highs-only images use the red side of that same color bar, and lows-only images use the blue side.

Several ternary images were also created for this work. These images are generated using three separate grids to represent the red-green-blue (RGB) or cyan-magenta-yellow (CMY) channels of the output image. RGB ternary images involve color addition, analogous to how different-colored light beams combine on a performance stage. When all three channels are present in full strength, pure white is the result. (Pure black indicates all three channels are absent.) CMY ternary images involve color subtraction, similar to colors resulting from the mixing of paint pigments. When all three channels are present in full strength, pure black is the result. (Pure white indicates all three channels are absent.) **Figure 17** explains in more detail how to interpret the full gamut of colors that can turn up in ternary images.

See also the list of abbreviations and acronyms supplied in this report to help decode the information contained within a given grid/image filename.

List of acronyms and abbreviations

agc	automatic gain control (appears in delivered file names)
Agc20	AGC when standard deviation=20 (in file names)
Alberta	Project area (appears in file names)
asig	analytic signal (appears in delivered file names)
colorbar	numerical values associated with image's color range (in file names)
CMY	cyan-magenta-yellow ternary (appears in delivered file names)
gray, grayscale	grayscale image (appears in delivered file names)
hgm	horizontal gradient magnitude (appears in delivered file names)
Highs	positive anomalies-only radial symmetry image (in file names)
HSI	hue, saturation and intensity (appears in delivered file names)
HTh	hysteresis thresholding was used during vectorization (in file names)
Int	structural intersections image (appears in delivered file names)
LgeRes	large-scale residual (appears in delivered file names)
lin	linear-stretch image (appears in delivered file names)
Lows	negative anomalies-only radial symmetry image (in file names)
LowsAndHighs	negative and positive anomalies radial symmetry image (in file names)
md	magnitude dependent radial symmetry result (in file names)
MedRes	medium-scale residual (appears in delivered file names)
mi	magnitude independent radial symmetry result (in file names)
OriDom	dominant orientation image (appears in delivered file names)
Pgrav	pseudogravity (appears in delivered file names)
PgravRes	residual of pseudogravity (appears in delivered file names)
PgravResHGM	HGM of residual of pseudogravity (appears in delivered file names)
res	residual (appears in delivered file names)
res25_100	25m-100m residual (appears in delivered file names)
RGB	red-green-blue ternary (appears in delivered file names)
RMI	residual magnetic intensity (appears in delivered file names)
RSym	radial symmetry image (appears in delivered file names)
RSym100	100m minimum radius radial symmetry image (in file names)
RTP	reduced-to-pole (appears in delivered file names)
SmRes	small-scale residual (appears in delivered file names)
Struct	structure image (appears in delivered file names)
Struct100	100m minimum wavelength structure image (in file names)
tern, ternary	ternary image (appears in delivered file names)
Thresh, thr, Th	image made via thresholding (appears in delivered file names)

List of acronyms and abbreviations (continued)

tilt	tilt angle (appears in delivered file names)
TMI	total magnetic intensity (appears in delivered file names)
Total	total structure image (appears in delivered file names)
vd	vertical derivative (a.k.a. 1VD) (appears in delivered file names)
vdmhgm	vertical derivative minus HGM (appears in delivered file names)
Vec	vectorized results file (appears in delivered file names)
Vert, V	shaded image where ‘sun’ is directly overhead (in file names)
vias	analytic signal of vertical integral (appears in delivered file names)
vint	vertical integral (appears in delivered file names)
X	directional derivative along X axis (appears in delivered file names)
Y	directional derivative along Y axis (appears in delivered file names)
Z	directional derivative along Z axis (i.e., vertical derivative) (in file names)

Project location map

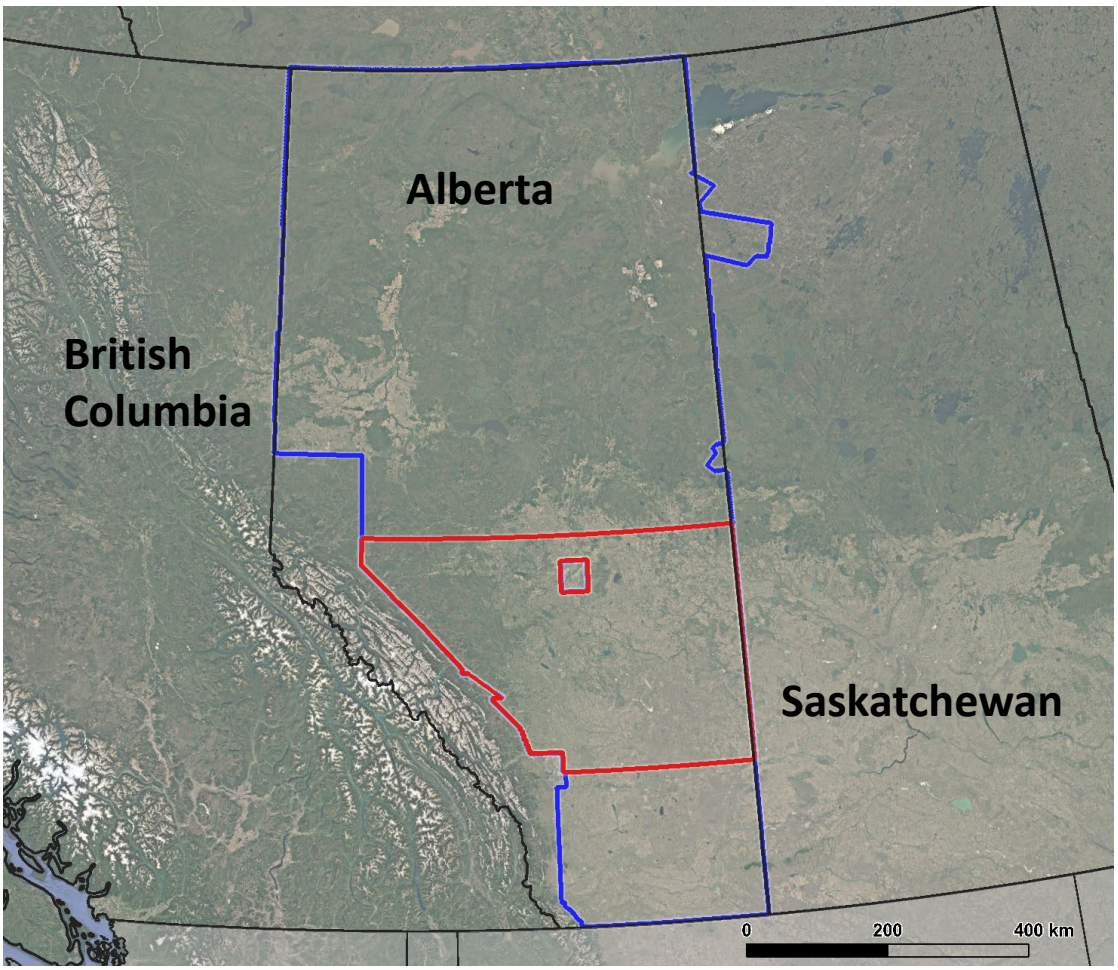

Figure 1: Location map for this project. The blue polygon indicates the outline of the merged Alberta magnetic dataset. The red polygon indicates the outline of the Central Alberta magnetic dataset.

Magnetic data-processing results images
▶ Total magnetic intensity (TMI)

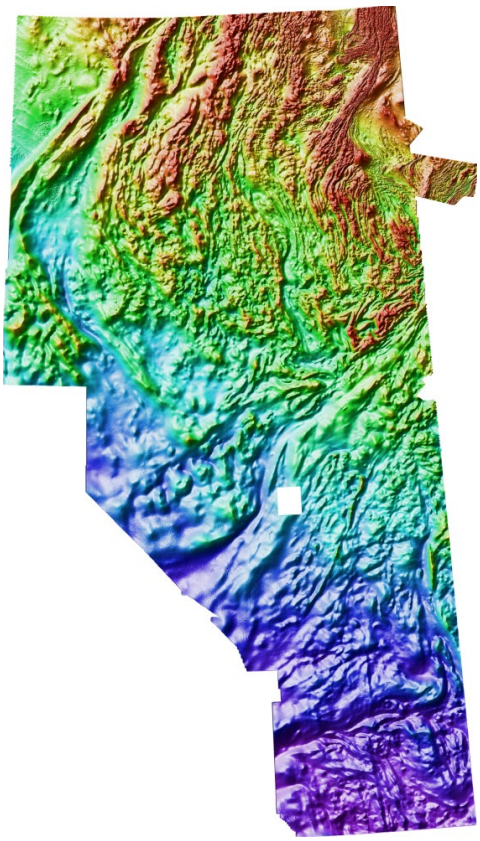

Alberta_TMIfinal_HSI_NW

Figure 2: Total magnetic intensity data for the project area. The indicative colorbar shown applies to all magnetic data-processing results images involving the HSI (hue, saturation, intensity) color display system.

Magnetic data-processing results images
▶ Reduction-to-pole (RTP)

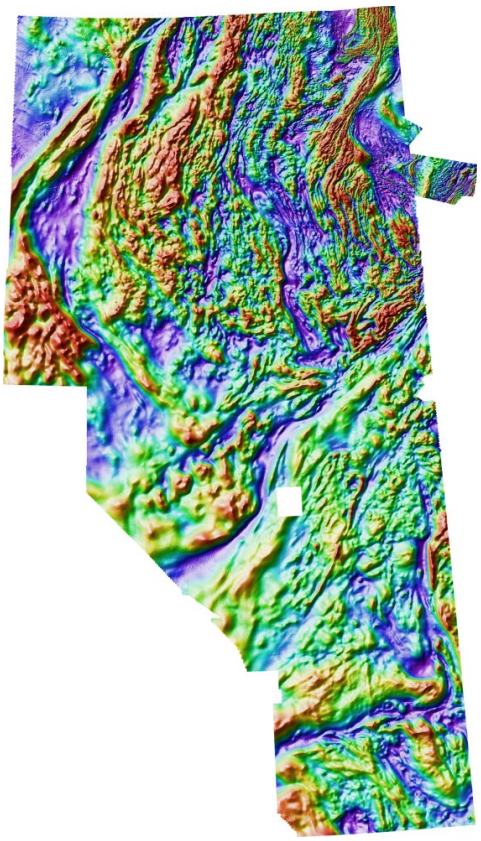

Alberta_RMIfinal_DRTP_HSI_NW

Figure 3: Reduced-to-the-pole magnetic data for the project area. The RTP filter attempts to produce the magnetic field that would be expected if the data were collected at the magnetic pole.

Magnetic data-processing results images (continued)
▶ Standard filtering — First vertical derivative

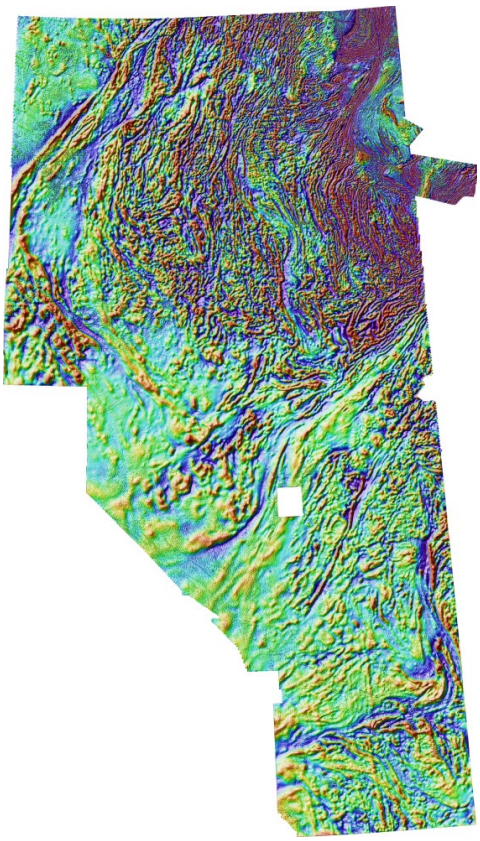

Alberta_RMIfinal_DRTP_vd_HSI_NW

Figure 4: The first vertical derivative (1VD) transform is the rate of change of the potential field in the vertical direction. Application of this filter has the effect of accentuating the shorter wavelength (higher frequency) components at the expense of longer wavelength (more regional) features.

Magnetic data-processing results images (continued)
▶ Standard filtering — Horizontal gradient magnitude

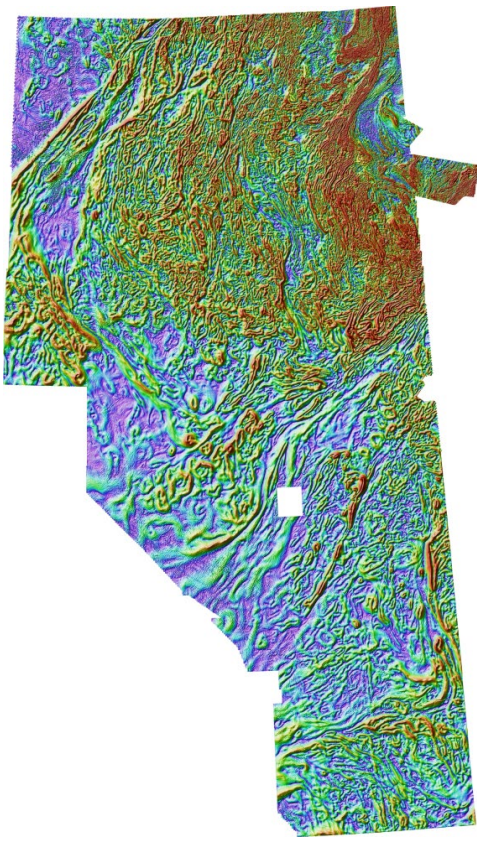

Alberta_RMIfinal_DRTP_hgm_HSI_NW

Figure 5: The horizontal gradient magnitude is calculated from the x- and y-derivatives of the data ($\sqrt{dx^2 + dy^2}$). This filter highlights the location of steep gradients in the data. Peaks in the HGM should occur at susceptibility contrasts in magnetic data and density contrasts in gravity data. These are likely to be locations of faults or contacts. Peaks will be offset in the down-dip direction for dipping bodies. The results are affected by remanent magnetization.

Magnetic data-processing results images (continued)
▶ Standard filtering — Vertical derivative minus HGM

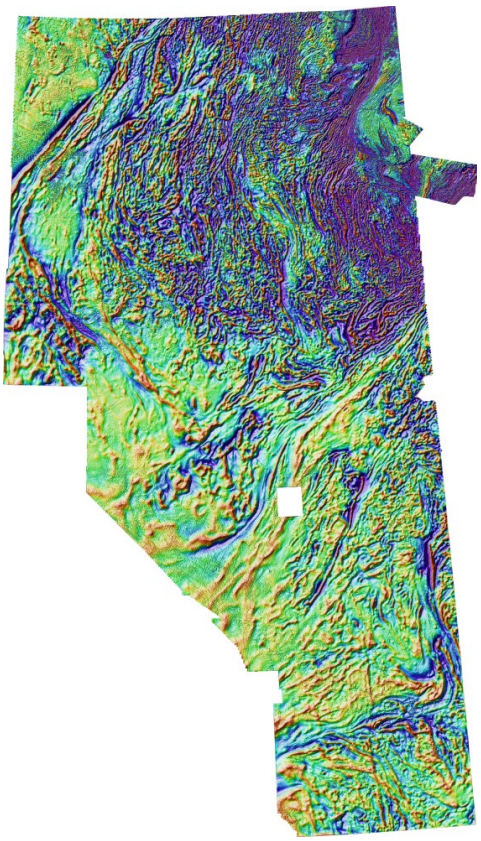

Alberta_RMIfinal_DRTP_vdmhgm_HSI_NW

Figure 6: The vertical derivative minus the HGM (VDMHGM) is a filter that accentuates the contrast in the first vertical derivative. This is useful for highlighting shallow sources in potential field data. It can also be useful when trying to pick the exact location to place a narrow magnetic unit or a narrow dense unit.

Magnetic data-processing results images (continued)

▶ Standard filtering — Tilt angle

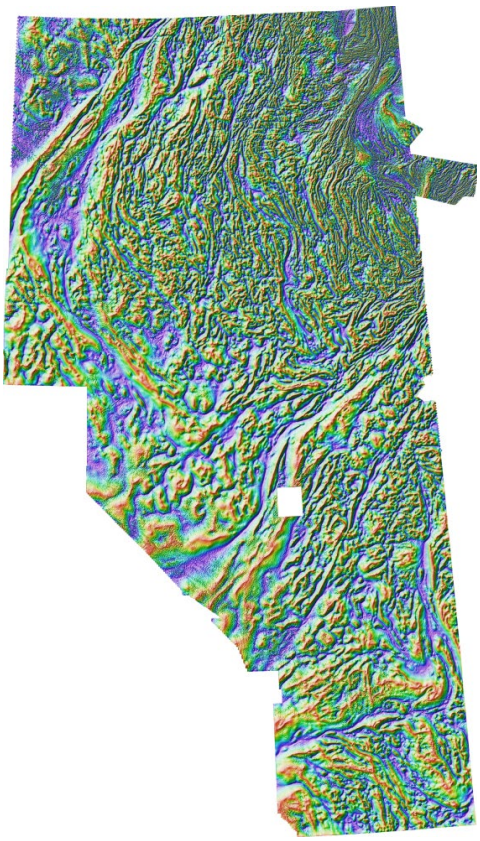

Alberta_RMIfinal_DRTP_tilt_HSI_NW

Figure 7: The tilt angle filter is the arctangent of the ratio of the vertical derivative to the horizontal gradient magnitude. This filter removes information about the amplitude of the signal, making the heights of peaks the same regardless of the susceptibility or density of the causative body. Structure and depth information are preserved. This makes it easier to see subtle features and some structures.

Magnetic data-processing results images (continued)
▶ Standard filtering — Analytic signal

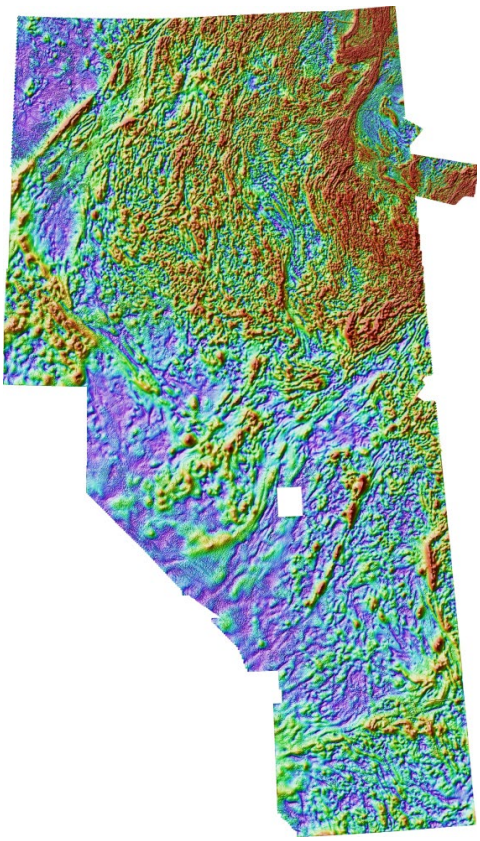

Alberta_RMIfinal_DRTP_asig_HSI_NW

Figure 8: Analytic signal of the RTP data. The analytic signal (also known as the total gradient magnitude) is calculated as $\sqrt{dx^2 + dy^2 + dz^2}$. This filter highlights the location of rapid changes in the data. Highs in the analytic signal correspond to high amplitudes in the vertical derivative (positive or negative) or high amplitudes in the horizontal gradient magnitude. Highs will occur over the top of small bodies with high susceptibility or high density contrast or at the edge of large-scale susceptibility or density contrast. Long-wavelength features are suppressed by this filter since it is based on derivative filters. This filter is relatively independent of magnetization direction and remanent magnetization.

Magnetic data-processing results images (continued)
▶ Standard filtering — Analytic signal of vertical integral

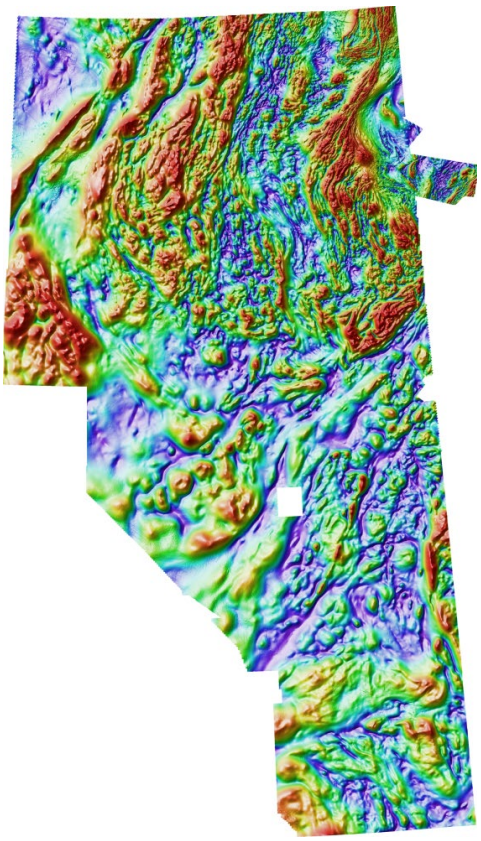

Alberta_RMIfinal_DRTP_vias_HSI_NW

Figure 9: The analytic signal filter was applied to the vertical integral of the magnetic data to produce this VIAS result. The analytic signal filter is described in the caption of **Figure 8**. Produces a grid with wavelength and amplitude characteristics that are similar to the RTP grid, but with reduced effects of remanent magnetization and magnetization direction.

Magnetic data-processing results images (continued)
▶ Standard filtering — Automatic gain control

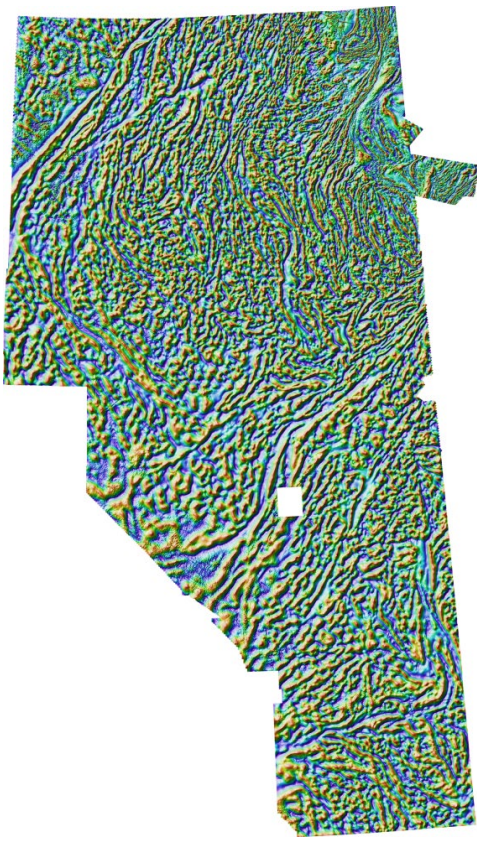

Alberta_RMIfinal_DRTP_AGC20_HSI_NW

Figure 10: The automatic gain control filter (AGC) is a means of evening out the amplitudes of anomalies. This makes more subtle features in the data visible. The filter also acts as a high-pass filter by suppressing the longer wavelengths.

Magnetic data-processing results images (continued)
▶ Standard filtering — Small-scale residual

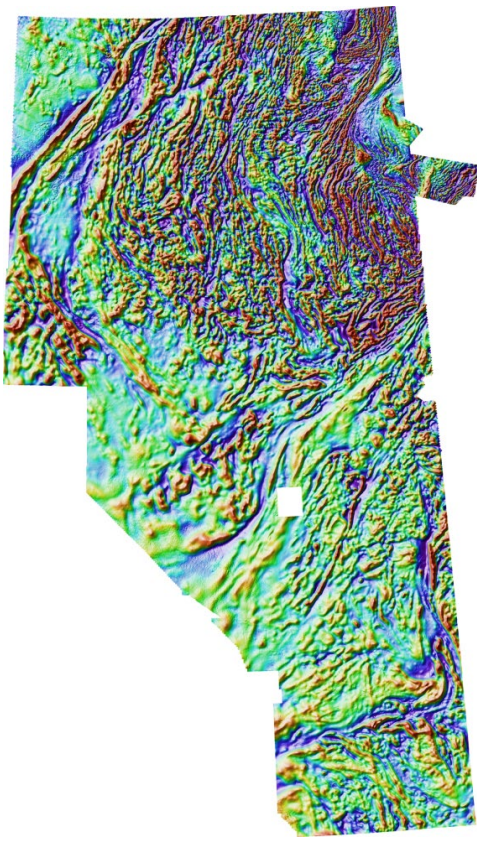

Alberta_RMIfinal_DRTP_res300_1500_HSI_NW

Figure 11: Differential upward continuation was applied to calculate the 300m-1500m residual of the RTP data in an attempt to separate sources from different depths (Jacobsen, 1987). The source depths should correspond to half of the upward continuation level. For this residual, that would be about 150m-750m depth.

Magnetic data-processing results images (continued)
▶ Standard filtering — Medium-scale residual

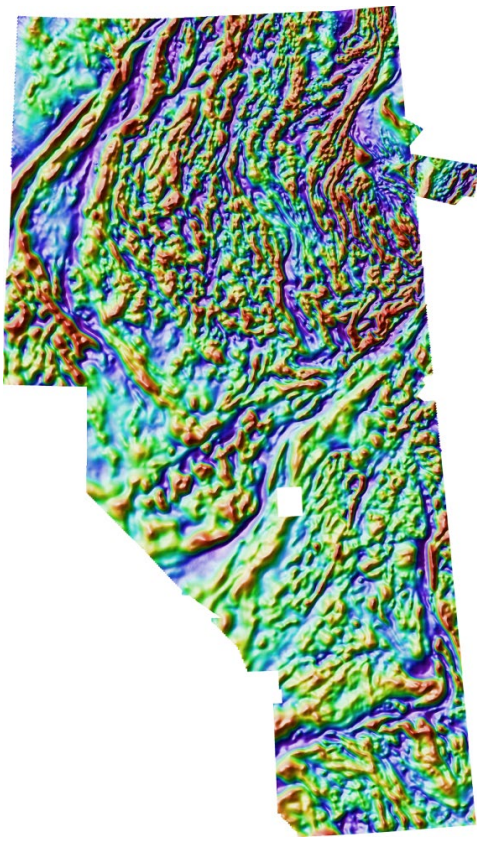

Alberta_RMIfinal_DRTP_res1500_6000_HSI_NW

Figure 12: Differential upward continuation was applied to calculate the 1500m-6000m residual of the RTP data in an attempt to separate sources from different depths (Jacobsen, 1987). The source depths should correspond to half of the upward continuation level. For this residual, that would be 750m-3000m depth.

Magnetic data-processing results images (continued)
▶ Standard filtering — Large-scale residual

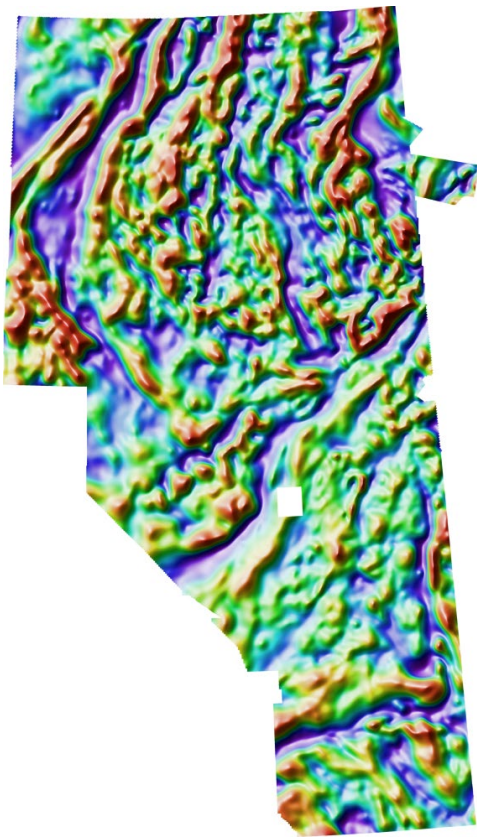

Alberta_RMIfinal_DRTP_res6000_15000_HSI_NW

Figure 13: Differential upward continuation was applied to calculate the 6000m-15000m residual of the RTP data in an attempt to separate sources from different depths (Jacobsen, 1987). The source depths should correspond to half of the upward continuation level. For this residual, that would be 3000m-7500m depth.

Magnetic data-processing results images (continued)

▶ Standard filtering — Pseudogravity

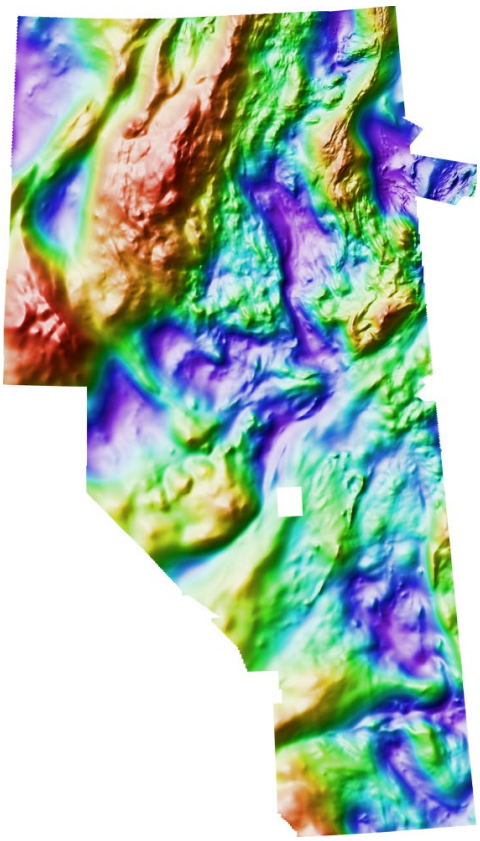

Alberta_RMIfinal_DRTP_PGrav_HSI_NW

Figure 14: Pseudogravity is generated by calculating the vertical integral of reduced-to-the-pole magnetic data and then using Poisson's relation (correlation between magnetic potential and gravitational potential) to scale the result. This generates a grid that is the expected gravity field if density were distributed in the same way as magnetic susceptibility in the project area. This is not a true gravity grid because it is highly unlikely that susceptibility and density are perfectly correlated. This filter enhances long-wavelength features and is good for highlighting large-scale features.

Magnetic data-processing results images (continued)
▶ Standard filtering — Pseudogravity residual

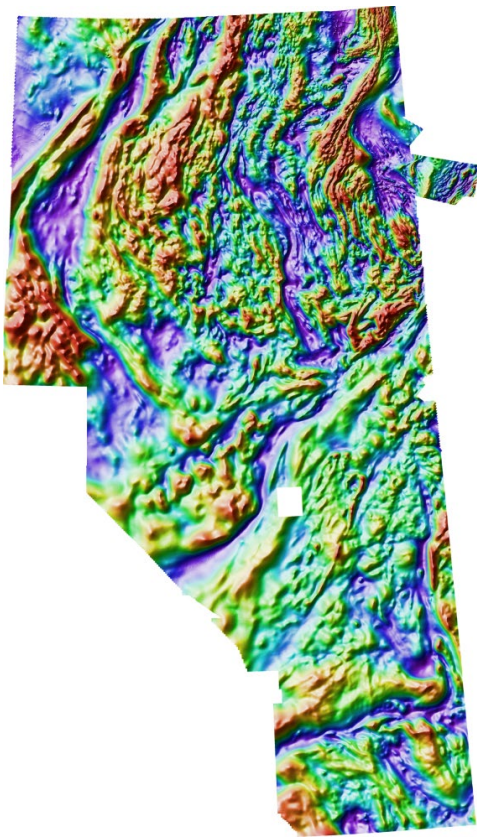

Alberta_RMIfinal_DRTP_PGravRes_HSI_NW

Figure 15: Differential upward continuation was applied to the pseudogravity grid to generate a 0-2000m residual. This removes the longest wavelength features to allow intermediate-scale features to be seen.

Magnetic data-processing results images (continued)
▶ Standard filtering — HGM of pseudogravity residual

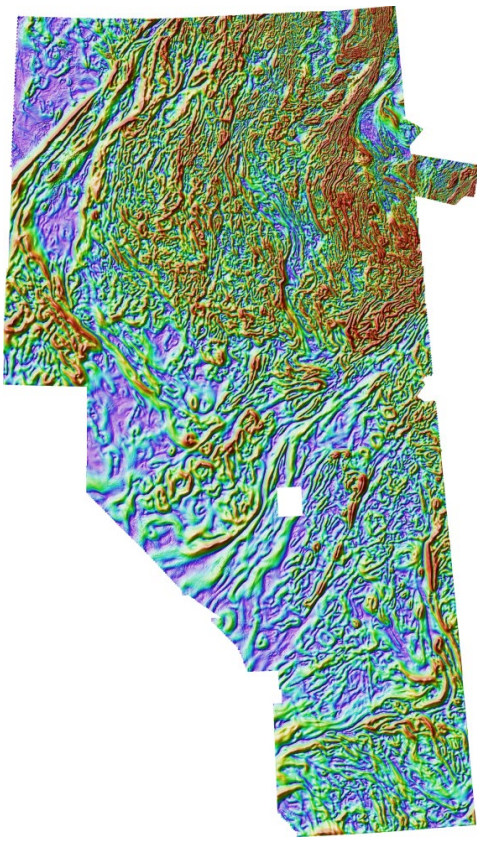

Alberta_RMIfinal_DRTP_PGravResHGM_HSI_NW

Figure 16: The horizontal gradient was calculated from the pseudogravity residual as described in the caption for **Figure 5**. The results highlight the edges of intermediate-scale features. However, this filter is affected by magnetization direction and remanent magnetization.

Magnetic data-processing results images (continued)
▶ Standard filtering images — Using ternary images

RGB

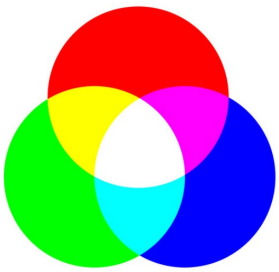

For RGB images:
Green + blue = cyan
Red + blue = magenta
Red + green = yellow
Red + green + blue = white
Low in red + green + blue = black

CMYK

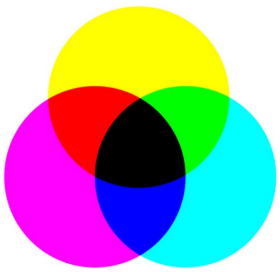

For CMY images:
Magenta + yellow = red
Cyan + yellow = green
Cyan + magenta = blue
Cyan + magenta + yellow = black
Low in red + green + blue = white

Figure 17: The information above shows how to interpret the colors in the RGB and CMY ternary images appearing in the next few figures, which are:

(i) Ternary of directional derivatives — This image encapsulates information about how steeply the gradient is changing in 3 orthogonal directions, namely the X and Y directions (within the plane of the image), and the Z direction (perpendicular to the plane of the image). All of this gradient information combines to help the observer intuitively identify the various major geological domains residing throughout the area of interest, and how these domains relate to each other.

(ii) Ternary of 1VD, tilt angle, and HGM — This image helps the observer intuitively understand where major structural features are situated, where breaks in the continuity of the magnetic 'fabric' occur, and how the textural character of the magnetic data changes from one locale to the next.

(iii) Ternary of residuals — Again, this image helps the observer intuitively understand where major structural features are situated, where breaks in the continuity of the magnetic 'fabric' occur, and how the textural character of the magnetic data changes from one locale to the next. However, features seen are generally coarser than those appearing in the ternary combining 1VD, tilt and HGM.

(iv) Ternary of RTP, VIAS, and analytic signal — This image helps the observer intuitively understand which subareas may be most affected by remanence (red locales in the CMY image).

(v) Ternary of pseudogravity results — This image combines three pseudogravity-related grids and produces an image that may assist the observer with intuitively grasping the geological affinity of features in the data.

Magnetic data-processing results images (continued)
▶ Standard filtering — Ternary of directional derivatives

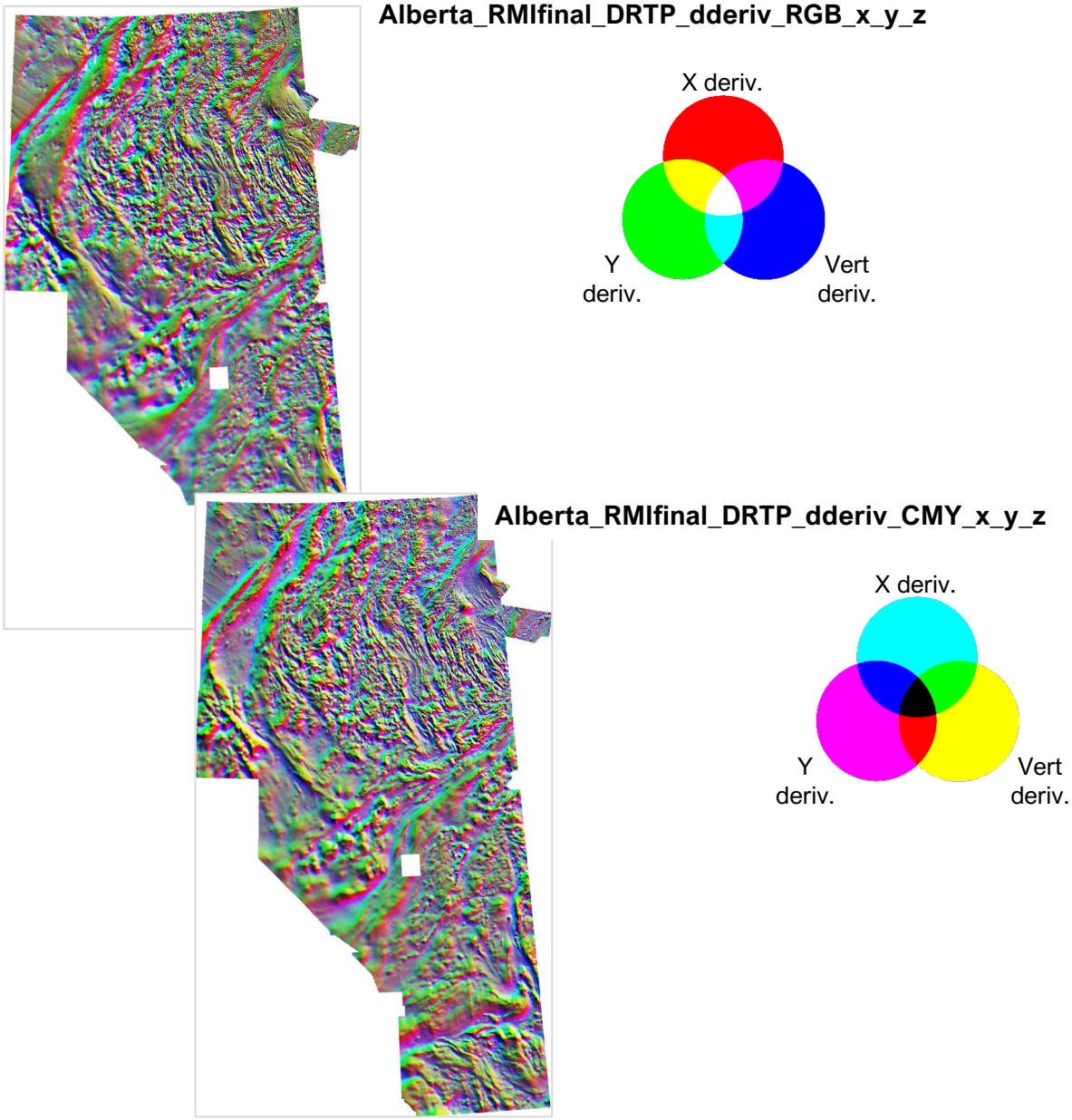

Figure 18: RGB and CMY ternary images co-displaying the X-gradient (R/C channels), Y-gradient (G/M channels), and Z-gradient (i.e., vertical derivative) (B/Y channels).

Magnetic data-processing results images (continued)

▶ Standard filtering — Ternary of 1VD, tilt, HGM

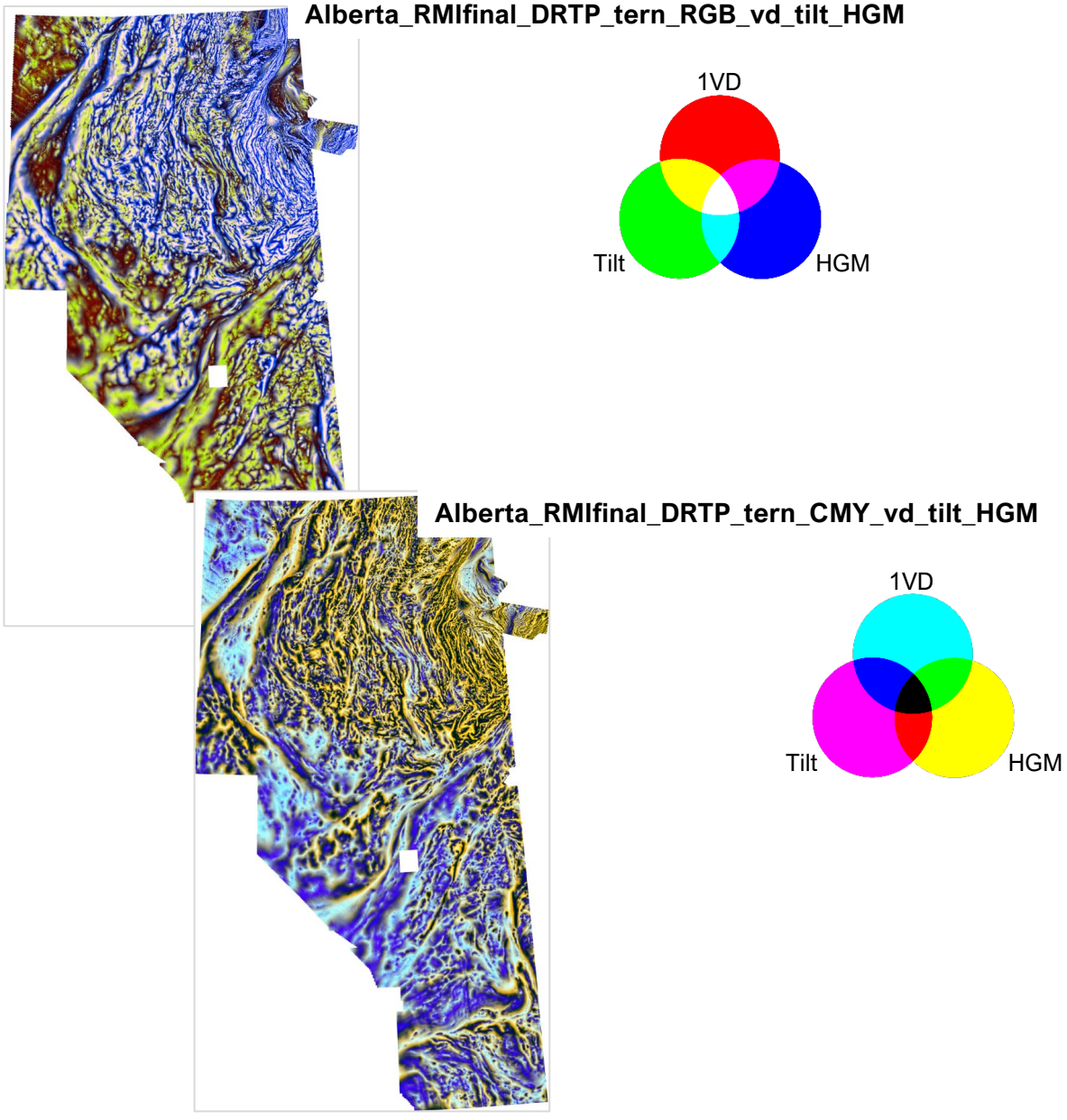

Figure 19: RGB and CMY ternary images co-displaying the vertical derivative (R/C channels), tilt angle (G/M channels), and HGM (B/Y channels).

Magnetic data-processing results images (continued)

▶ Standard filtering — Ternary of residuals

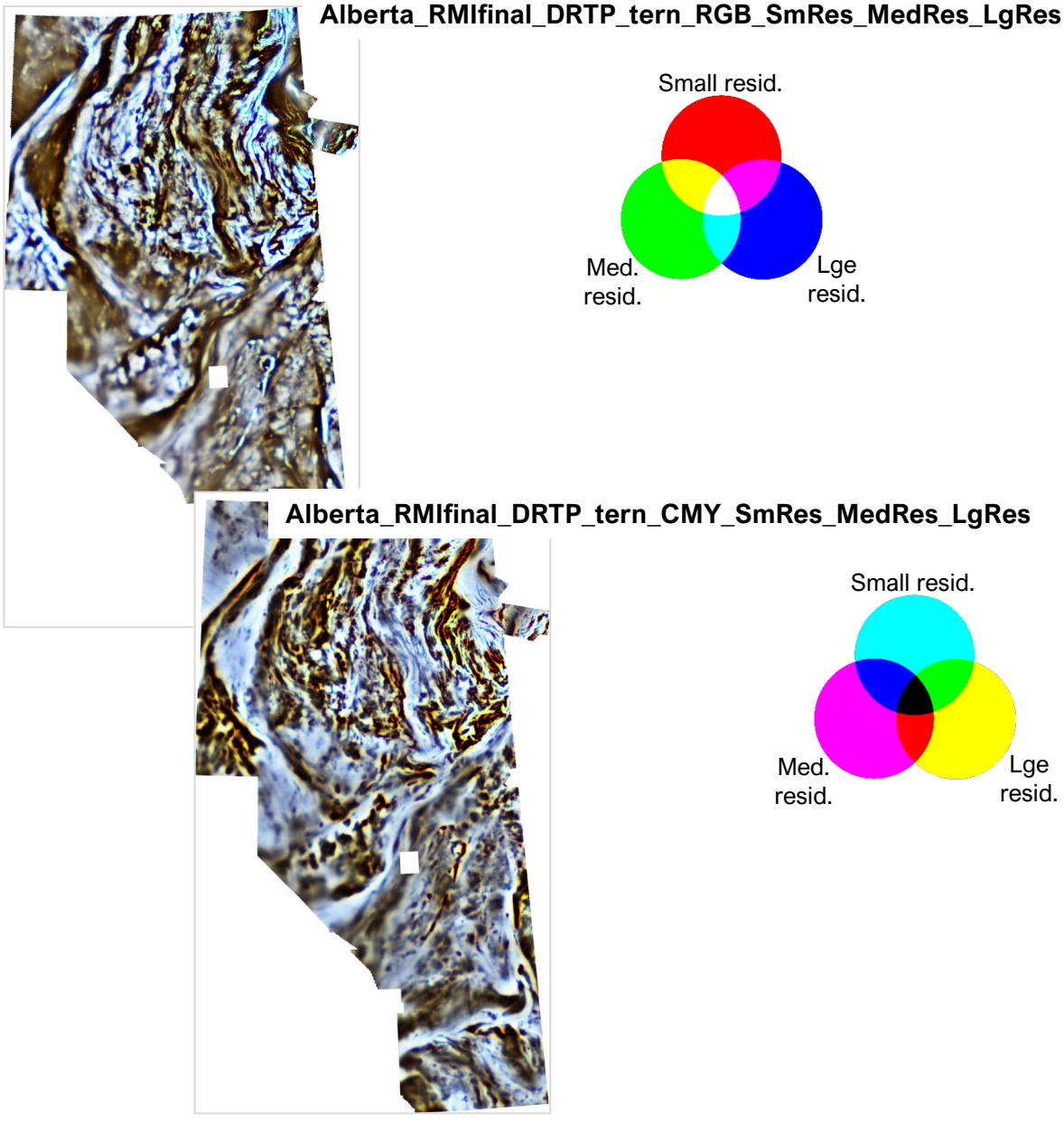

Figure 20: RGB and CMY ternary images co-displaying the small-scale (R/C channels), medium-scale (G/M channels), and large-scale residuals (B/Y channels).

Magnetic data-processing results images (continued)

▶ Standard filtering — Ternary of RTP, VIAS, Asig

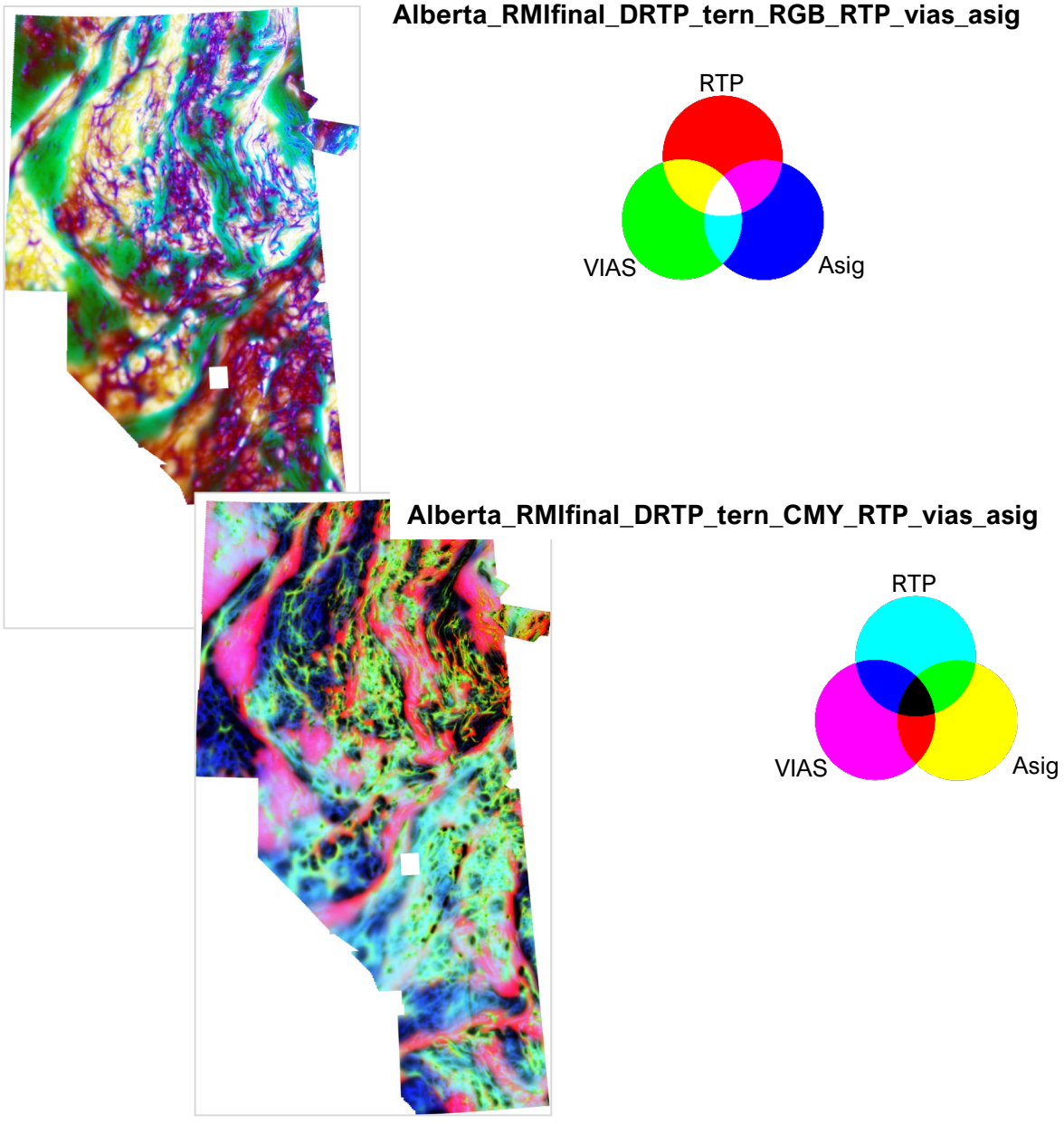

Figure 21: RGB and CMY ternary images co-displaying the RTP (R/C channels), VIAS (G/M channels), and analytic signal (B/Y channels).

Magnetic data-processing results images (continued)

▶ Standard filtering — Ternary of pseudogravity results

Alberta_RMIfinal_DRTP_tern_RGB_PGrav_PGravRes_PGravResHGM

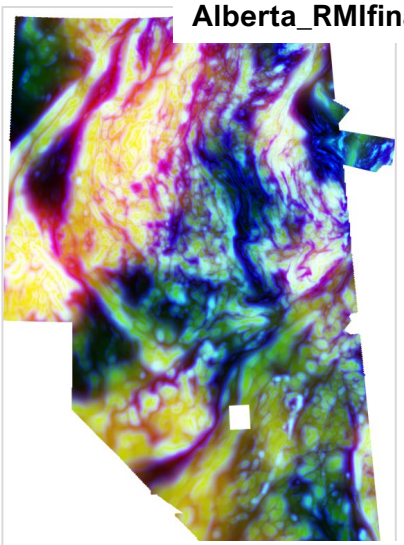

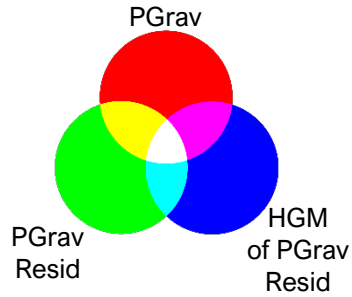

Alberta_RMIfinal_DRTP_tern_CMY_PGrav_PGravRes_PGravResHGM

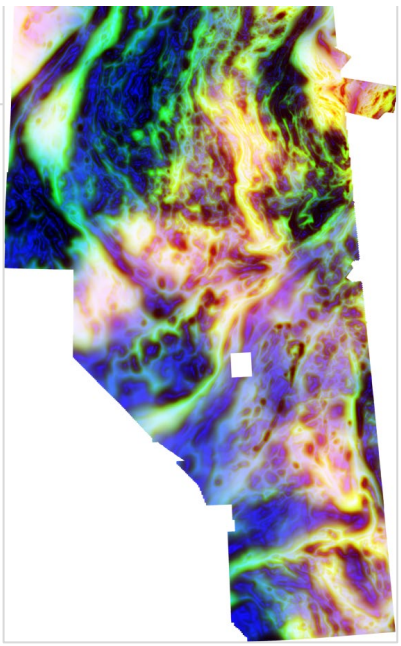

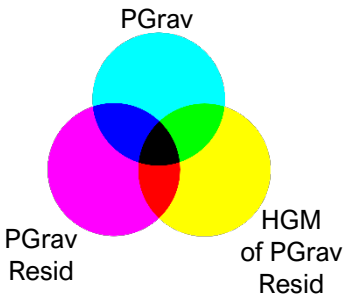

Figure 22: RGB and CMY ternary images co-displaying pseudograv (R/C channels), pseudograv residual (G/M channels), and HGM of pseudograv residual (B/Y channels).

Magnetic data-processing results images (continued)

▶ Total structure detection — Analysis of RTP

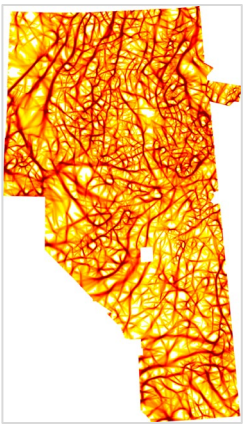

Figure 23: Representative image** showing 4000m structure detection results for the RTP data. TOP: Total structure detected. MIDDLE: Map of thresholded structural orientations. BOTTOM: Total structure in vectorized form (black lines with displayed thickness varying according to median value) over the project area's RTP image.

Alberta_RMIfinal_DRTP_Struct4000_Total

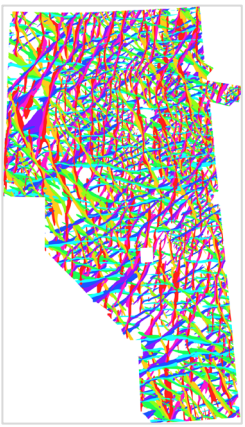

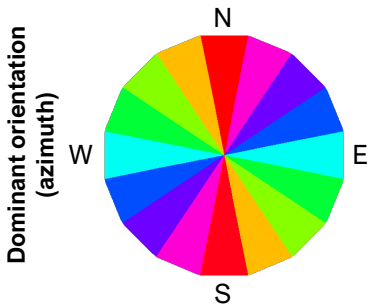

Alberta_RMIfinal_DRTP_Struct4000_OriDom_Th

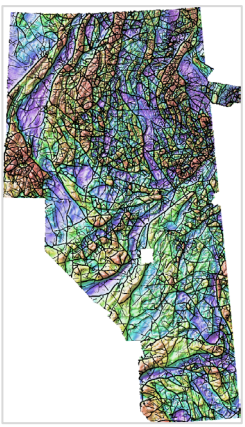

Alberta_RMIfinal_DRTP_Struct4000_Total_Vec

Alberta_RMIfinal_DRTP_HSI_NW

** *Further scales of results also delivered.*

Magnetic data-processing results images (continued)

▶ Total structure detection — Analysis of RTP

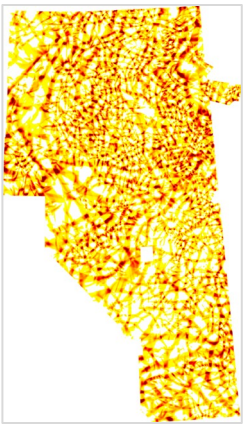

Figure 24: Representative image** showing 4000m structure detection results for the RTP data. TOP: Total structure intersections detected. MIDDLE: Intersections co-displayed with same-scale structures (line color and thickness varies according to structure's median value). BOTTOM: Intersections co-displayed with strong intersections (black-lined polygons) over gray RTP.

Alberta_RMIfinal_DRTP_Struct4000_Int

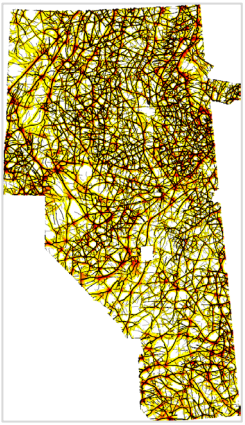

Alberta_RMIfinal_DRTP_Struct4000_Int

Alberta_RMIfinal_DRTP_Struct4000_Int_HTh_Vec

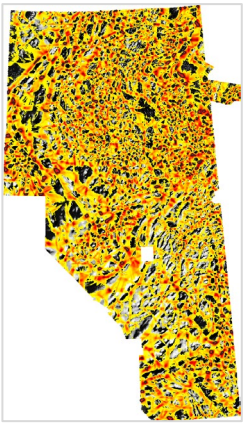

Alberta_RMIfinal_DRTP_Struct4000_Int

Alberta_RMIfinal_DRTP_Struct4000_Int_HTh_Vec

Alberta_RMIfinal_DRTP_HSI_NW (grayscale)

** *Further scales of results also delivered.*

Magnetic data-processing results images (continued)

▶ Total structure detection — Analysis of AGC

Figure 25: Representative image** showing 4000m structure detection results for the RTP's AGC. TOP: Total structure detected. MIDDLE: Map of thresholded structural orientations. BOTTOM: Total structure in vectorized form (black lines with displayed thickness varying according to median value) over the project area's RTP image.

Alberta_RMIfinal_DRTP_AGC60_Struct4000_Total

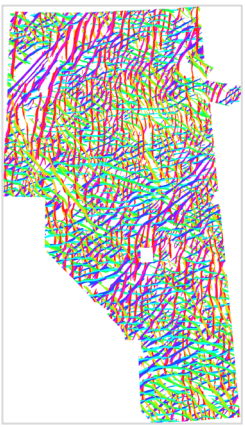

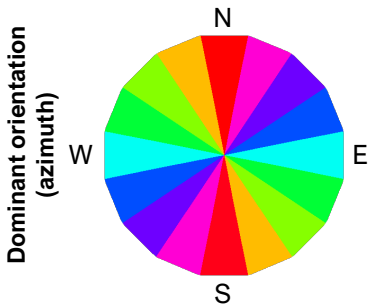

Alberta_RMIfinal_DRTP_AGC60_Struct4000_OriDom_Th

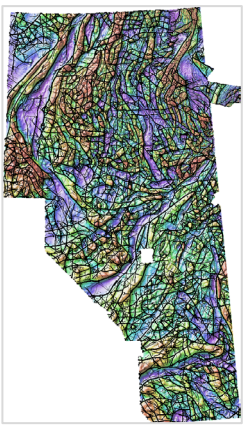

Alberta_RMIfinal_DRTP_AGC60_Struct4000_Total_Vec

Alberta_RMIfinal_DRTP_HSI_NW

** *Further scales of results also delivered.*

Magnetic data-processing results images (continued)

▶ Total structure detection — Analysis of AGC

Figure 26: Representative image** showing 4000m structure detection results for the RTP's AGC. TOP: Total structure intersections detected. MIDDLE: Intersections co-displayed with same-scale structures (line color and thickness varies according to structure's median value). BOTTOM: Intersections co-displayed with strong intersections (black-lined polygons) over gray RTP.

Alberta_RMIfinal_DRTP_AGC60_Struct4000_Int

Alberta_RMIfinal_DRTP_AGC60_Struct4000_Int

Alberta_RMIfinal_DRTP_AGC60_Struct4000_Total_Vec

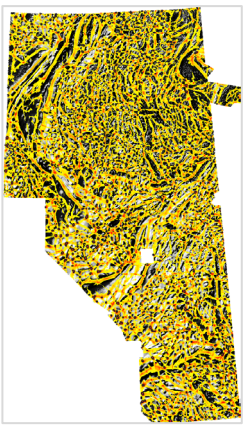

Alberta_RMIfinal_DRTP_AGC60_Struct4000_Int

Alberta_RMIfinal_DRTP_AGC60_Struct4000_Int_HTh_Vec

Alberta_RMIfinal_DRTP_HSI_NW (grayscale)

** *Further scales of results also delivered.*

Magnetic data-processing results images (continued)
▶ Parallel/cross structure — RTP fabric orientation

Alberta_RMIfinal_DRTP_Fab_Ori

Figure 27: The orientation of magnetic units was determined by taking the AGC of the RTP magnetic data and applying an anisotropic diffusion filter to highlight linear features. Ridge lines were extracted from the enhanced grid and the orientation of the ridge lines was determine. The resulting orientations were interpolated and smoothed to generate the map shown above. The green areas are dominated by WNW to NW trends. The blue and cyan areas are dominated by ENE to EW trends while the magenta indicates NE to NNE trends. The reds and oranges indicate areas that are dominated by NNW to N-trending features.

Magnetic data-processing results images (continued)

▶ Parallel/cross structure — RTP

Figure 28: Representative image** showing 4000m belt-parallel structure detection results for the RTP data. TOP: Parallel structures detected. MIDDLE: The same results in vectorized form (displayed line thickness varies according to structure's median value). BOTTOM: Vectorized results co-displayed with the RTP image.

Alberta_RMIfinal_DRTP_Struct4000_Para

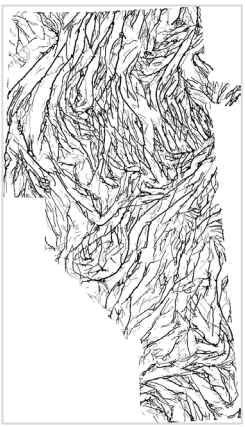

Alberta_RMIfinal_DRTP_Struct4000_Para_Vec

Alberta_RMIfinal_DRTP_Struct4000_Para_Vec

Alberta_RMIfinal_DRTP_HSI_NW

** *Further scales of results also delivered.*

Magnetic data-processing results images (continued)

▶ Parallel/cross structure — RTP

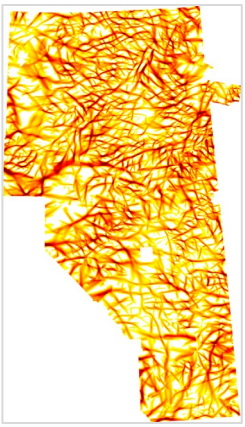

Figure 29: Representative image** showing 4000m belt-crossing structure detection results for the RTP data. TOP: Cross structures detected. MIDDLE: The same results in vectorized form (displayed line thickness varies according to structure's median value). BOTTOM: Vectorized results co-displayed with the RTP image.

Alberta_RMIfinal_DRTP_Struct4000_Cross

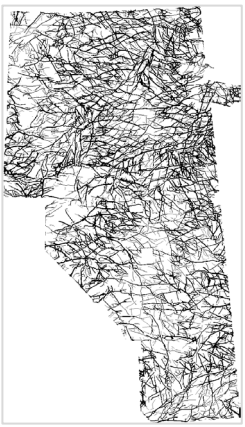

Alberta_RMIfinal_DRTP_Struct4000_Cross_Vec

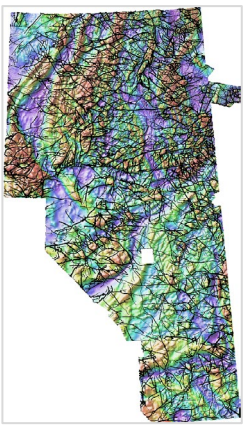

Alberta_RMIfinal_DRTP_Struct4000_Cross_Vec

Alberta_RMIfinal_DRTP_HSI_NW

** *Further scales of results also delivered.*

Magnetic data-processing results images (continued)

▶ Parallel/cross structure — AGC

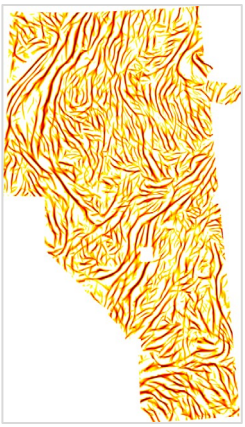

Figure 30: Representative image** showing 4000m belt-parallel structure detection results for the RTP's AGC. TOP: Parallel structures detected. MIDDLE: The same results in vectorized form (displayed line thickness varies according to structure's median value). BOTTOM: Vectorized results co-displayed with the RTP image.

Alberta_RMIfinal_DRTP_AGC60_Struct4000_Para

Alberta_RMIfinal_DRTP_AGC60_Struct4000_Para_Vec

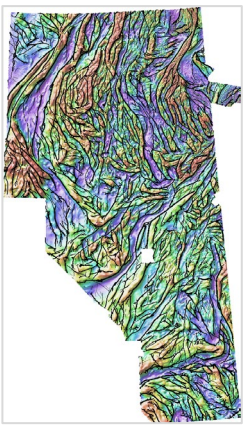

Alberta_RMIfinal_DRTP_AGC60_Struct4000_Para_Vec

Alberta_RMIfinal_DRTP_HSI_NW

** *Further scales of results also delivered.*

Magnetic data-processing results images (continued)

▶ Parallel/cross structure — AGC

Figure 31: Representative image** showing 4000m belt-crossing structure detection results for the RTP's AGC. TOP: Cross structures detected. MIDDLE: The same results in vectorized form (displayed line thickness varies according to structure's median value). BOTTOM: Vectorized results co-displayed with the RTP image.

Alberta_RMIfinal_DRTP_AGC60_Struct4000_Cross

Alberta_RMIfinal_DRTP_AGC60_Struct4000_Cross_Vec

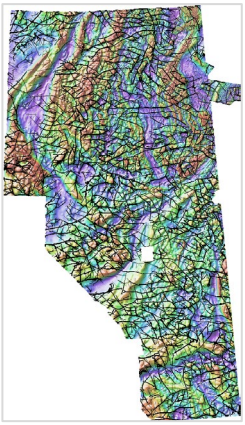

Alberta_RMIfinal_DRTP_AGC60_Struct4000_Cross_Vec

Alberta_RMIfinal_DRTP_HSI_NW

** *Further scales of results also delivered.*

Magnetic data-processing results images (continued)

▶ Radial symmetry analysis — RTP

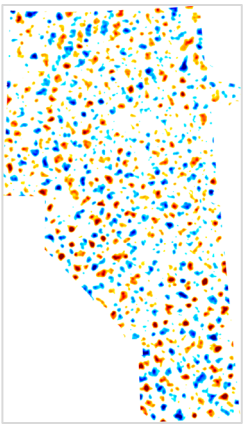

Figure 32: Representative image** showing 8000m magnitude-independent radial symmetry results for the RTP data. TOP: Radially symmetric features detected (both positive and negative anomalies). MIDDLE: Vectorized polygons representing strong anomalies obtained via thresholding. BOTTOM: Polygons co-displayed with the RTP image.

Alberta_RMIfinal_DRTP_res2000_32000_RSym8000_mi_highs_and_lows

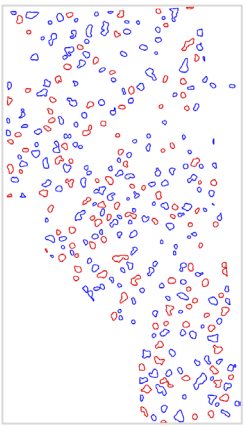

Alberta_RMIfinal_DRTP_res2000_32000_RSym8000_mi_HTh_Vec_highs

Alberta_RMIfinal_DRTP_res2000_32000_RSym8000_mi_HTh_Vec_lows

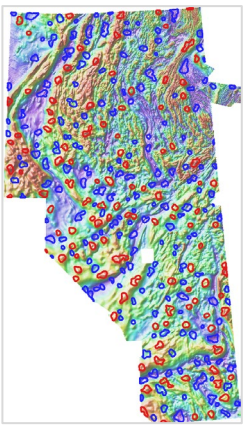

Alberta_RMIfinal_DRTP_res2000_32000_RSym8000_mi_HTh_Vec_highs

Alberta_RMIfinal_DRTP_res2000_32000_RSym8000_mi_HTh_Vec_lows

Alberta_RMIfinal_DRTP_HSI_NW

** *Further scales of results also delivered.*

Magnetic data-processing results images (continued)

▶ Depth to basement — Depth

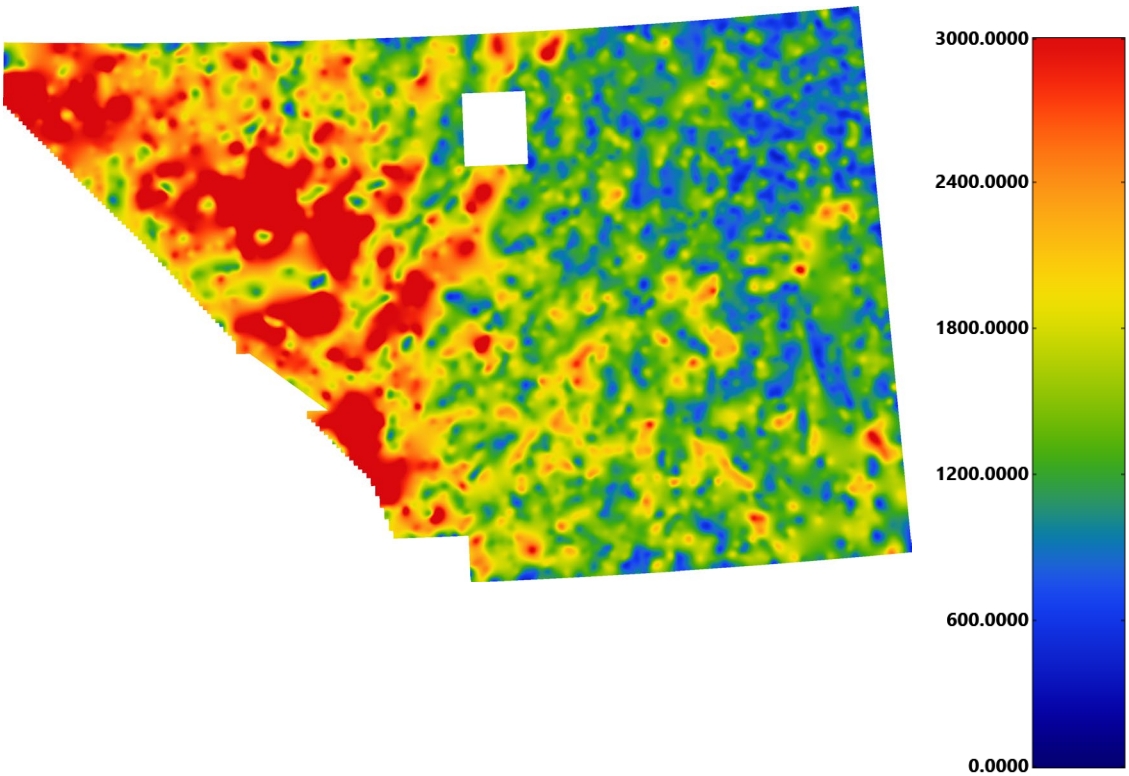

AlbertaCenter_RMI_RTP_Depth_to_Magnetic_Source

Figure 33: The depth to magnetic source results are shown colored according to the color bar on the right. The units are in meters below the topographic surface. The depths increase to the west with the magnetic rocks being buried by more than 3km in the areas with the most cover. The least cover is in the northeast. The whole area appears to have some cover present though small amounts of basement could outcrop in the NE.

Magnetic data-processing results images (continued)

▶ Depth to basement — Surface elevation

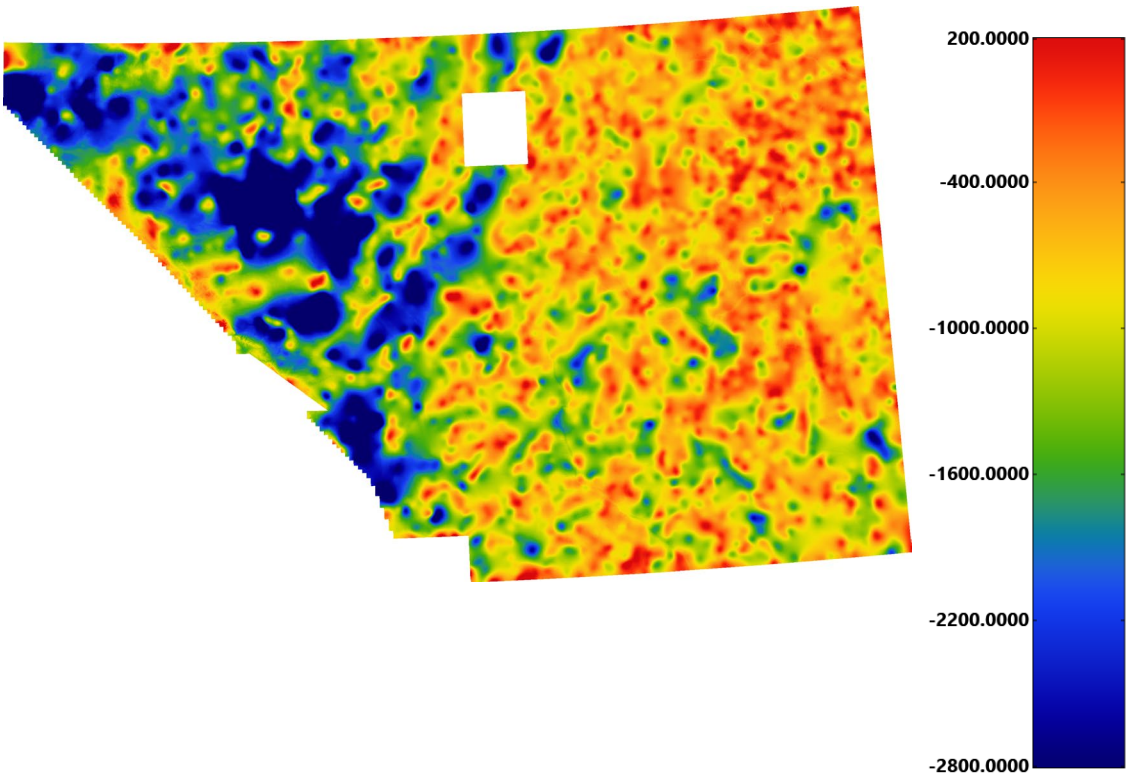

AlbertaCenter_RMI_RTP_Magnetic_Basement_Surface

Figure 34: The elevation of the magnetic basement surface is shown colored as indicated by the color bar to the right of the image. The grid is basically the inverse of the depth to source grid with the magnetic rocks close to the surface in the northeast and getting down to and RL below -2800 in parts of the west.

Appendix 1: Structure detection algorithm

The goal in developing structure detection was to move towards automated interpretation of potential field data that would be most similar to an interpretation by a person. The structure detection is a phase congruency algorithm based on oriented exponential filters (**Kovesi, 1999**).

The structure detection filter is a feature detection algorithm used to highlight ridges, valleys or edges in gridded data. The results are significantly different from other feature detection routines.

Perhaps the biggest difference is that the results are a measure of symmetry or asymmetry, irrespective of amplitude. This is because the analysis is completed using the local phase rather than the signal amplitude.

This means that features in areas of low contrast are highlighted just as well as those in areas of high contrast, as long as the frequencies are present. High values in the structure grid indicate that the structure is close to a step edge. A small step change will have a higher value than a higher amplitude change that is more gradual.

The method is also multi-scale by design. For structures to be highlighted, they must be present at more than one scale. This eliminates more-minor edges that may be present over a narrow frequency range.

The use of exponential filters to determine the scale allows for some inference as to the depth of the structures detected when the filter is applied to potential field data. The wavelength in the filename is the shallowest upward continuation level used and the approximate depth should range between 0.5 and 1 times this wavelength.

This depth estimate is based on **Jacobsen (1987)**. This method is not perfect at separating sources from different depths. It is possible to generate long-wavelength features from shallow sources as evidenced by the fact that there are long wavelength features present in radiometric data, which do not have a significant depth component. However, the method should provide a good first pass estimate of which features extend to depth and which are only surficial. It is possible for deep tapping structures to be missed if there is not a significant property contrast across them.

Appendix 1: Structure detection algorithm (continued)

The structure detection filter produces orientation grids that show the orientation of the strongest edge at a given location. When these orientation grids have been thresholded to remove low amplitude features, it's easier to see the prominent structural orientations.

References

Kovesi, P., 1999, Image Features From Phase Congruency. Videre: A Journal of Computer Vision Research, v. 1, no. 3.

Jacobsen, B.H., 1987, A case for upward continuation as a standard separation filter for potential-field maps. Geophysics, v.52, no. 8, pp. 1138-1148.

Appendix 2: Radial symmetry algorithm

The goal in developing the radial symmetry filter is a move towards automated interpretation of potential field and topographic data that would be most similar to an interpretation by a person.

The filter highlights round features (as opposed to linear features) in the data. This allows us to locate areas that have a higher likelihood of being intrusive bodies or discrete alteration zones.

We have developed several radial symmetry filters. The filter that was used for this project is a gradient-based filter that looks for points where the grid slopes away in all directions. Detected locations are magnetic highs that are discrete bodies. Discrete magnetic lows are areas where the grid slopes toward the location from all directions. This algorithm is based on **Loy and Zelinsky (2002)**.

The filter can be used in a magnitude independent (MI) or magnitude dependent (MD) mode. The MI measure is a strict measure of radial symmetry, making it a direct measure of how round an anomaly is, irrespective of the magnitude of the gradients involved there. The MD measure is the MI measure scaled according to the magnitude of the gradients in the grid.

The filter looks for features with a radius between a base radius and two times that radius. It will not locate features that are significantly smaller than the range used. The filter will highlight the center of some features that are larger than the radius range.

References

Loy G., Zelinsky A., 2002, A Fast Radial Symmetry Transform for Detecting Points of Interest. In: Heyden A., Sparr G., Nielsen M., Johansen P. (eds) Computer Vision — ECCV 2002. ECCV 2002. Lecture Notes in Computer Science, vol 2350. Springer, Berlin, Heidelberg